

SOLID-SUPPORTED POLYMER BILAYERS AS MEMBRANE MIMICS

Inauguraldissertation

zur

Erlangung der Würde eines Doktors der Philosophie

vorgelegt der

Philosophisch-Naturwissenschaftlichen Fakultät

der Universität Basel

von

Serena Belegriou

aus

Deutschland

Basel, 2010

Genehmigt von der Philosophisch-Naturwissenschaftlichen Fakultät auf Antrag von

Prof. Dr. Wolfgang Meier

und

Prof. Dr. Uwe Pieleles

Basel, den 22.06.2010

Prof. Dr. Eberhard Parlow

Dekan

to To

and

Kasia

„Viel wichtiger als die großen Systeme, die in den Köpfen anderer Leute erdacht wurden, sind die kleinen Dinge auf die man selber kommt.“

*aus Sputnik Sweethart
von Haruki Murakami*

Danksagung/Acknowledgements

Ich möchte *Prof. Dr. Wolfgang Meier* für die Möglichkeit danken, ein spannendes, interdisziplinäres Projekt in seiner Arbeitsgruppe bearbeitet haben zu können, in einer freundschaftlichen Atmosphäre, die genügend Freiraum zur wissenschaftlichen und persönlichen Entfaltung ließ.

Ich danke *Prof. Dr. Uwe Piele*s für die konstruktive, enthusiastische Begutachtung der Arbeit, sein damit verbundenes Interesse, und die unterhaltsamen und lehrreichen Gespräche.

Besten Dank an *Prof. Dr. Thomas Pfohl* für die sofortige Zusage zur Übernahme des Prüfungsvorsitzes.

I am greatly indebted to *Kasia, Dr. Katarzyna Kita-Tokarczyk*, for her role as (former) office mate, fitness (and sometimes drill) instructor, psychologist, motivator, proof reader, scientific collaborator, and, most important, as an incredibly helpful friend.

Besonderer Dank gebührt *Dr. Jan Dorn*. Ohne seine engagierte Zusammenarbeit wäre diese Arbeit in der Form erst gar nicht möglich gewesen. Danke auch für die perfekte Organisation der zahlreichen Mess-Sessions am MPIP und natürlich auch für die Einhaltung der „work-life-balance“ in Mainz.

Vielen Dank an *PD Dr. Daniel Häussinger* für die Durchführung und Auswertung der DOSY Messungen.

Dem *Fonds der Chemischen Industrie* danke ich für die finanzielle Unterstützung in Form eines Kekulé-Stipendiums und für die professionelle Betreuung während und nach der Stipendiumslaufzeit.

I want to thank the former and present members of “Gruppe Meier” for the great time we had! Besonders danke ich *Dirk de Bruyn* und *Kasper Renggli* dafür, dass sie die wahren IT Spezialisten in der Gruppe sind, *Gabriele Persy* für die TEM Messungen, *Dr. Nico Bruns* für die geduldige Beantwortung aller (un)möglichen Fragen, *Ruth Pfalzberger* für ihr graphisches Talent, *Esther Stalder* für die zuverlässige Abwicklung der zahlreichen administrativen Angelegenheiten, *Dr. Lucy Kind* für ihre ansteckende Fröhlichkeit, *dziękuję to Agnieszka Jagoda* for being such a pleasant office mate, *Thomas Schuster* und *Stefan Egli* für die lustigen Cargo-Bar-, Grill- und Kochabende, unter anderem mit Weißwurst und Weißwurstersatzprodukten, *Sven Kasper* für die -vor allem in letzter Zeit- häufigen Passivraucherpausen, die tolle Zeit auch außerhalb der Uni und auch dafür, dass er der einzig wahre Lab-Sheriff ist und *Dr. Diana Sebök* dafür, dass sie in so kurzer Zeit zu einer wirklich guten Freundin wurde und dafür, dass sie (fast) die selben Unmengen an Essen wie ich verdrücken kann.

Danke auch den *Ulmer Chemikern* für die tollen Jahre in Ulm, inklusive Höhentrainingslager, die zum Glück noch fortgesetzt werden.

Mille grazie a *Meme, Raffaella* e famiglia per farmi sentire a Basilea immediatamente come a casa propria.

Ich danke meinen „Wölfinnen“, *Ma* und *Tante*, ebenso *Wolfgang* und *Onkel Reinhold*. Ihr habt mir die Grundvoraussetzungen mitgegeben diesen Weg zu bestreiten.

Und natürlich möchte ich dir, *Tobi*, für so ziemlich alles danken. Trotz all deiner Ermahnungen („Wir sind ja net zum Spaß da!“), war und ist die Zeit mit dir sehr spaßig, vor allem die letzten paar Jahre. Ich muss es dir eigentlich gar nicht „nur mal eben sagen“, denn du weißt ja, dass du das Größte für mich bist!

Abstract

Membranes are one of Nature's most remarkable designs. Due to their importance in numerous cellular processes, they are prominent subjects of biochemical and biophysical fundamental research. In particular, it is crucial to understand the membrane morphology, the role of individual membrane components, and also to correlate the membrane structure to its various functions. Besides, systems inspired by natural membranes are of high interest for technological applications, such as water purification, drug screening, or sensing. However, the complexity and fragility of natural membranes often limit their direct use. For that reason, the development of membrane models is indispensable. Suitable building blocks for model systems could be lipids or amphiphilic polymers.

In this thesis, robust solid-supported membrane models from amphiphilic diblock copolymers were designed by combining different methods of polymer synthesis, membrane preparation, and surface analytics. Anionic polymerization yielded a well-defined poly(butadiene)-*b*-poly(ethylene oxide) polymer in terms of overall molecular weight and individual block length. Through a chemical modification procedure, a sulfur-functionalized derivate of the polymer was obtained, which served for covalent immobilization of the polymer monolayers on ultrasmooth gold surfaces.

For membrane preparation two different procedures were employed: on the one hand, individual polymeric monolayers were deposited on the gold supports by a combination of the well-controllable Langmuir film transfer techniques. On the other hand, in a one-step procedure, polymer superstructures were spread either on gold or on glass surfaces to yield solid-supported polymer membranes. The membranes with a covalently immobilized proximal leaflet by sulfur/gold chemistry possess high mechanical stability, and at the same time, a certain degree of mobility resulting from the non-covalent coupling of the individual sheets.

The membranes were characterized by surface-sensitive techniques such as atomic force microscopy and surface plasmon resonance spectroscopy to gain insights into morphology, homogeneity, and thickness of the layers. To demonstrate the membranes' biomimetic potential, they were incubated with peptides, polymyxin B and α -haemolysin. Occurring interactions were detected by electrochemical impedance spectroscopy.

In summary, this thesis might impact fundamental membrane science as well as prospective biotechnological applications.

Abbreviations and symbols

<i>A</i>	area
AFM	atomic force microscopy
ATR-IR	attenuated total reflection infrared spectroscopy
Bd	1,3-butadiene
BL	bilayer
BLM	black lipid membrane
BodiPy	boron-dipyrromethene (4,4-difluoro-3a,4a-diaza- <i>s</i> -indacene)
BuLi	butyllithium
BuP ₄	phosphazene base
<i>C</i> , <i>C</i>	capacitor, capacitance
CAC	critical aggregation concentration
CPE	constant phase element
C_s^{-1}	compressibility modulus
δ	chemical shift
δ_{diff}	diffusion constant
DCM	dichloromethane
DF	degree of functionalization
DLS	dynamic light scattering
DMAP	4-(dimethylamino)pyridine
DMF	dimethylformamide
DOSY	diffusion ordered spectroscopy
EDC·HCl	1-ethyl-3-(3-dimethylaminopropyl)carbodiimide hydrochloride
EIS	electrochemical impedance spectroscopy
EO	ethylene oxide
GPC	gel permeation chromatography
λ	wavelength
LA	lipoic acid (1,2-dithiolane-3-pentanoic acid))
LB	Langmuir-Blodgett (transfer)
LS	Langmuir-Schaefer (transfer)
MEK	methyl ethyl ketone (2-butanone)
NMR	nuclear magnetic resonance

ML	monolayer
MMA	mean molecular area
M_n	number average molecular weight
M_w	weight average molecular weight
n	refractive index
N	number of repeating units
NEt ₃	triethylamine
OH	hydroxyl group
π	surface pressure
PAA	poly(acrylic acid)
PB	poly(butadiene)
PBS	phosphate buffered saline
PDI	polydispersity index
PEE	poly(ethyl ethylene)
PEO	poly(ethylene oxide)
PS	poly(styrene)
ρ	density
R, R	resistor, resistance
r_h	hydrodynamic radius
SPR	surface plasmon resonance (spectroscopy)
TEM	transmission electron microscopy
θ	(phase) angle
T_g	glass transition temperature
THF	tetrahydrofuran
TMRA	tetramethylrhodamine-5-carbonyl azide
TSG	template stripped gold
Z	impedance

Table of contents

1	Introduction	1
1.1	Models of non-supported membranes	3
1.2	Block copolymer membranes	6
1.2.1	General aspects of self-assembly	6
1.2.2	Thermodynamic and kinetic stabilization	7
1.3	Solid-supported membrane models	10
2	Motivation and concept	14
3	Results and discussion	16
3.1	Synthesis of PB-PEO-OH	16
3.2	Synthesis of PB-PEO-LA	18
3.3	PB-PEO membranes <i>via</i> Langmuir transfer techniques	21
3.3.1	Monolayers at the air-water interface	21
3.3.2	Monolayers on gold	23
3.3.2.1	Characterization by ATR-IR	24
3.3.2.2	Thickness determination by SPR	25
3.3.2.3	Characterization by AFM	26
3.3.3	Bilayer membranes on gold	29
3.3.3.1	Thickness determination by SPR	29
3.3.3.2	Characterization by AFM	31
3.3.3.3	Scratching experiments	32
3.3.3.4	Membrane stability	33
3.4	Membranes <i>via</i> spreading of PB-PEO superstructures	37
3.4.1	Formation and characterization of PB-PEO superstructures	37
3.4.1.1	Solvent-free preparation	38
3.4.1.2	Solvent displacement techniques	41
3.4.2	Aggregate spreading by non-covalent interactions	50
3.4.3	Aggregate spreading by covalent interactions	52
3.4.3.1	Characterization by AFM	52
3.4.3.2	Characterization by EIS	59
3.5	Influence of peptides on PB-PEO bilayers	65

4	Conclusions and outlook	70
5	Experimental part.....	72
5.1	Synthesis of PB-PEO-OH.....	72
5.2	Synthesis of PB-PEO-LA	74
5.3	Mono- and bilayer preparation	75
5.3.1	Gold substrate preparation.....	75
5.3.2	Monolayer transfer	75
5.3.3	Bilayer preparation by LS transfer	75
5.3.4	Preparation of PB-PEO superstructures	76
5.3.5	Spreading of PB-PEO superstructures	76
5.3.6	Bilayer incubation with peptides.....	76
5.4	Mono- and bilayer characterization	77
5.4.1	Characterization at the air-water interface	77
5.4.2	Contact angle measurements.....	77
5.4.3	ATR infrared spectroscopy	78
5.4.4	Surface plasmon resonance spectroscopy	78
5.4.5	Atomic force microscopy	78
5.4.6	Electrochemical impedance spectroscopy.....	79
5.4.7	Dynamic light scattering	79
5.4.8	Transmission electron microscopy.....	80
6	Additional polymers synthesized	81
6.1	Biotin-functionalized PB-PEO	81
6.2	Fluorophore-functionalized PB-PEO.....	83
7	References.....	85
	Curriculum vitae.....	90
	Publications and conference posters	91

1 Introduction

Membranes are ubiquitous and essential for all living organisms. For instance, in the human body, we encounter about 100 km^2 of membranes, barely 5 nm thick, forming the boundary of the cells and cell-organelles, such as mitochondria, Golgi-apparatus, endoplasmatic reticulum, or lysosomes.^[1]

Membranes are highly complex assemblies, consisting of lipids, proteins, and oligosaccharides, and far from only inert separation layers. Apart from compartmentalizing and protecting cells and cell organelles from their environment, they are involved in a multitude of biochemical processes. Membrane-related functions comprise, for instance, passive and active transport of ions between the intra- and extracellular space in order to maintain electrochemical gradients across the membrane. These gradients are of fundamental importance for the energy generation and storage, the cell metabolism, or the signal transduction. Furthermore, membranes are involved in dynamic processes such as cellular differentiation or cell migration.^[2]

The structure of a cell membrane can be described by the “fluid mosaic model” proposed by Singer and Nicolson in 1972.^[3] It is depicted in Figure 1.

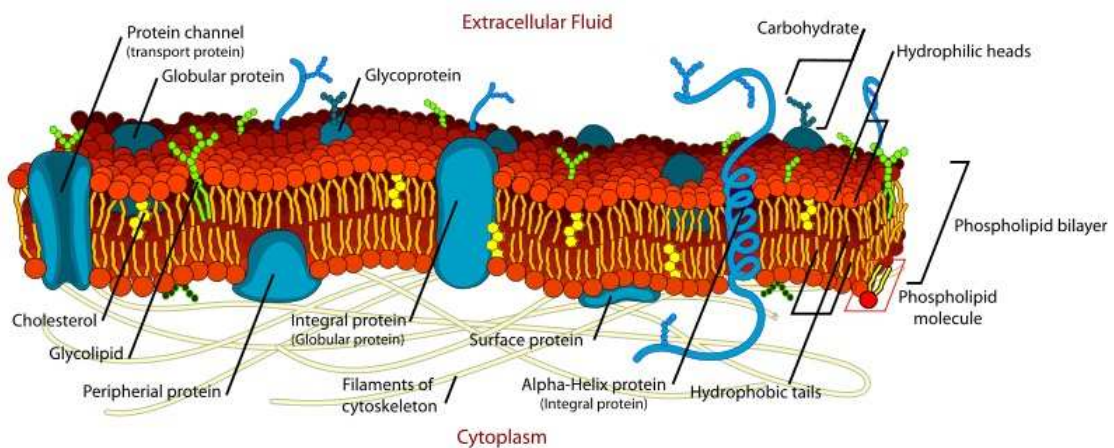


Figure 1. A fluid mosaic model of the cell membrane.^[4]

According to this model, the central structural element is the lipid bilayer. It is arranged in such a way, that the fatty acid chains face towards each other and form the hydrophobic membrane core, whereas the hydrophilic parts are exposed to the intra- or extracellular space, respectively.

This arrangement is driven by the lipid geometry and the hydrophobic effect.^[5-7] The two individual leaflets of the lipid bilayer are held together by (non-covalent) hydrophobic interactions. Steroids, e.g. cholesterol, are embedded in the lipid matrix, mainly to stabilize the structure. Membrane proteins can be embedded in the bilayer as integral proteins, or/and associated to one side of the bilayer as peripheral proteins. Thus, the cell membrane can be formally considered as a two-dimensional solution of proteins in a viscous lipid bilayer solvent.^[3] The exact composition of biological membranes varies depending on the type and function of the cell or a membrane region.^[8]

Since the cell membrane with its vital functions is the most important interface in living organisms, modern research focuses on the investigation of its structure, properties, and functions. Membranes are valuable for addressing biophysical and biochemical questions such as studies of individual membrane-related processes, investigations of membrane components at a single-molecule level, or ligand-receptor binding. In pharmaceuticals, they are very important as therapeutic targets, since antibiotics or virus receptors interact with membranes. Furthermore, integral proteins are one of the key targets for drugs. However, due to their high hydrophobicity, investigations have to be performed in their natural environment, i.e. in a lipid membrane.^[1] The thorough investigation of integral proteins in lipid membranes is a fundamental step in drug design and development.^[9] Besides basic research, membranes are also highly attractive for industrial research. Membranes might be technologically interesting, e.g. for water purifications and desalination applications.^[10, 11] Moreover, they could act as platform for sensor devices, with potential applications in trace analysis or in biosensing.^[10, 12]

However, natural membranes as highly specialized and complex multi-component assemblies are not always suitable to investigate and understand distinct membranes functions. Furthermore, their complexity is disadvantageous for many technological and industrial processes. Therefore, the development of simplified biomimetic model membranes (either in solution or on surfaces) is necessary. In order to break down the complexity of natural membranes, model systems usually consist of only a few membrane components, mainly mimicking a characteristic feature of the membrane, e.g. the central bilayer structure.

Following Nature, commonly (phospho)lipids are implemented as building blocks to create membrane mimics. Even though some reports on advanced lipid-based systems were already published,^[13-15] they still suffer from some drawbacks. Lipids are prone to oxidation, and chemical modification of lipids with functional groups is limited. Moreover, lipid membranes may not possess sufficient stability, mechanically and against air,^[16] which - depending on the conditions - limits their use for technological applications.

These drawbacks can be overcome by employing alternative building blocks, i.e. amphiphilic block copolymers. These polymers are already well-known in the field of materials science, surface coatings or tissue engineering.^[17-20] Recently, amphiphilic block copolymers also attracted considerable interest as constituents for model membranes,^[21-24] and proved to be a suitable platform to study specific (membrane) proteins and protein-related processes in a non-natural environment.^[25-29] With an appropriate molar mass and hydrophilic to hydrophobic block ratio, amphiphilic block copolymers adopt the bilayer structure in water.^[30, 31] Since the molecular weight of polymers can be considerably higher compared to lipids, the resulting membranes thickness can be also larger than that of lipid membranes, thus making polymer membranes mechanically more stable.^[32] Polymer synthesis allows for the adjustment of such parameters as block length, molecular weight, chemical composition, hydrophilic/hydrophobic balance, and molecular architecture. Hence, a wealth of possibilities are accessible to tailor customized block copolymer membranes.^[23, 33]

1.1 Models of non-supported membranes

In the development of membrane models, cues can be taken from self-assembly of amphiphilic molecules. The common characteristic feature of amphiphiles such as surfactants, lipids, or amphiphilic block copolymers, is the covalent linkage of parts with different polarities, which favor different solvents. The covalent bond prevents macroscopic phase separation. When exposed to a selective solvent, amphiphiles can self-assemble into lyotropic phases such as micelles or lamellae (vesicles). Self-assembly into mesophases takes place in the dilute regime, but the amphiphile concentration has to exceed the critical aggregation concentration (CAC).^[34, 35]

Long-range repulsive interactions between the parts of different polarity, as well as short-range attractive forces by covalent bonds between the incompatible parts, are involved at the same time during the microphase separation process.^[19] The aggregates themselves are held together solely by non-covalent interactions.^[21]

The superstructures formed upon self-assembly of amphiphilic molecules such as lipids or polymers can serve as membrane models. The most prominent membrane models in solution, i.e. black lipid membranes, Langmuir monolayers, and vesicles (liposomes) are depicted in Figure 2 and will be briefly presented in this section.

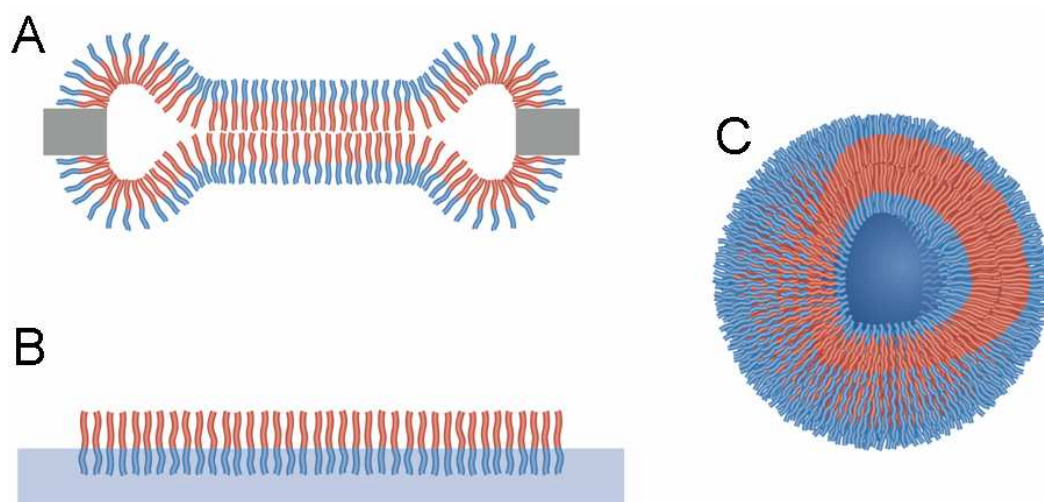


Figure 2. Models of non-supported membranes: (A) black lipid membrane, (B) Langmuir monolayer, and (C) vesicle.

Black lipid membranes (BLMs), or *black polymer membranes*,^[36, 37] are free-standing bilayers, spanned over a small aperture in a hydrophobic material such as TeflonTM.^[38-40] BLMs are well suited for measurements of transmembrane currents on a single-channel level.^[41] Even though they provide valuable information about transport processes in membranes, their potential for technological use is restricted: they are mechanically fragile and their long-term stability is limited.^[16]

Langmuir monolayers are monomolecular thin films floating at the air-liquid interface.^[42, 43] They can be produced by spreading a solution of a surface-active and water insoluble compound, e.g. a lipid or an amphiphilic polymer, on the free surface of a liquid subphase. Since they resemble, in contrast to BLMs or vesicles, only a monolayer, they are less suited to investigate transmembrane processes, but they are appropriate to study interactions occurring at the membrane surface.^[44] In particular studies of binary polymer-peptide or polymer-lipid mixtures revealed interesting insights into the behavior of mixed phases.^[45, 46]

Vesicles are hollow, lamellar spherical structures, with dimensions ranging from nanometers to several tens of micrometers. If the vesicle constituents are lipids, they are referred to as *liposomes*. Vesicles can be prepared either by solvent-free techniques, such as rehydration or electroformation,^[47] or by solvent displacement techniques utilizing a co-solvent.^[48] Further treatments like extrusion,^[49] chromatography,^[50] freeze-thawing,^[51] or a combination of these methods can be applied to create a homogeneous dispersion of vesicles with defined sizes. With vesicles, it was possible to investigate, for example, permeability and solute transport through bilayers.^[28, 52] Furthermore, vesicular membrane models proved to be useful for membrane protein reconstitution.^[53-55]

Vesicles from amphiphilic block copolymers (*polymersomes*) were first described by Eisenberg and co-workers.^[56] Those bilayer structures in solution very well mimic biological membranes and as such have found several applications.^[28, 57] Contrary to lipids, however, self assembly processes in polymer solutions are more complex, in particular due to the large polymer size. In the following sections, we will describe the concepts of polymer self assembly in solution and discuss some aspects of thermodynamic and kinetic stabilization.

1.2 Block copolymer membranes

In general, block copolymers are built of two constitutionally different blocks A and B, which are linearly linked. Within the sequence, one block type can appear repeatedly to yield, for example, an ABA sequence. In the case of amphiphilic block copolymers, the constitutionally diverse blocks should differ also concerning their polarity. Polymer synthesis allows for the alteration of amphiphilic properties through different chemical composition, absolute chain length, or relative block length.^[33]

1.2.1 General aspects of self-assembly

Similar to their low molecular weight counterparts (e.g. lipids, surfactants), amphiphilic block copolymers self-assemble in block-selective solvents and form lyotropic phases such as micelles or lamellae.^[17, 18, 21, 23] Amphiphilic self-assembly can be described by geometrical and thermodynamic aspects. The determining factor for aggregate shape is the volume ratio of the hydrophobic block to the hydrophilic one, because it controls the interfacial curvature.^[58] By changing this ratio, specific self-assembled nanostructures such as spheres, cylinders, or bilayers can be targeted according to the “packing parameter”.^[5]

A theoretical description of amphiphilic self-assembly was given by Wang.^[59] In brief, depending on the block copolymer composition, a curved bilayer as found in vesicles may become favored over a flat one. Similarly, Antonietti and Förster^[58] consider the lower free energy of curved bilayers as compared to flat ones as the driving force for vesicle formation. If the sheet-like aggregates are large enough, they close to vesicles as illustrated in Figure 3.

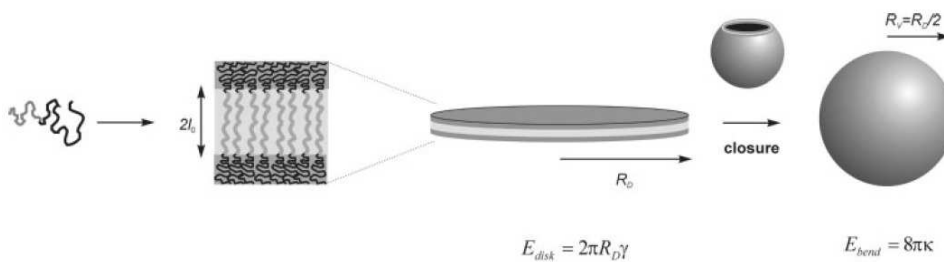


Figure 3. Schematic illustration of the formation of bilayers and their closure to vesicles.^[58]

The minimization of the system's total free energy is the driving force for amphiphile aggregation. The free energy can be decreased by energetic and entropic contributions. On the one hand, a decrease of the free energy can be achieved by decreasing the interfacial energy of the hydrophobic-hydrophilic interface, which, in turn, can be accomplished by reducing the interfacial contact area.^[58] On the other hand, aggregation decreases the total entropic loss, because the contacts between water molecules and hydrophobic blocks are minimized ("hydrophobic effect").^[7] In other words, amphiphile aggregation leads to an entropic gain of the water molecules. However, many amphiphilic block copolymers have a considerably low CAC - for such polymers, morphology and size of the aggregates are usually not based on molecular exchange and equilibrium processes, but are rather trapped by the preparation conditions.^[58] Hence, block copolymer self-assemblies can be considered as non-equilibrium structures, as explained in detail in the following section. The non-equilibrium state is strongly coupled with the morphological variety and the complexity of polymer aggregates. Among others, the preparation conditions determine the aggregate shape, by inducing a certain bilayer asymmetry that leads to spontaneous curvature minimizing the energy for the system of interest.^[58]

1.2.2 Thermodynamic and kinetic stabilization

One of the first reports describing multiple block copolymer morphologies was published by Zhang and Eisenberg.^[56] By varying the hydrophilic content of poly(styrene)-*b*-poly(acrylic acid) (PS-PAA) block copolymers, different morphologies of "crew-cut" aggregates (where corona-forming hydrophilic blocks are much shorter than core-forming hydrophobic blocks) were obtained. More precisely, by gradually decreasing the PAA content, micelle morphology changed from spherical to rod-like, and finally vesicles were obtained. The preparation of the aggregates was aided by organic solvents, i.e. DMF, swelling the hydrophobic PS cores. Upon DMF removal by e.g. dialysis against water, the core structures became kinetically frozen at room temperature due to the glassy nature of PS.

The polymorphism of block copolymer aggregates was also demonstrated by Bates and co-workers. The aggregation structure of PEO-based block copolymers could be controlled by varying the PEO content.^[60] Analogous to the reports from the Eisenberg group, a decrease of the hydrophilic volume ratio led to morphological transitions from spheres to cylinders to bilayers, which is in accordance with a decrease in curvature.

The morphology of PS-PAA aggregates described by Eisenberg results from the balance of three main contributions to the free energy: chain stretching in the core, interfacial energy or tension, and repulsion between corona chains.^[56] They control the aggregate architecture and upon their alteration, morphological changes of block copolymer aggregates can be induced.^[61] They can be altered by parameters such as the absolute block length, the block ratio, the polymer concentration in the stock solution, temperature, the presence of electrolytes, the nature of the common solvent, and the process of water addition (speed, volume). In particular, the last parameter was systematically investigated by Yu and Eisenberg.^[31] At low water content *versus* the common solvent, the exchange of polymer chains between bulk solution and aggregates is assumed to take place. Thus, at this stage, the self-assembly is under thermodynamic control. As the water content increases, the exchange rate of polymer chains slows down, resulting in kinetically frozen (trapped) intermediate structures. These experimental observations even allowed for the postulation of aggregate formation mechanisms. In accordance with the considerations by Förster and Antonietti,^[58] lamellae were considered as precursors of (large) vesicles.

According to a recent review, it is believed that the morphologies of block copolymer aggregates containing rather liquid hydrophobic cores, e.g. consisting of poly(butadiene) (PB) or poly(ethyl ethylene) (PEE), are not dictated by the kinetically frozen hydrophobic blocks.^[62] However, from a careful literature study, it becomes apparent that the arguments for the formation of kinetically trapped PS-containing aggregates, account also for PB- or PEE-containing superstructures.^[63, 64] As explained above, the formation of trapped intermediate, non-equilibrium structures originates mainly in extremely slow component exchange kinetics. Additionally, large chain length and high aggregate surface viscosity^[64] are assumed to hamper the establishment of a global equilibrium.^[63] However, a local equilibrium can be achieved by adopting the shape with minimal energy.^[64]

In this context, Jain and Bates used the term “nonergodicity” to explain the phenomena observed by Eisenberg and co-workers.^[63]

Still, the long-lasting discussions about the thermodynamic state of block copolymer aggregates are far from concluded. Eisenberg group reported about thermodynamically controlled block copolymer aggregates,^[65-67] since the size of PS-PAA vesicles responded reversibly to changes in the solvent composition.^[65, 66] Changes of vesicle sizes are driven by the interfacial energy contribution to the free energy in such a way, that the system minimizes the surface area by increasing the vesicle size and decreasing the total number of vesicles. This was experimentally achieved by addition of water. Hence, at low water contents the vesicle radii were smaller. The intrinsic polymer polydispersity stabilizes such high curvature vesicles by segregation of the PAA blocks. Fluorescence quenching experiments showed that shorter chains will be located at the inner side of the vesicle membrane, whereas the longer chains are present on the outer vesicle shell.

The examples of amphiphilic self-assembly discussed so far exclusively refer to block copolymer aggregates in solution. On the other hand, for studying membrane functions, individual membrane components, or membrane-related processes, and also for specific technological applications, e.g. sensing, the membrane confinement on solid surfaces may be highly desirable. Moreover, in-detail structural investigations can be performed on surface-immobilized systems, since they are accessible to surface characterization tools, such as atomic force microscopy or surface plasmon resonance spectroscopy. These arguments principally motivated the development of solid-supported membrane models.

1.3 Solid-supported membrane models

This particular class of membrane models was developed in the 1980s. Common preparation techniques for such membranes are Langmuir film transfers,^[68-70] or vesicle spreading.^[71, 72] Early attempts comprised the direct deposition of lipid bilayers onto solid substrates by vesicle fusion.^[73, 74] This resulted in membranes, only separated from the solid support by an ultrathin (1-2 nm) water film.^[75, 76] However, this concept suffers from a number of intrinsic difficulties. The mere physical coupling between the lipid bilayer and the solid support eventually may lead to partial detachment of membrane constituents or replacement by other surface-active compounds.^[77] Furthermore, as depicted in Figure 4 a, the membrane-substrate distance is usually not large enough to avoid direct contact between incorporated membrane components (e.g. integral proteins) and the solid surface.^[78] Some of the proteins envisaged for basic biophysical studies or technological applications, however, possess functional units which protrude far out from the bilayer.^[77] Strong interactions and/or frictional coupling between the substrate and incorporated proteins might lead to partial loss of functionality or even to complete protein denaturation.^[77]

Next generations of solid-supported membranes were therefore optimized in such a way that unfavorable contacts between the substrate and integral membrane components can be avoided. Two major concepts, depicted in Figure 4 b and c, are used to achieve this improvement: lipid bilayers are either “cushioned” on polymer or polyelectrolyte films,^[75, 76, 78, 79] or covalently coupled to the substrate by anchor or spacer groups (and are often referred to as “tethered bilayer membranes”).^[77, 79, 80] Recent attempts involved the introduction of spacer units like peptides, oligomers, or polymers.^[13, 78, 80-83]

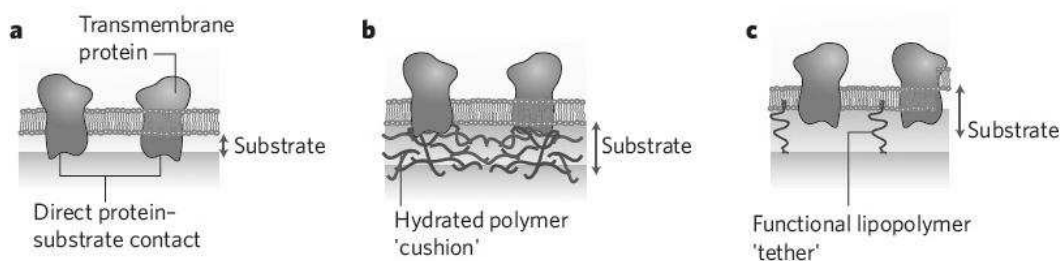


Figure 4. Different types of solid-supported membranes. (a), the bilayer is deposited directly onto the solid substrate, (b) the bilayer is decoupled from the substrate by a polymer cushion, or (c) by a particular tether unit.^[78]

In particular, the approach of covalent tethering is of central importance to this thesis. This concept guarantees a mechanically and chemically robust attachment of the bilayer to the solid support, while at the same time the membrane retains its fluid character.^[80] However, despite these advantageous properties, lipid-based solid-supported membranes still suffer from some drawbacks. As mentioned before, lipid membranes lack mechanical stability, their long-term stability, in particular in gaseous environment is limited, and they also lack chemical versatility. Therefore amphiphilic block copolymers might be a suitable alternative to lipids as membrane building blocks.

In contrast to lipid-based solid-supported membranes, the research area of solid-supported block copolymer membranes has just emerged a few years ago. So far, basically two different architectures of solid-supported polymeric membranes have been reported: they consist either of planar bilayers,^[84, 85] or well-defined polymer aggregates.^[27, 86]

Concerning the latter system, two recent publications^[27, 86] made use of the specific and strong streptavidin-biotin binding assay to immobilize triblock copolymer vesicles on glass. Rosenkranz *et al.* employed this approach to investigate protein folding at a single-molecule level. Proteins, encapsulated in triblock copolymer nanocontainers, could be individually observed for extended time periods. So far, this was impossible to accomplish for freely diffusing molecules in solution.^[86]

Moreover, this immobilization method proved useful for studying enzymatic conversions on precisely patterned surfaces. Grzelakowski *et al.* encapsulated an enzyme in surface-bound hybrid protein-polymer nanoreactors.^[27] A fluorogenic substrate was introduced into the nanoreactors *via* a previously incorporated channel protein. By enzymatic conversion, it became insoluble and fluorescent, thus detectable by laser scanning microscopy. This approach of tethering polymer vesicles to solid surfaces represents the first attempt towards potential applications in the field of analytics, in particular sensing, or in microfluidics.

In parallel, Rakhmatullina *et al.* presented first attempts towards planar solid-supported block copolymer membranes. The membranes were prepared either by surface-initiated radical polymerization (“grafting-from”),^[84] or by vesicle fusion through adsorption.^[85] In the very first report,^[84] atom transfer radical polymerization was applied to prepare surface-grafted triblock copolymer membranes on gold. A

variety of different surface-analytical techniques not only provided information about the layer thickness and surface topography, but also allowed for insights into the block orientation. It was revealed that during the growth of the individual blocks, the polymer chains became oriented in such a way that they tilted increasingly towards the gold surfaces.^[84]

Amphiphilic triblock copolymer membranes have also been prepared by vesicle fusion through adsorption of polyelectrolyte vesicles^[87] on different substrates. In particular, on mica, defect-free block copolymer membranes could be produced through electrostatic interactions between the positively charged polymer vesicles and the negatively charged, hydrophilic mica surface.^[85] Such a membrane is depicted in Figure 5.

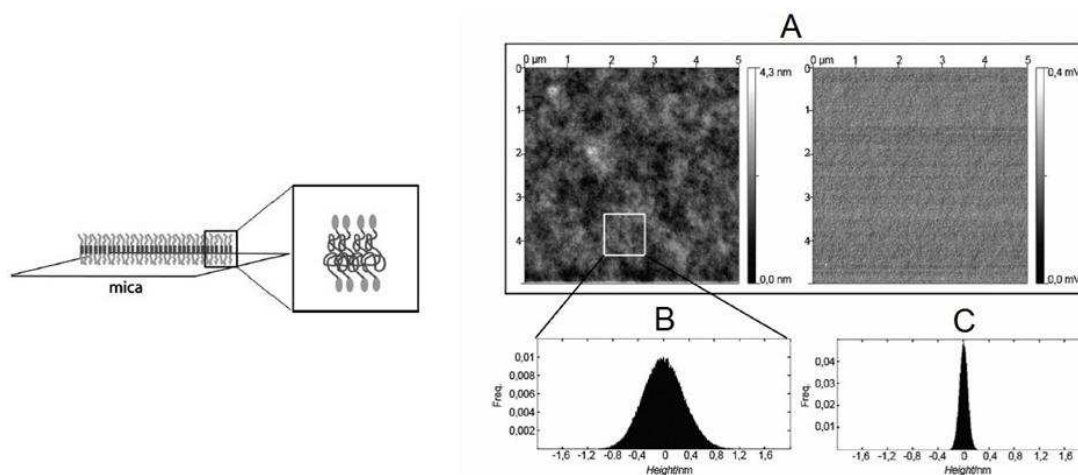


Figure 5. Sketch and AFM images of a solid-supported triblock copolymer membrane on mica. (A) Defect-free copolymer membrane on mica (topography and phase image). The surface histograms, taken before (C) and after vesicle deposition (B) show an increase of surface roughness.^[85]

Potential applications of solid-solid supported membranes as sensing devices for instance, may require successful incorporation of biological moieties, such as membrane proteins. However, the polycationic character of the membranes prepared by vesicle spreading might impede functional incorporation of biological molecules. Additionally, the grafted membranes on gold might be too densely packed for protein incorporation and considerable synthetic efforts might be needed to reduce (and control) the chain packing density. Therefore, these first attempts towards solid-supported polymer membranes can be improved in order to create systems with a well-

controlled packing density. This could be achieved by the application of amphiphilic self-assembly instead of surface chemistry or electrostatics. Self-assembly allows for fast preparation of well-defined polymer membranes with large surface coverage. Additionally, polymers with very different chemical compositions can be used,^[24] unrestricted by the limitations of surface grafting methods. This versatility should lead to membranes that can be possibly applied in biophysical studies, sensor developments, or nanotechnology.

2 Motivation and concept

Despite remarkable advances in the development of membrane models in the past decades,^[79, 80] there is still a great demand for further improvements. The commonly used lipid-based models suffer from some fundamental drawbacks, such as limited chemical functionality and versatility. Moreover, poor stability against air^[16] and the lack of long-term mechanical stability are particularly disadvantageous for prospective technological applications, e.g. in drug screening or sensor development.

Therefore, the aim of this work is to develop a new generation of stable and versatile solid-supported membranes, based on amphiphilic block copolymers: such bilayers are expected to outperform lipid-based membranes. Regarding their preparation and the resulting properties, the major advantages are: (i) chemical tailoring of the membrane building polymers, due to the availability of numerous monomers with various functionalities; (ii) the possibility of using controlled polymerization techniques for the adjustment of the overall molecular weight, thus for adjusting the membrane thickness; (iii) the tunability of hydrophilic to hydrophobic ratio, thus controlling the physicochemical properties and polymer self-assembly; (iv) enhanced mechanical stability, due to high polymer molecular weight and the resulting thicker membranes.

Considering these points, the major goal of this thesis, i.e. to prepare solid-supported block copolymer membranes, was approached through the following objectives:

- (i) to demonstrate the feasibility of the self-assembly approach to create solid-supported polymer bilayers
- (ii) to explore different preparation strategies
- (iii) to thoroughly characterize the membranes
- (iv) to investigate membrane stability, particularly in air
- (v) to study the biomimetic potential of the supported bilayers

To realize these objectives, diblock copolymers based on poly(butadiene)-*b*-poly(ethylene oxide) (PB-PEO) were chosen. These polymers were previously shown to produce fluid vesicular membranes^[60, 88] and monolayers at the air-water interface.^[89] It was also demonstrated that vesicles from PB-PEO do not exhibit toxic effects on living cells^[88] and are able to host membrane-active peptides.^[90]

The bilayer architecture can be achieved by two different methods: on the one hand, a combination of sequential Langmuir film transfer techniques was employed to deposit individual polymer monolayers on ultrasmooth gold surfaces. On the other hand, a one-step procedure, i.e. spreading of polymer aggregates on gold or glass substrates, was applied. The resulting membranes can be analyzed by surface-sensitive techniques, such as contact angle measurements, atomic force microscopy, and surface plasmon resonance spectroscopy, to gain insights into morphology, homogeneity, and thickness of the layers. Finally, the ability of the membranes to act as a hosting matrix for biologically active moieties could be probed by electrochemical impedance spectroscopy.

3 Results and discussion

The first two sections of this chapter focus on the synthetic part, i.e. polymer synthesis, purification, functionalization, and characterization. The following two sections include the preparation and characterization of solid-supported poly(butadiene)-*b*-poly(ethylene oxide) (PB-PEO) membranes, and are dedicated to membranes prepared by Langmuir film transfer techniques, and by spreading of polymer superstructures, respectively.

3.1 Synthesis of PB-PEO-OH

PB-PEO block copolymers were synthesized by sequential living anionic polymerization. This technique allows for the synthesis of tailor-made polymers,^[91, 92] with well-defined polydispersities, molecular weights, and hydrophilic volume fractions.

More precisely, a procedure was followed that utilizes the phosphazene base *t*BuP₄.^[93, 94] This base prevents the strong association of the living PEO chain ends with the Li⁺ counter-ions from the initiator, and therefore allows for a sequential one-step polymerization without intermediate steps. The reaction scheme is depicted in Figure 6.

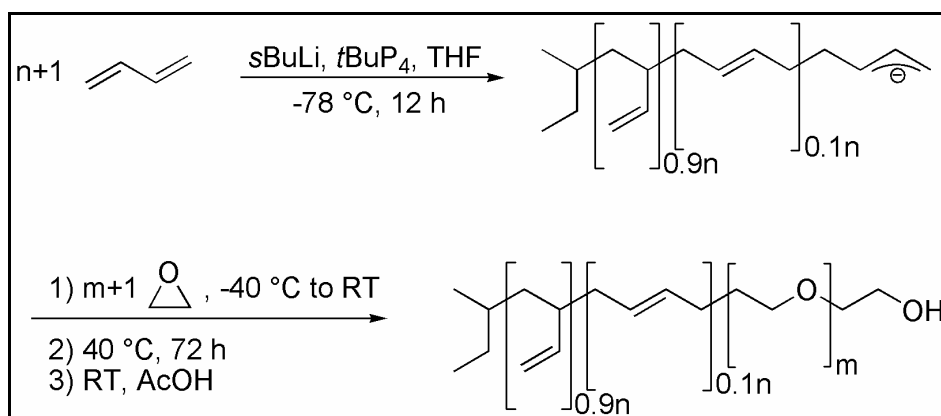


Figure 6. Reaction scheme of the one-pot anionic copolymerization of 1,3-butadiene and ethylene oxide.

Polymers synthesized by anionic polymerization can be obtained in high yields and almost pure, because side products should not form and non-reacted monomers can be removed under vacuum. Usually, purification comprises only precipitation. However, in this case, the phosphazene base could neither be fully removed by repeated precipitations in appropriate solvents such as acetone, water, methanol, or ethanol, nor by addition of an ion exchange resin. In some cases, the *t*BuP₄ content was up to 60%, as determined by ¹H-NMR. This contamination might negatively affect prospective applications, where the polymer is in contact with sensitive biological compounds such as transmembrane proteins. Therefore, repeated extractions with water and 10% (v/v) HCl were performed, followed by additional precipitations. In this way, it was possible to lower the *t*BuP₄ content to less than 1%.

The polymerization reaction yielded 90% 1,2 and 10% 1,4 isomer, as determined by ¹H-NMR. The isomers are statistically distributed. A representative spectrum of PB-PEO-OH is shown in Figure 7.

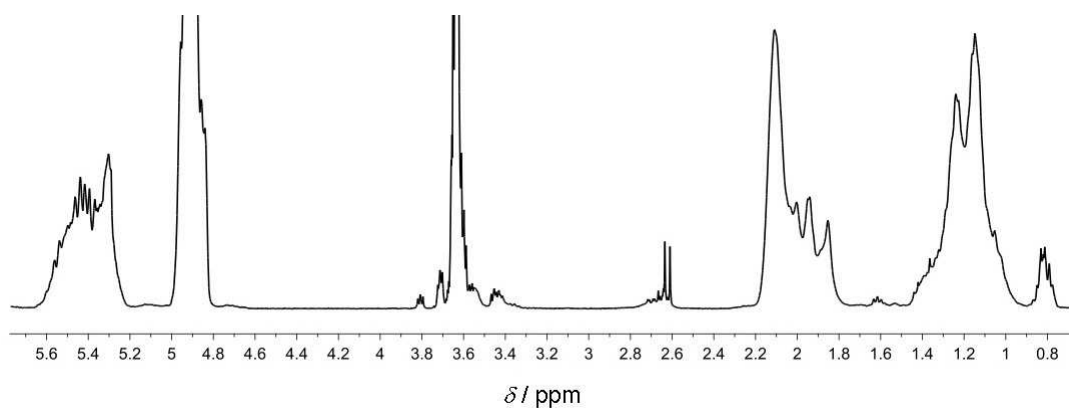


Figure 7. Representative ¹H-NMR spectrum of purified PB-PEO-OH. The signals at $\delta = 2.6$ ppm are assigned to *t*BuP₄. Analysis of the integrals revealed a *t*BuP₄ residue of less than 1%. A detailed peak assignment is presented in the experimental part.

The molecular weight of the block copolymer was determined by GPC and ¹H-NMR. First, a PB aliquot, drawn prior to the sequential copolymerization, was analyzed by GPC with THF as eluent. Narrow poly(butadiene) standards were used to calculate M_n , M_w , and the polydispersity index (PDI) of the PB block ($N_{PB} = 52$). The number of the ethylene oxide repeating units ($N_{PEO} = 29$), thus the molecular weight, was

calculated from the integral ratios in the $^1\text{H-NMR}$ spectrum of the block copolymer. The results are summarized in Table 1 (see section 3.2).

3.2 Synthesis of PB-PEO-LA

PB-PEO-OH was modified with lipoic acid (LA). The reaction was performed under classical esterification conditions, as shown in Figure 8.

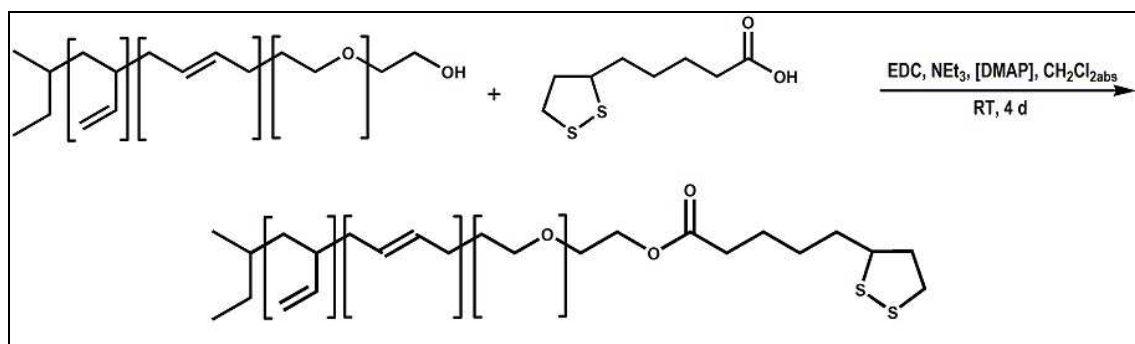


Figure 8. Reaction scheme of PB-PEO end-functionalization with lipoic acid.

This provided an easy synthetic route to a sulfur-functionalized polymer PB-PEO-LA, which can serve for covalent immobilization on gold substrates. As sulfur is integrated as disulfide in a dithiolane ring, no special precautions have to be taken and the handling is much easier than with the more sensitive free thiols. A similar approach was used for tethering phospholipids to ultrasMOOTH gold substrates.^[83]

Figure 9 shows a representative $^1\text{H-NMR}$ spectrum of PB-PEO-LA. Compared to the spectrum of the hydroxyl-terminated PB-PEO (see Figure 7), new signals, which can be assigned to the LA end group, are present. The discrete lipoic acid signals are highlighted in orange. The signal marked in blue corresponds to the methylene group of the PB-PEO backbone adjacent to the newly formed ester group. This hints already towards covalent functionalization of PB-PEO with lipoic acid.

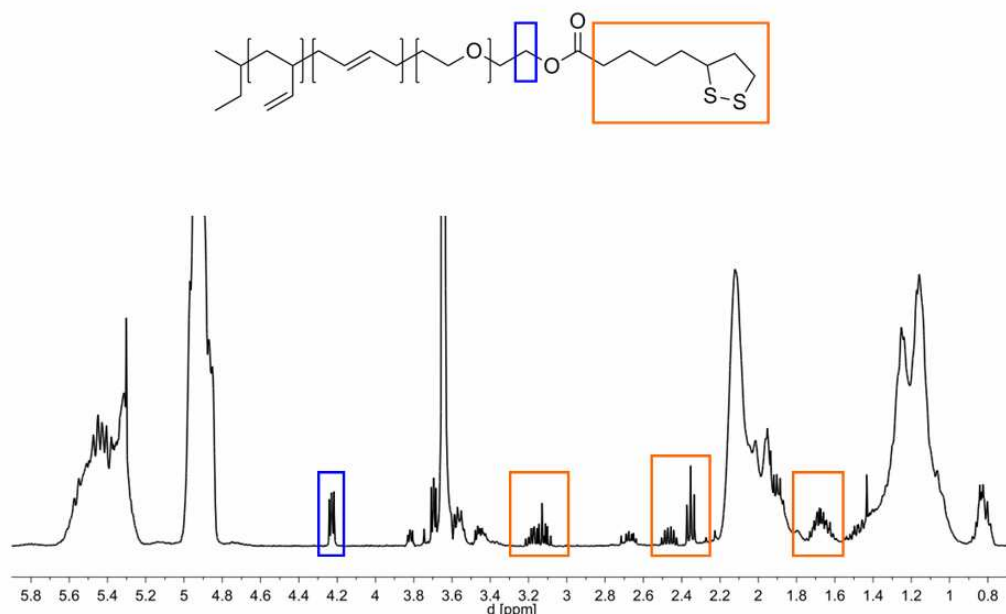


Figure 9. Structure and representative ¹H-NMR spectrum of PB-PEO-LA. The signals from the lipoic acid group are highlighted in orange. The signal at $\delta = 4.22$ ppm, highlighted in blue, corresponds to the methylene group in the backbone, which is adjacent to the newly formed ester group. A detailed peak assignment is presented in the experimental part.

The degree of functionalization was determined by ¹H-NMR. The distinct signal of the terminal protons of the 1,2 isomer at $\delta = 4.85$ - 4.97 ppm served as reference signal. Two-dimensional diffusion ordered spectroscopy (DOSY) was applied to prove covalent linkage of PB-PEO-OH to all functionalization reagents present in the system after the work-up procedure. DOSY is based on a pulse-field gradient spin-echo NMR experiment, in which components experience different diffusion, for instance according to their size or shape. Since this technique is capable to resolve components whose diffusion coefficients differ only by a few percent, it is a valuable tool for identifying individual components in complex mixtures.^[95, 96]

The diffusion coefficients ascribed to distinct signals from the polymer backbone and the end-groups are in the same order of magnitude, indicating the same diffusion behavior for backbone and end-group in the applied field gradient. Thus, end-functionalization of the polymer was successful. Table 1 summarizes the results.

Table 1. Polymer characterization results obtained by GPC, ¹H-NMR, and DOSY.

	N _{PB}	N _{PEO}	M _n [g/mol]	PDI	DF %	δ _{diff} [m ² /s]	
						endgroup	polymer backbone
PB-PEO-OH	52	29	4100	1.07			
PB-PEO-LA	52	29	4300	1.09	85	2.18×10 ⁻¹⁰ 2.16×10 ⁻¹⁰	

N_{PB} and N_{PEO} are the numbers of repeating units, M_n is the number average molecular weight calculated from GPC and ¹H-NMR, PDI is the polydispersity index denoted as M_w/M_n with M_w the weight average molecular weight. DF is the degree of functionalization calculated from ¹H-NMR and δ_{diff} is the diffusion constant obtained from DOSY measurements. The constants are assigned to clearly identified peaks of the end group and the polymer backbone.

3.3 PB-PEO membranes *via* Langmuir transfer techniques

This section is subdivided into three parts, with the first two parts discussing PB-PEO monolayers at the air-water interface, as well as on gold. The third part deals with the characterization of PB-PEO bilayers on gold, including experiments on membrane stability.

3.3.1 Monolayers at the air-water interface

The polymers used for the assembly of solid-supported membranes by Langmuir monolayer transfer were PB-PEO-OH and PB-PEO-LA. First, they were characterized at the air-water interface by surface pressure-area isotherms (π -A).

Representative isotherms recorded at 20 °C on ultrapure water are presented in Figure 10 (A: PB-PEO1-OH, B: PB-PEO1-LA). Unlike low molecular weight amphiphiles, polymers usually do not display clear, well-defined phase transitions.^[97] In order to gain deeper insight in possibly occurring transitions, compressibility moduli $C_s^{-1} = -A(\partial\pi/\partial A)_T$ were calculated, using the first order derivatives of the isotherms.^[98]

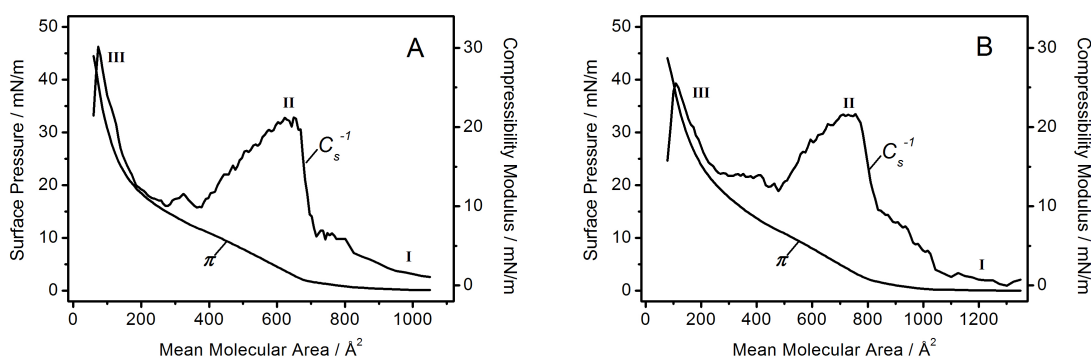


Figure 10. Surface pressure (π) and compressibility modulus C_s^{-1} versus mean molecular area for the PB-PEO-OH and -LA. Part A refers to the OH-terminated and B to the LA-functionalized block copolymer. The isotherms were recorded at $T = 20$ °C. I, II, and III are explained in the text.

At low surface pressures and mean molecular areas $>800 \text{ \AA}^2$ (I) it is assumed that the polymer films are in an expanded state (“pancake” conformation), with the hydrophobic PB blocks lying flat at the air-water interface. The insoluble PB chains are anchored to the interface by water-soluble PEO blocks. The PEO segments are assumed to adopt a flattened conformation at the interface.^[99] In this relaxed state, no difference in the π -A-isotherms of the two polymers was recognizable.

Upon compression, an increase in surface pressure and compressibility modulus of both polymers was measured (II), indicating that the films undergo a transition from a gas-like to a more condensed phase. The maxima of the compressibility moduli of both polymers in this phase were calculated to 21 mN/m, corresponding to liquid expanded regimes.^[100] At smaller mean molecular areas, approximately 380 \AA^2 for the OH-terminated polymer (Figure 10 A) and 485 \AA^2 for the LA-terminated polymer (Figure 10 B), a second phase transition was revealed, as characterized by stagnating C_s^{-1} values. These phase transitions did not show any temperature dependence in the range from 14 to 28 °C, which means that the observed transitions are rather related to conformational rearrangements of the PEO blocks in the subphase than to first order phase transitions. As reported before,^[99] such transitions are assigned to the dissolution of the PEO blocks in the subphase. In this region, the PEO blocks extend into the subphase increasing intermolecular interactions by hydrogen bonding^[99] while the water-insoluble PB blocks serve as an anchor to the interface. This “pseudo-plateau” region becomes more pronounced with increasing PEO block length.^[89, 99, 101] The block copolymers used in this work bear only about 29 PEO units, and therefore the plateau is not clearly visible. However, the first derivative of the isotherms reveals the constant C_s^{-1} region with proceeding partial PEO dehydration.

Further compression led to a slightly less compressible, i.e. liquid-like, phase with similar C_s^{-1} values for both polymers (III). At a mean molecular area of 100 \AA^2 , the compressibility moduli of 30 mN/m for the OH-terminated polymer and 26 mN/m for the LA-terminated polymer, respectively, suggest a qualitatively similar organization pattern for the two polymers. Finally, the surface pressure of both polymers increases steeply until the films collapse at 44 mN/m.

Upon multiple compression-expansion-cycles no hysteresis could be detected. Hence, the isotherms were fully reversible, meaning that the films elastically responded to area changes, and the polymers did not dissolve in the subphase.

Additionally, polymer organization at the air-water interface was investigated by Brewster angle microscopy. The observed monolayers were smooth and did not show any significant features over the whole compression range.

In order to create defect-free bilayers by consecutive Langmuir-Blodgett-/Schaefer film deposition, film stability is crucial. Therefore, the polymer monolayers were compressed to the surface pressure applied in the transfer experiments, which was monitored over time. The compressed monolayers maintained the pressure for longer than 100 min, which was the usual duration for the transfers, indicating high film stability.

3.3.2 Monolayers on gold

Covalent immobilization of sulfur-containing PB-PEO-LA monolayers on ultrasmooth gold substrates was accomplished by Langmuir-Blodgett (LB) transfer, as depicted in Figure 11. A major advantage of the LB transfer technique is the ability to produce highly ordered monolayers without major defects on very large scales compared to the size of its components. It has been applied for the controlled fabrication of highly ordered monomolecular films^[102] and successfully employed for lipid bilayer preparation.^[14, 74, 103]

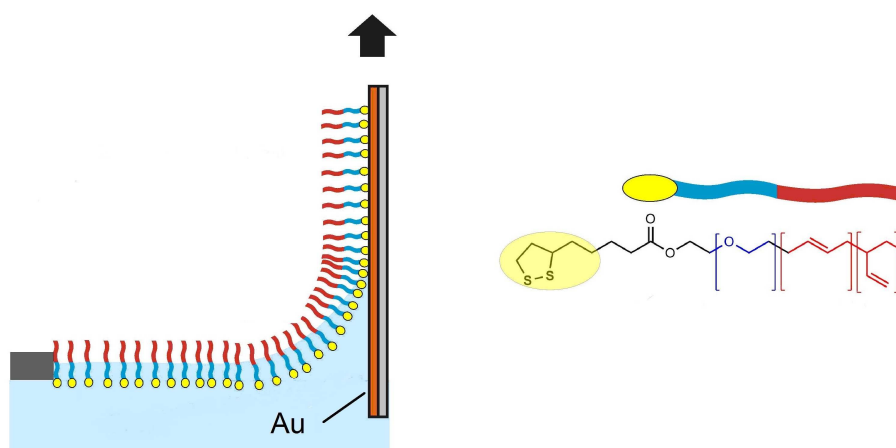


Figure 11. Monolayer transfer: The gold substrate is covalently coated with a monolayer of sulfur-functionalized polymer on the dipper upstroke.

Film depositions were performed at the surface pressure of 35 mN/m, which refers to 80% of the collapse pressure. The corresponding compressibility modulus of the monolayer is 26 mN/m. In this phase, the polymer films assume the most densely packed brush-like order. The transfer ratios are approximately 1.3. Since the transfer ratio is an approximate indication of the transfer quality,^[104] our value moderately deviating from unity is acceptable and suggests successful monolayer transfer.

In order to follow the surface functionalization process, contact angle measurements were carried out on the bare gold surface and the transferred LB film. Contact angles increased from 60° for freshly cleaved gold substrates to at least 90° for the PB-PEO-LA-covered substrates. The contact angle values were obtained from at least five different individual measurements on the same sample. The changes towards higher values stem from the hydrophobic poly(butadiene) blocks facing away from the gold surface.

3.3.2.1 Characterization by ATR-IR

The transfer ratios and the contact angle measurements already hint towards successful immobilization of a sulfur-functionalized PB-PEO monolayer on gold. Furthermore, attenuated total reflection infrared spectroscopy (ATR-IR) was applied to investigate the sample. A blank gold slide was measured as a reference, for which no adsorption bands could be detected.

Spectra of PB-PEO-OH and PB-PEO-LA monolayers on gold were recorded. First, the measurements were performed immediately after transfer. The spectra are shown in Figure 12, with the full triangles referring to the lipoic acid-modified polymer and the full circles to the hydroxy-terminated polymer. The spectra clearly show the CH and CH₂ absorption bands of the polymer backbones.

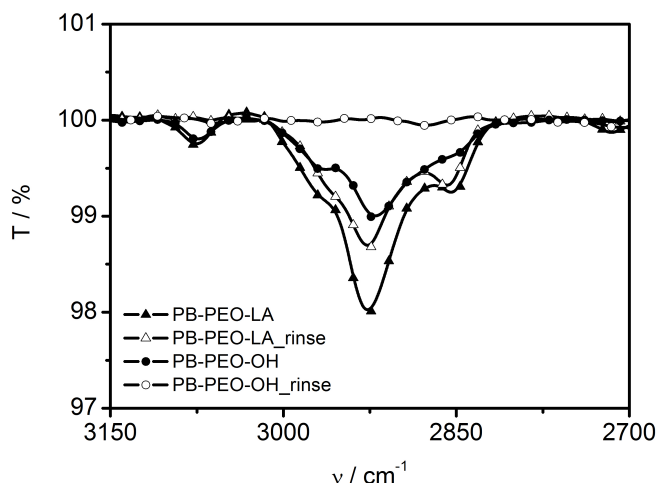


Figure 12. Section of an ATR-IR spectrum of hydroxyl- and lipoic acid-functionalized PB-PEO. Full symbols refer to measurements directly after transfer and the open symbols to measurements upon rinsing.

In order to prove covalent immobilization, the functionalized gold slides were rinsed with good solvents such as THF or CHCl_3 . The non-covalently bound PB-PEO-OH film could be fully removed upon rinsing, since the PB-PEO absorption signals are not present any more (empty circles). In contrast, the covalently immobilized PB-PEO-LA monolayer could not be removed by rinsing with a good solvent, thus the polymer backbone absorption bands are still present (empty triangles).

This experiment confirms covalent functionalization of the polymer with lipoic acid, as well as covalent immobilization of the polymer on the gold substrates.

3.3.2.2 Thickness determination by SPR

Monolayer formation was also characterized by surface plasmon resonance spectroscopy (SPR). This optical method allows for non-invasive thin film characterization and is very sensitive to small changes in adsorbed mass. A major advantage of this technique is the label-free detection. Figure 13 shows the representative angular spectra of a blank gold substrate and of a gold slide functionalized with a PB-PEO-LA monolayer.

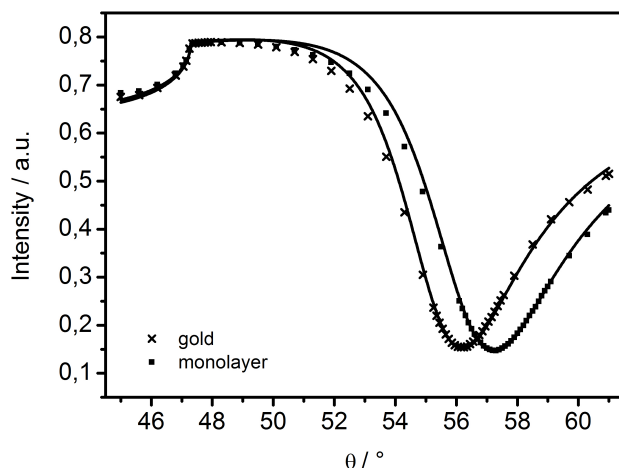


Figure 13. Representative angular SPR spectra measured in ultrapure water showing the shift of the reflectivity minimum from blank gold to the covalently attached PB-PEO-LA monolayer. The solid lines represent the fit.

The shift of the reflectivity minimum from the blank gold (crosses) to the PB-PEO-LA monolayer (full squares) is clearly visible in Figure 13. From Fresnel equation-based calculations, the optical thickness of the monolayer can be obtained. Assuming a refractive index of 1.5 for the block copolymer, a mean geometrical thickness of 6.1 ± 0.4 nm was calculated. The experiments were performed in air as well as in water and data analysis resulted in the same monolayer thickness which means that neither strong swelling nor drying alters the monolayer thickness. We note that SPR yields average mass thicknesses, meaning that it cannot distinguish rough or patchy films from plane layers.

3.3.2.3 Characterization by AFM

To study local film morphology, atomic force microscopy (AFM) was applied for monolayer characterization. Information about homogeneity, structural defects, and roughness of the monolayers can be obtained by this method. AFM measurements were performed in air as well as in aqueous media. A typical height image and cross section of a film in water are presented in Figure 14.

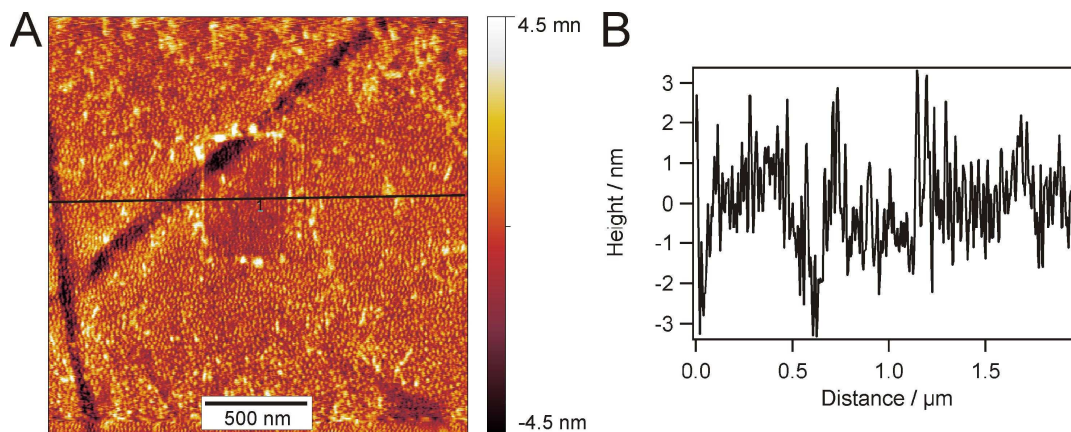


Figure 14. An AFM image (A), recorded in water, and the corresponding cross section (B) of the covalently immobilized monolayer, which was scratched with a hard cantilever. The two dark stripes result from cracks in the epoxy glue due to cutting the slide prior to monolayer transfer.

The film surrounding the square in the centre of the image is completely unperturbed, while the part in the middle was scratched with the AFM-tip. The unaltered film does not show any defects on the micrometer scale. Roughness (root-mean-square) does not exceed 0.5 nm over one square micrometer. We note that there is a small amount of material adsorbed on top of the monolayer which might result from impurities during film transfer. What can be seen as well is the monolayer film exhibiting a very fine structure on the length scale of about 10 nm. This might be due to rearrangements of amphiphilic polymers with chain lengths comparable to the size of these microstructures. This is not surprising since the image was recorded in water so that the hydrophobic poly(butadiene) chains tend to minimize their free energy by rearranging on the surface. However, the freedom to reorient is limited by the covalent attachment to the substrate. AFM scratching experiments show that the monolayer cannot be scratched away, but some loosely bound material is wiped away by the tip. This loose material likely stems from impurities during film transfer. The dark stripes in the image are cracks in the epoxy-glue underneath the gold which result from cutting large substrates into halves.

In addition to the height images, force-distance curves provide information about the mechanical properties. By repeatedly approaching and retracting the cantilever from the surface, adhesive and repulsive forces yielding information about structural details can be obtained. All force measurements were performed with a hydrophilic, bare oxide sharpened silicon nitride AFM tip. Since structures, such as presented in this work, have not been reported so far, there are no literature references concerning the force curves to compare. However, a lot is known about force measurements on supported lipid bilayers.^[105]

For the monolayer one does not expect any characteristic features since the covalently bound polymer chains have only very limited ability to reorganize upon perturbation by the cantilever. Also the hydrophilic cantilever should be repelled from the hydrophobic surface. Exactly this behavior can be seen in Figure 15.

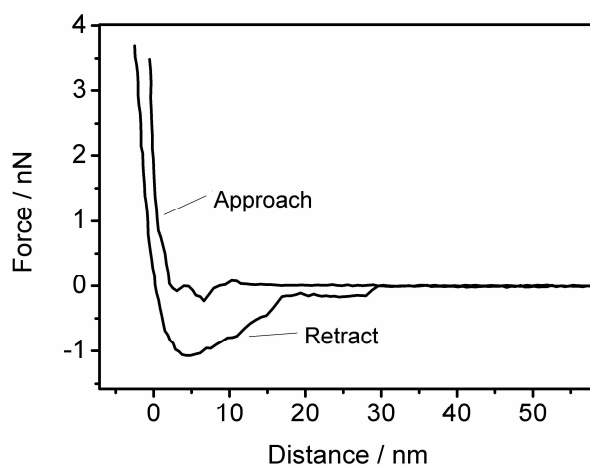


Figure 15. Force-distance curve recorded on the monolayer.

3.3.3 Bilayer membranes on gold

The Langmuir-Schaefer (LS) technique was applied for the transfer of the second monolayer to the PB-PEO-LA-covered substrate in order to obtain a complete bilayer membrane. A substrate, which had been previously coated with a PB-PEO-LA monolayer, was placed horizontally above a PB-PEO-OH Langmuir film and subsequently pressed through the air-water interface. The procedure is depicted in Figure 16. After transfer, the sample was assembled into the measurement cell and kept hydrated throughout surface analysis experiments.

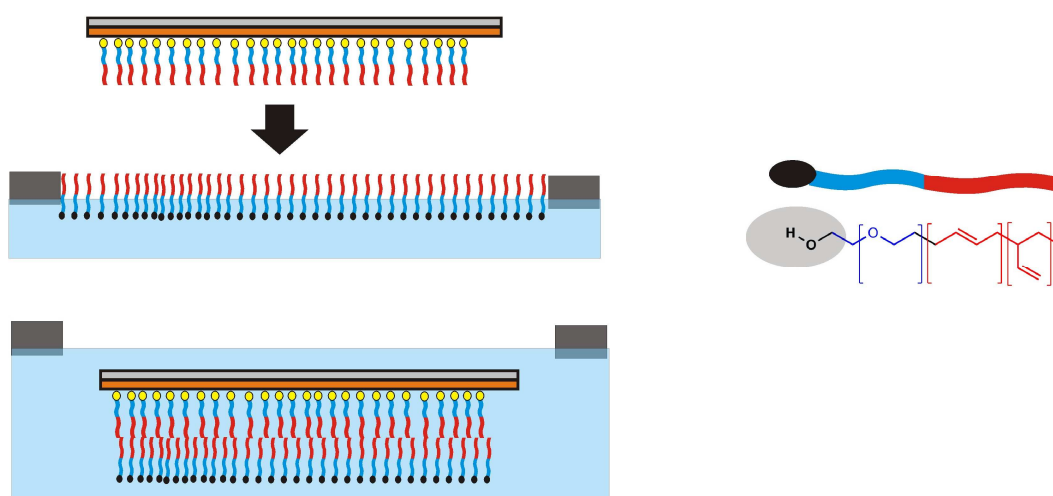


Figure 16. Langmuir-Schaefer transfer of a PB-PEO-OH monolayer to a PB-PEO-LA-covered substrate.

3.3.3.1 Thickness determination by SPR

SPR measurements were performed to investigate the film thickness. The angular scans in Figure 17 show the shift of the reflectivity minimum upon bilayer deposition (open circles) with respect to the blank gold substrate (crosses) and the monolayer (full squares).

From the fit, assuming $n = 1.5$, a mean bilayer thickness of 11.3 ± 0.5 nm was obtained. The doubling of the layer thickness suggests a bilayer structure of the type hydrophilic-hydrophobic-hydrophilic.

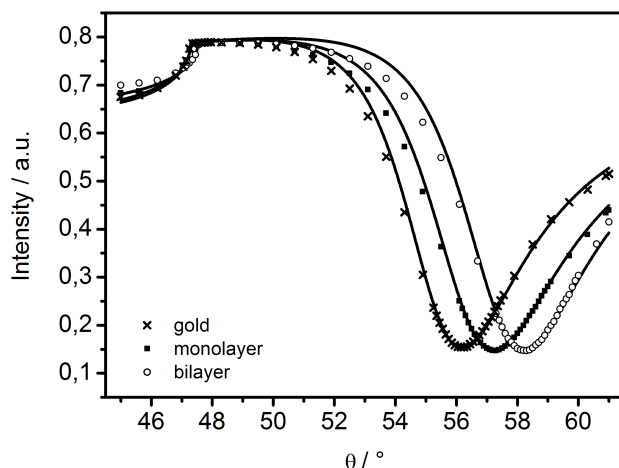


Figure 17. A representative angular SPR spectrum measured in ultrapure water showing the shift of the reflectivity minimum from blank gold to the covalently attached PB-PEO-LA monolayer and to the bilayer. The solid lines represent the fit.

The bilayer thickness is in good agreement with results reported earlier,^[32] where a PB-PEO diblock copolymer was investigated, having similar molecular weight and a comparable hydrophilic to hydrophobic block ratio to the polymer reported here.

The attachment of the second layer to the previously immobilized monolayer is governed mainly by hydrophobic interactions between the poly(butadiene) blocks. The resulting membrane architecture is supposed to be an intermediate structure between completely unperturbed chains, like it is the case with low molecular weight amphiphiles, and an interdigitated structure.^[30, 106] However, minor entanglement of the individual polymer chains in the opposing leaflets is expected due to the rather low molecular weight of the polymer.

3.3.3.2 Characterization by AFM

Homogeneity and roughness of the bilayer membranes were investigated by AFM measurements in water. The height image presented in Figure 18 A shows a uniform and homogeneous film. Sections across the image (Figure 18 B) and statistical analysis proved the root-mean-squared roughness to be approximately 0.35 nm over the area of $1 \mu\text{m}^2$. High uniformity and smoothness were accomplished on large areas up to several hundreds of square micrometers.

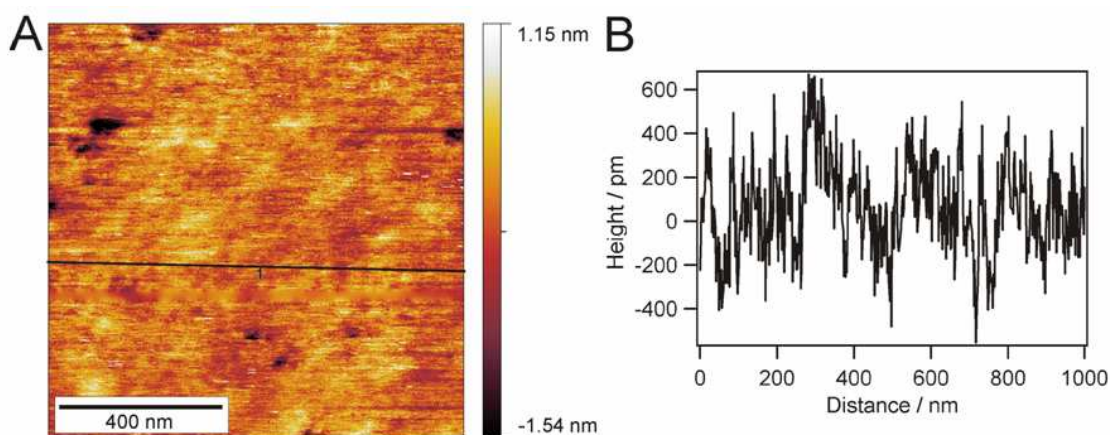


Figure 18. An AFM image of the intact bilayer after Langmuir-Schaefer transfer (A) and the corresponding cross section (B) shows homogenous transfer over an area of $1 \mu\text{m}^2$ with negligible defects.

Force-distance measurements were also performed on the bilayer. In contrast to the monolayer, the bilayer curves showed characteristic features, as presented in Figure 19. The molecules of the top layer tend to re-organize when the tip penetrates the surface. Since there is a lateral pressure within the membrane plane that has to be overcome, a rise of the force curve can be observed at the beginning. At a certain point, the applied force is high enough and the cantilever snaps into the bilayer, which can be seen at a distance below 10 nm where the force temporarily decreases until the lower part of the substrate is reached. This characteristic step has been observed for various supported lipid bilayer systems.^[105] The jump in the force-distance curve appears even after several tens of approach-retract cycles which shows that the polymer chains are mobile enough to cure the small hole made by the cantilever. The width of the jump corresponds to ca. 7 nm, which fits approximately the thickness of an individual

polymer layer. Since the cantilever was not calibrated and the nominal spring constant was taken for scaling, it was not possible to determine absolute force values from these measurements. However, a qualitative statement can be made.

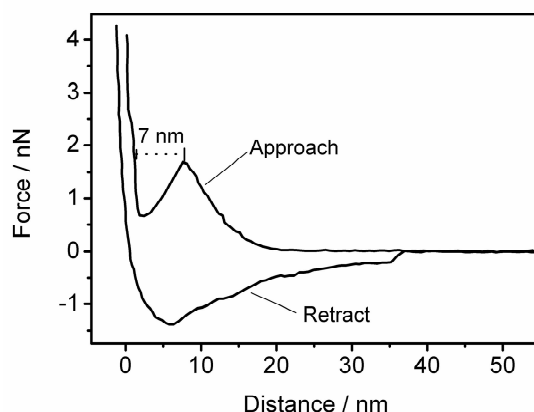


Figure 19. Force–distance curves measured on the bilayer. A distinct jump in the approach curve indicates the penetration of a distinct layer. These measurements were performed using the same cantilever as for the monolayer experiments.

3.3.3.3 Scratching experiments

In order to prove the presence of the second bilayer leaflet, scratching experiments were performed with a hard cantilever, able to remove material from the surface. Figure 20 A clearly shows that the upper layer can be selectively removed from the surface which is not possible by scratching the covalently attached monolayer (see Figure 14). The corresponding section (Figure 20 B) shows the height difference between monolayer and bilayer more evidently. The formation of a well with a homogeneous depth indicates complete removal of the second layer. However, as shown in Figure 20 B, the section depth of the trace is merely 3 nm. The hard cantilever (2 N/m) used for this experiment is not able to map the actual height, but partially penetrates the membrane. Unfortunately it is not possible to exchange the hard tip by a soft one without losing the position of the scratch under the microscope. If a soft cantilever (spring constant 0.32 N/m) is used to image the scratched area, the expected monolayer thickness of approximately 6 nm will be found.

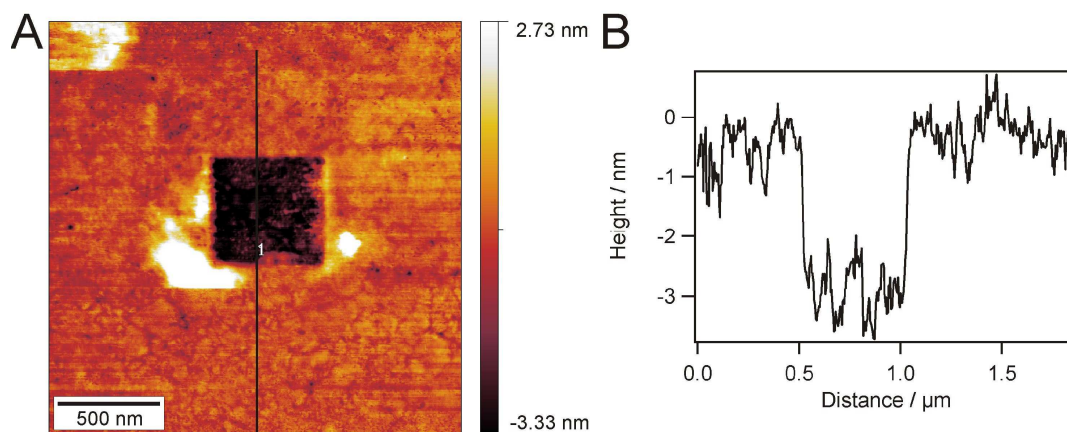


Figure 20. An AFM image after a scratching experiment (A) and a section through A along the indicated line (B).

3.3.3.4 Membrane stability

In order to probe stability, the membrane was thoroughly rinsed with ultrapure water (18.2 MΩ m) in a flow cell and SPR reflectivity changes versus time at the incident angle of 56° were investigated. For that, the membrane was permanently kept under water. This kinetic measurement did not reveal any significant changes in reflectivity upon the harsh rinsing process. Consequently, no loss of mass was detected and the membrane stayed intact during and after the rinsing procedure.

When rinsing was carried out using a good solvent for the PB-PEO diblock, such as THF or CHCl₃, the non-covalently bound upper leaflet of the membrane was washed away and the reflectivity minimum (solid line) returned to the value obtained for a monolayer (full squares), as shown in Figure 21.

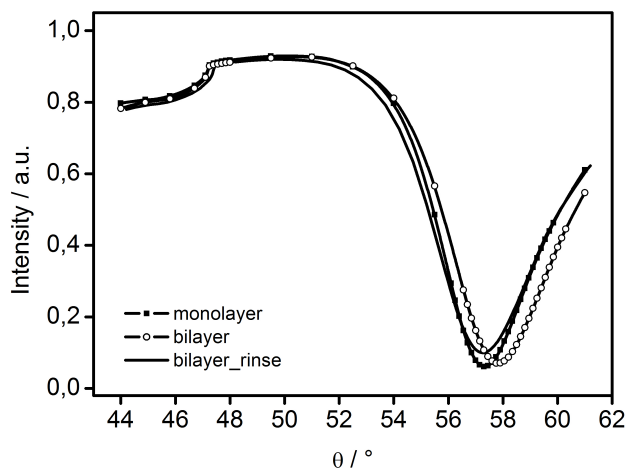


Figure 21. SPR spectrum of a bilayer rinsed with an organic solvent. Upon rinsing, the reflectivity minimum returned to the monolayer value, indicating the removal of the non-covalently bound upper bilayer leaflet.

Furthermore, the membrane stability in air was studied. Therefore the membrane was dried under a stream of nitrogen at room temperature, left dry for two hours, and later rehydrated with ultrapure water. SPR measurements shown in Figure 22 hardly revealed any shift of the reflectivity minimum after drying and rehydration of the membrane (solid line). This indicates that the material adsorbed on the surface was not removed and did not collapse during this experiment.

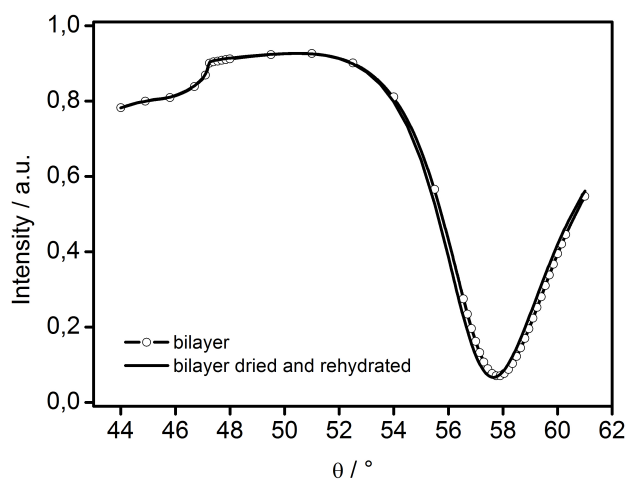


Figure 22. SPR spectrum of a dried bilayer. Since the reflectivity minimum of the dried bilayer hardly shifted compared to a hydrated bilayer, air stability to a certain extent can be postulated.

In addition to the optical measurements, AFM images in Figure 24 A show that the architecture does not change significantly upon drying for short times up to two hours. This unambiguously proves the high stability of the polymer architecture compared to common lipid systems. Usually, supported and tethered lipid bilayers decompose directly when brought into contact with air, whereas solid-supported phospholipid systems resisting a rinsing procedure have already been reported.^[15, 107] So far, the closest attempts towards air-stable supported lipid bilayers employed the stabilising effect of sugars^[108] or polymer layers.^[109] However, these approaches have the drawback of potentially hindering the access of proteins or substrates to the membrane. A recent publication from Deng *et al.*^[110] describes an air-stable membrane tethered *via* cholesterol anchor groups which remains fluid after several cycles of drying (2 h) and rehydration.

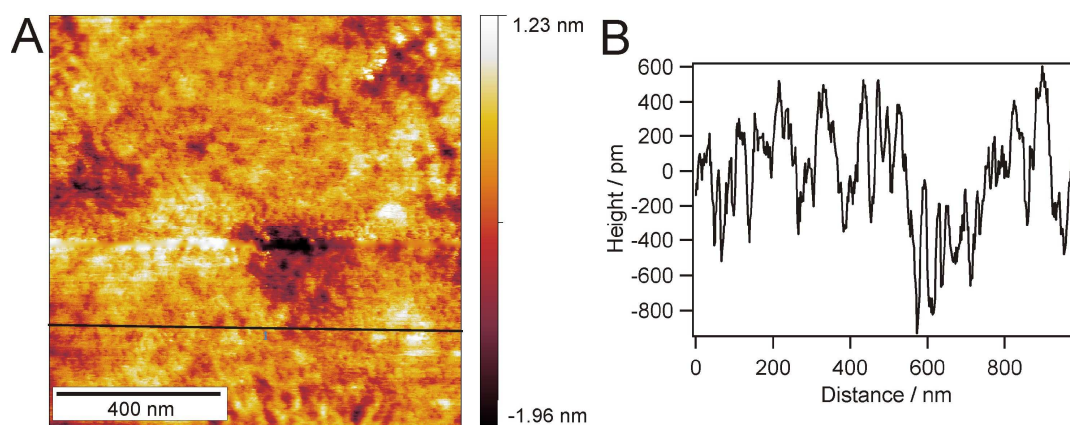


Figure 23. AFM image and cross-section of bilayer dried for 2 h.

Drying of our polymeric bilayer for longer than 12 h led to a significant change in morphology, as seen in Figure 24 A. Objects of 10-20 nm in height were present everywhere on the surface, which suggests the disassembly of the architecture. Most likely the polymer chains reassembled into micellar structures in order to minimize their energy. This assumption is supported by the measured height of these objects, which is in the dimension of a complete bilayer. Consequently, it can be concluded, that water is still necessary to stabilize the bilayer structure on the long term scale.

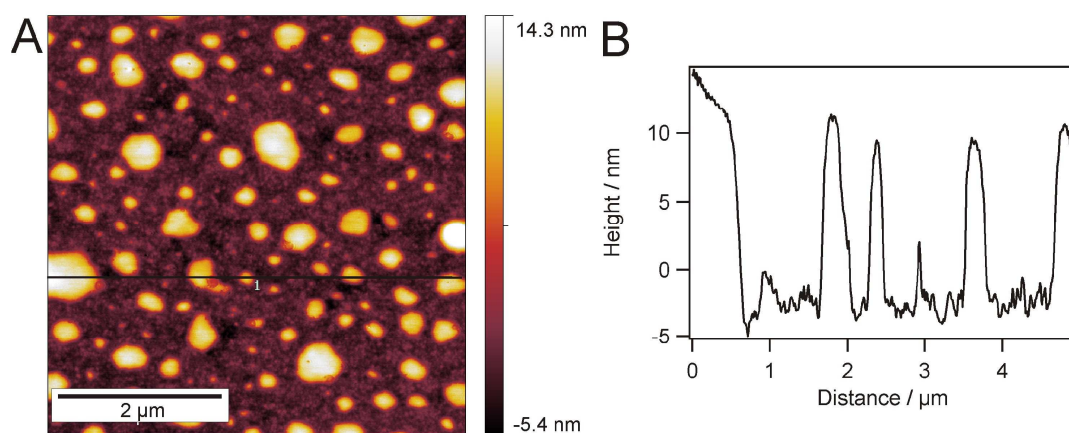


Figure 24. AFM image and cross-section of bilayer dried for 12 h.

An explanation for this observation could be insufficient coupling between the two individual polymer layers. This suggests a rather low entanglement of the polymer chains. This is in accordance with the literature for the particular chain length of the polymers used here.^[111] Probably, membrane stability against drying can be increased by using longer block copolymers. In this case, a higher degree of interdigitation between the two opposing leaflets, thus enhanced membrane stabilization, is expected. On the other hand, a higher degree of entanglement and an increase in thickness, due to the use of longer polymers, might minimize fluidity and hinder incorporation of proteins. This is disadvantageous for a prospective purpose of this membrane system, i.e. serving as matrix for protein incorporation.

3.4 Membranes *via* spreading of PB-PEO superstructures

In this section, supported planar PB-PEO membranes were produced by spreading of pre-organized polymer superstructures. First, the formation and the characterization of these superstructures will be discussed. Afterwards, two preparation pathways differing regarding substrates and polymers, as well as regarding the interactions between them, will be presented and discussed.

3.4.1 Formation and characterization of PB-PEO superstructures

The PB-PEO polymers used for membrane built-up contain 52 PB and 29 PEO repeating units. The hydrophilic weight fraction of these polymers is 0.31, which corresponds to a hydrophilic volume fraction of 0.26. According to the morphology diagram from Jain and Bates^[112] mainly bilayer morphologies (vesicles) should form upon self-assembly in aqueous media.

Common preparation methods were applied to prepare PB-PEO self-assemblies, i.e. electroformation, film rehydration (swelling), and solvent displacement techniques. Optical, fluorescence, and transmission electron microscopy (TEM), as well as dynamic light scattering (DLS) were used to investigate the resulting polymer superstructures.

The intention of these experiments was to develop a protocol for reproducible self-assembly, tailor-made for spreading experiments presented in the sections 3.4.2 and 3.4.3. One aim for instance, was the identification of a method that yields the highest aggregate concentration possible. By dilution, one batch can be used for several experiments, which improves reproducibility. The protocol should also ensure maximal concentration control. Furthermore, the required preparation time was also a decisive factor. Methods using solvents are probably unfavorable due to solvent traces that might disturb experiments with sensitive biological moieties. Nevertheless, as explained in detail below, the self-assembly of the particular polymers used herein, occurred faster applying solvent-aided methods compared to solvent-free methods.

In the following, the results of PB-PEO self-assembly by solvent-free and solvent-aided methods, respectively, will be presented and discussed, in particular focusing on the fulfillment of the above criteria.

3.4.1.1 Solvent-free preparation

By electroformation, giant unilamellar PB-PEO-OH polymersomes could be produced. The diameters of the vesicles reached several tens of micrometers, as seen in the optical micrograph shown in Figure 25. However, the yield was very low, which is likely due to the employed experimental setup and conditions, i.e. dip-coating of platinum wires with polymer solution. The polymer films produced this way were rather thick and inhomogeneous, which might have impeded vesicle formation to a certain extent. Additionally, it was very difficult to detach the vesicles from the electrodes, even at low frequencies, which usually favor detachment.^[113] Consequently, the aliquots taken from the electroformation cell contained only a very small amount of vesicles.

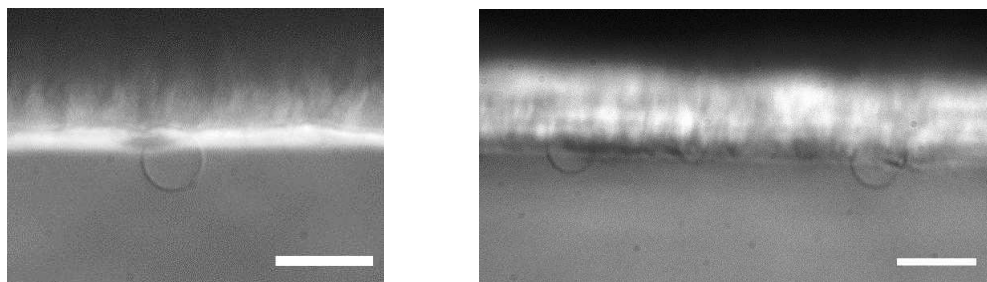


Figure 25. Optical micrograph of giant PB-PEO-OH vesicles. The images were taken in the phase-contrast mode. The scale bars correspond to 40 μm .

Besides electroformation, film rehydration was applied as well to prepare vesicles. PB-PEO-OH and PB-PEO-LA were self-assembled by film rehydration, using either bidistilled water, PBS (phosphate buffered saline; $\text{pH} = 7.4$), or sucrose (0.2 M) as rehydration medium. Both polymers formed superstructures by film rehydration in all aqueous media used.

Figure 26 shows a representative optical micrograph of PB-PEO-OH vesicles. For the presented experiment, sucrose was used as rehydration medium. Some vesicles are highlighted for better visibility.

Regardless the aqueous medium, rehydrations yielded approximately the same results concerning vesicle size. Vesicle diameters ranged from several micrometers up to several tens of micrometers.

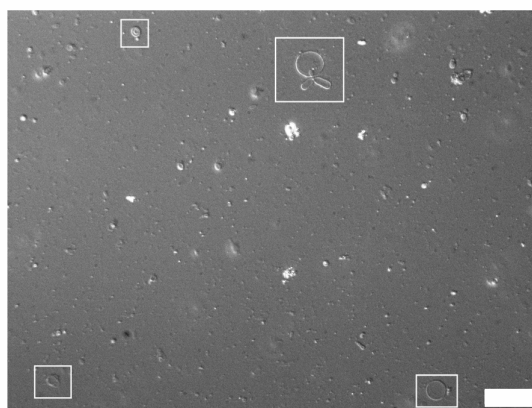


Figure 26. Optical micrograph of PB-PEO-OH giant vesicles prepared by rehydration in sucrose. Among the highlighted objects, not only spherical and unilamellar, but also oblong or multilamellar vesicles can be detected. The scale bar corresponds to 40 μm .

Thus, vesicle sizes were in the same range as obtained by electroformation. However, by film rehydration a higher amount of self-assemblies could be produced. In contrast to electroformation, rehydration yielded vesicles that were more inhomogeneous concerning size, lamellarity, and morphology. Besides perfectly spherical vesicles also deformed elongated morphologies could be observed.

To better visualize these observations, the samples were stained with fluorescent dyes (BodiPy 505/515; 2.5 μM ; Invitrogen, Switzerland) and investigated by fluorescence microscopy. The dyes were either added before, or after vesicle formation. Staining was successful in both cases. Figure 27 shows some dye labeled giant vesicles. The previously mentioned differences such as lamellarity or variety in morphology can be clearly distinguished. For instance a multilamellar aggregate can be seen in the upper part of the image. This aggregate shows another interesting feature as well: a little spherule on the left part of the aggregate. This is reminiscent of exocytosis or budding, processes also known from lipids^[114, 115] or similar block copolymers.^[58] The vesicle visible in the lower right corner might also undergo a morphological change such as an exo- or endocytosis-like process. Probably it is also undergoing a fusion or fission process like it was reported for other block copolymers.^[116-118]

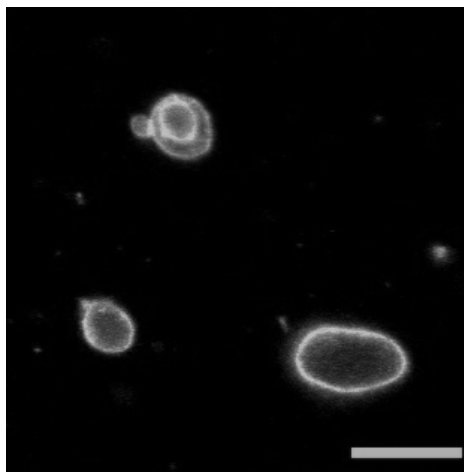


Figure 27. Stained giant vesicles visualized by fluorescence microscopy. The scale bar corresponds to 10 μm .

In conclusion, electroformation as well as film rehydration yielded giant PB-PEO vesicles. However, in particular concerning electroformation, the yield was extremely low. In contrast, by film rehydration larger amounts of vesicles could be obtained, though in a very irreproducible way. In most of the experiments, the polymer films either remained attached to the flask wall, or the polymer partly precipitated. This refers in particular to PB-PEO-OH. Several treatments, such as rehydration under rotation or shaking at elevated temperatures (37 to 60 °C) in an incubator, were applied. Since the glass transition temperature of the polymer is rather high (close to 0 °C),^[119] particularly heating was supposed to promote self-assembly by increasing fluidity and mobility of the polymer. This treatment had a more pronounced effect on PB-PEO-LA, than on PB-PEO-OH. In the case of PB-PEO-LA, the aqueous phase became slightly turbid within approximately one week in the incubator at elevated temperatures. In contrast, PB-PEO-OH self-assembly hardly proceeded within several weeks by applying the same conditions. Long-term treatments at elevated temperatures necessary for the self-assembly of a PB-based block copolymer have been also reported in literature.^[120]

Apparently the quality of the film strongly influenced the formation of vesicles. Since the films were not always of exactly the same quality, i.e. homogenous and thin, self-assembly did not proceed perfectly reproducibly either.

3.4.1.2 Solvent displacement techniques

Since the self-assembly by solvent-free techniques proceeded in an irreproducible way and fairly slowly, solvent displacement techniques were also used to prepare polymersomes. Furthermore, solvent displacement techniques are known to produce vesicles in large numbers.^[21, 121]

PB-PEO polymers were dissolved in either water immiscible CHCl_3 or water miscible THF. The aqueous phase, bidistilled water or buffer, was added drop-wise under vigorous stirring. Further, the organic solvent was evaporated under gentle stirring at ambient conditions within 3-4 days. Merely the evaporation of CHCl_3 was also performed under reduced pressure, as explained below.

Self-assembly of PB-PEO-OH in water upon CHCl_3 removal

The optical micrograph in Figure 28 gives an overview of the shape variety and the complexity of PB-PEO-OH self-assembly in bidistilled water. The morphological variety, already known from the rehydration experiments (see section 3.4.1.1), is also present here. Apart from merely spherical, also oblong or kidney-shaped structures can be seen in Figure 28. Such structures are known from other amphiphiles such as lipids^[114, 115] and have been also reported for a similar block copolymers.^[58, 113]

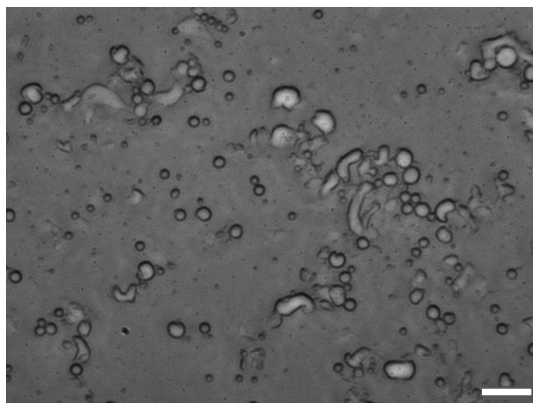


Figure 28. Bright field optical micrograph showing a variety of PB-PEO-OH superstructures prepared in water by chloroform displacement. The scale bar corresponds to 20 μm .

Further, the samples were extruded through smaller pore sizes (0.2 μm) and investigated by DLS. The analysis revealed a bimodal distribution. Larger assemblies with hydrodynamic radii $r_h = 110$ nm and smaller ones with $r_h = 10$ -15 nm could be detected. The polydispersity of the samples was below 0.2. It has to be stated, that even after extrusion, the samples were still rather disperse, as it is confirmed by TEM and discussed in detail below.

In order to gain deeper insight into size and shape of the assemblies, TEM was performed. Representative images are shown in Figure 29 A-C. In Figure 29 A an overview image covering an area of approximately $100 \mu\text{m}^2$ is depicted. Objects can be identified, which occupy roughly spherical areas with diameters of 150 nm up to more than 500 nm. These objects possess a sub-structure consisting of “arranged”, partly bent rod-like structures, which can be seen in detail in Figure 29 B. The average diameter of the rods is 30 nm. Apart from the rod-like structures, also spherical morphologies with varying size could be detected, as depicted in Figure 29 C. The radii of the spherical structures range from 5 nm to 160 nm. As mentioned above, DLS measurements gave already a hint towards such a multimodal size distribution.

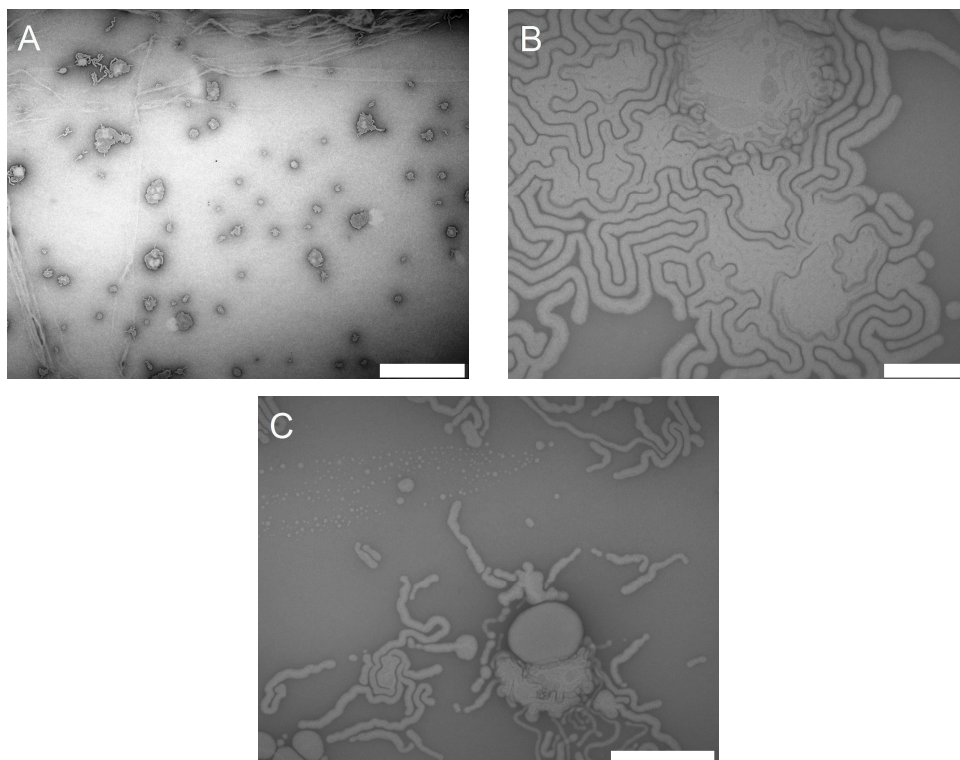


Figure 29. PB-PEO-OH aggregates, prepared in bidistilled water by chloroform displacement, visualized by TEM. The scale bars correspond to 2 μm (A), 200 nm (B), and 500 nm (C).

Further, interesting structures consisting of a rod-like and a spherical part can also be detected in Figure 29 C. Among all morphologies observed, however, the typical signs of hollow structures, i.e. dark fringes at the walls, are missing. Instead, light intensity, corresponding to the electron density, is uniformly distributed throughout the whole aggregates. This suggests a flat, lamellar-like structure.^[31, 63] Probably the extrusion process or the conditions during the TEM measurements altered the previously observed hollow structures of the aggregates (see Figure 28).

It might still be questionable whether the rod-like structures are worm-like micelles or flat, lamellar assemblies. Worm-like micelles are usually known to be very long, up to several micrometers, and thus very often entangled. None of these characteristics can be recognized in Figure 29, suggesting that the PB-PEO-OH assemblies shown are not worm-like micelles. Similar structures to the ones presented in Figure 29, even though referring to different polymers, were reported in the literature.^[31, 67] More precisely, depending on the water content and on the time-dependent evolution, it was possible to obtain also shorter and thicker rod-like aggregates. These short rods further undergo transitions to lamellae. When apparent as hybrid morphologies consisting of a rod-like and a spherical part, these structures were referred to as “paddle-shaped” lamellae, and considered as intermediate state to vesicle formation.^[67]

Theoretically, the hydrophilic fraction of PB-PEO-OH is 0.26 and the final concentration of polymer aggregates in water is $>0.1\%$, which should result in dispersed vesicles.^[112] However, as explained in detail in the introduction, the observation of intermediate structures is due to the preparation conditions employed, which might lead to kinetically frozen structures. In particular, methods aided by organic solvents are known to favor kinetically frozen structures.^[60] In this case, the transition of short rods to lamellae is a fast step in the formation kinetics of vesicles, whereas the second step, the closure of a lamella to a vesicle, is slow, thus the rate-determining step.^[67] Apparently, the chosen preparation conditions “froze” the rod-like and paddle-shaped lamellar morphologies. Hence, the anyway slow closure step to vesicles could not be achieved with the employed preparation conditions.

In summary, this method yielded indeed larger amounts of polymer self-assemblies compared to the solvent-free methods. As it was stated at the beginning of the chapter, a high vesicle concentration was desired. However, other decisive parameters, i.e. preparation time and concentration control, could not be fully achieved by this method. CHCl_3 evaporation proceeded very slowly, since it had to diffuse through the water phase. Even under stirring, evaporation could not be notably accelerated. Hence, the solvent was removed under reduced pressure. Hereby a considerable amount of water evaporated as well, even leading to partial precipitation of the polymer. Consequently, the final concentration could not be determined accurately.

In order to improve the procedure, PB-PEO self-assembly was also probed using a water-miscible solvent. Since the organic solvent should also be a good solvent for the whole block copolymer, THF was chosen. In the following sections PB-PEO self-assembly in aqueous media by THF evaporation will be discussed.

Self-assembly of PB-PEO-OH and PB-PEO-LA upon THF removal

Within this series, the suspensions were directly extruded through 0.2 μm pore-sized membranes and investigated by DLS and TEM.

First, PB-PEO-OH assemblies prepared in PBS will be discussed. DLS of aggregates prepared in PBS revealed mainly one population with hydrodynamic radii $r_h = 75$ nm. Only at larger scattering angles (above 120°) a peak-tailing towards smaller radii could be detected. Even though the peak was not resolved, it is probable that a population of smaller aggregates formed as well. The PDI was below 0.1.

The samples were further characterized by TEM. In Figure 30, micrographs of PB-PEO-OH assemblies prepared in PBS are shown. The aggregates cover roughly distinct areas of the TEM grid, similar to the TEM images of PB-PEO-OH self-assemblies prepared upon CHCl_3 evaporation (see Figure 29 A). A magnification, as shown in Figure 30 B, reveals once more a rod-like lamellar sub-structure of the polymer domains. The rod diameters range approximately from 20 nm to 50 nm, which is in agreement with the results shown in Figure 29. Once more, bulbs approximately 110 nm in diameter, mainly located at the end of the rods, can be detected. In accordance with the discussion and interpretation of PB-PEO-OH self-assembly in water upon CHCl_3 evaporation, these structures are interpreted as paddle-shaped

lamellae as well. Actually, these paddle-shaped morphologies with spherical end caps are even more pronounced than before. Such end caps were reported to be energetically more favorable.^[63, 112] Due to the dimensions of the rods and the spherical end caps, it is unlikely that micelles were observed.

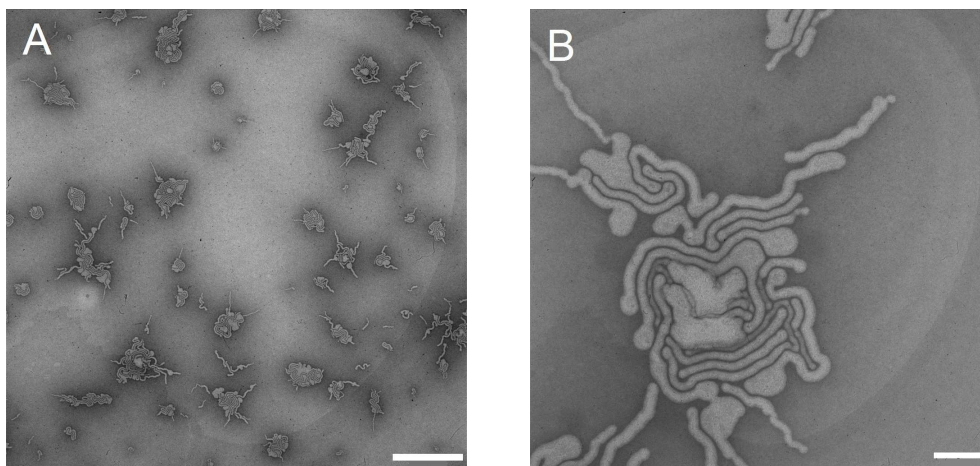


Figure 30. Transmission electron micrographs of PB-PEO-OH assemblies prepared in PBS upon THF evaporation. The scale bars correspond to 2 μm (A) and 200 nm (B), respectively.

Next, self-assembly of PB-PEO-OH in bidistilled water upon THF evaporation is discussed. In contrast to self-assembly in PBS, DLS investigations clearly revealed two distinct populations. The hydrodynamic radii of the larger assemblies ranged from 85 nm to 105 nm, whereas the radii of the smaller population ranged from 15 nm to 35 nm. TEM analysis revealed that the smaller population is predominant, as depicted in Figure 31. Besides small spherical aggregates, rods and oblong structures can be also identified in the magnification shown in Figure 31 B. The spherical objects strongly differ in size, whereas the main population consists of small spherical structures with an average diameter of about 30 nm. The rods are slightly thicker than the spheres and have diameters of ca. 45 nm. This is almost consistent with the previous results, i.e. self-assembly of PB-PEO-OH in water upon CHCl_3 evaporation and in PBS upon THF evaporation. However, the amount of the small spherical aggregates, this time presumably micelles, is significantly higher compared to the previous experiments.

A comparison of PB-PEO-OH self-assembly regarding the employed conditions does not reveal a clear trend, neither concerning the size nor the morphology of the formed superstructures. Aggregation in bidistilled water upon CHCl_3 displacement and aggregation in PBS upon THF displacement mainly yielded oblong structures that can be assigned to rod-like lamellae. Merely self-assembly in bidistilled water upon THF evaporation resulted in a predominant population of spherical self-assemblies, probably micelles. However, it is questionable whether these spherical structures are really micelles, or hollow assemblies (probably small vesicles). Since their diameters are about 30 nm, they are actually too large for micelles consisting of the polymers used herein. According to the results presented in section 3.3, micelle diameters of 10-15 nm were expected. In this case, however, it is by factor of about 2.5 larger, which could hint towards hollow structures.

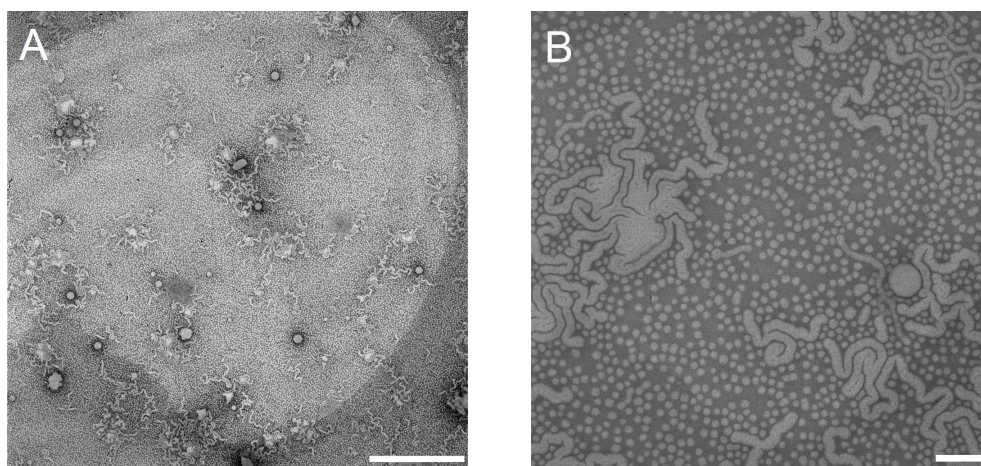


Figure 31. Transmission electron micrographs of PB-PEO-OH self-assemblies prepared in bidistilled water upon THF evaporation. The scale bars correspond to 2 μm (A) and 200 nm (B), respectively.

In the following, PB-PEO-LA self-assembly in bidistilled water upon THF evaporation will be discussed. Preparation in PBS was also probed, however, in this case polymer precipitation was observed several minutes after PBS addition.

The self-assembly of PB-PEO-LA in bidistilled water yielded mainly one population with $r_h = 90\text{-}110$ nm and dispersities below 0.1, as analyzed by DLS. The visualization by TEM revealed interesting morphological features. Representative TEM images of two different batches, prepared following the same protocol, are shown in Figure 32 A, B and Figure 32 C. In Figure 32 A, some roughly spherical objects ranging from 90 to

230 nm in diameter, as well as higher aggregates of these objects can be identified. The biggest aggregates reach diameters of about 1 μm . Contrary to the rather loosely assembled rod-like sub-structures of PB-PEO-OH aggregates discussed before (see Figure 29 A and Figure 30 A), here the shape of the assemblies is rather spherical and more homogeneous. By having a closer look on the magnification shown in Figure 32 B, a lamellar-like sub-structure in the interior of the spherical assemblies can be detected. Additionally, groove-like features can be detected in some of the assemblies (see also Figure 32 A and C). They might be a hint for partially cross-linked and broken assemblies, probably due to the electron beam. However, the cross-linking process would have to proceed very fast, since no changes of the assemblies were detected during the TEM measurements. Furthermore, these features were observed very rarely and should be considered as a general phenomenon.

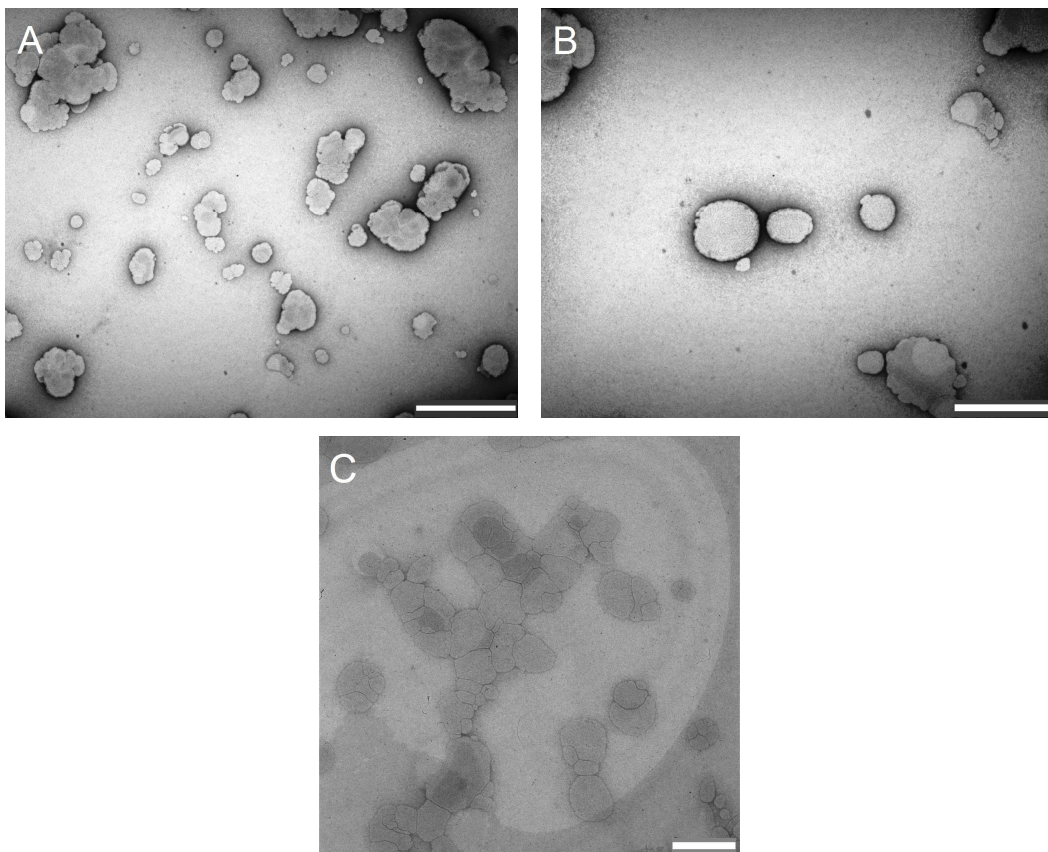


Figure 32. Transmission electron micrographs of PB-PEO-LA self-assemblies prepared in bidistilled water. Scale bars correspond to 1 μm (A) and 500 nm (B, C), respectively.

Further characteristic morphological features of PB-PEO-LA self-assemblies in bidistilled water are shown in Figure 33. In contrast to the structures shown in Figure 32 (B and C), this time, the aggregates do not display a defined, uniform shape. Partly, rod-like structures are present. Interestingly, almost every rod seems to have a spherical-like end cap. This might be the energetically most favorable state for these structures.^[63, 112] Such structures have also been reported by Jain and Bates and referred to as “octopi-like” structures.^[63] These structures were interpreted as flat bilayers with cylindrical micelles protruding along the edges. The cylindrical structures in Figure 33 are about 27 nm in diameter, hence slightly thicker than expected. According to the thickness measurements of solid-supported PB-PEO membranes by SPR and AFM (see section 3.3), thickness of a bilayer is about 11-12 nm. Hence, micellar PB-PEO aggregates, be it spherical or cylindrical, should have as well a thickness of ca. 11-12 nm. It was also shown in literature that the wall thickness of polymer vesicles is in agreement with the diameter of worm-like or spherical micelles.^[113] Therefore, it is questionable whether the rod-like structural elements are really cylindrical micelles.

Another difference to the literature report is the shape of the middle parts.^[63] In the report, the core part was almost perfectly spherical. However, in our case, the middle parts are mainly deformed.

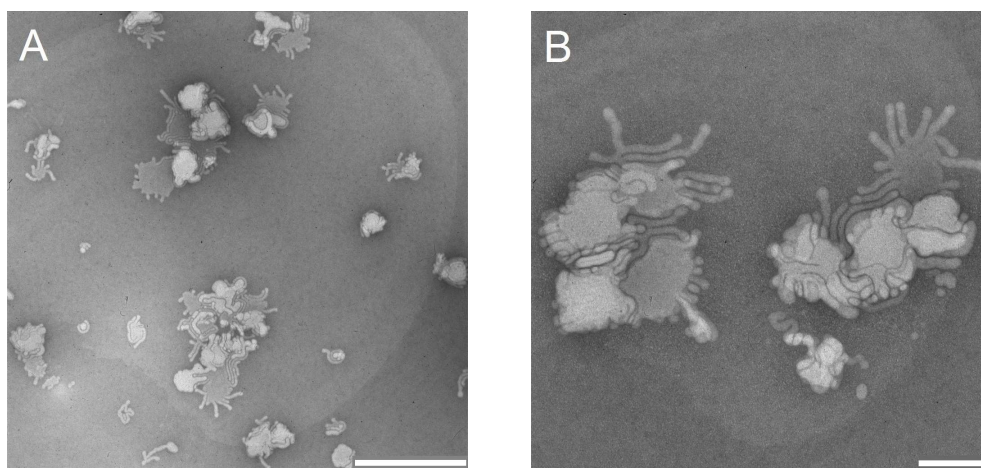


Figure 33. Transmission electron micrographs of PB-PEO-LA self-assemblies prepared in bidistilled water. Scale bars correspond to 1 μm (A) and 200 nm (B), respectively.

As already mentioned before, the short rods can be regarded as a preliminary stage to vesicles, *via* lamellar intermediate structures. Apparently this time, the aggregates were investigated at a later stage. In Figure 33 the predominant fraction are not the short rods, but structures resembling bent lamellae. They are also intermediate, kinetically frozen structures, however, kinetically a step closer to the formation of vesicles. Interestingly, the preparation protocol for PB-PEO-OH and PB-PEO-LA self-assembly was exactly the same, but only in the case of PB-PEO-LA the bent lamellae morphology was that pronounced. Probably this effect derives from the different end-groups. It is known from the literature that different end-groups affect the self-assembly behavior.^[122]

These experiments show that the preparation and characterization of controlled and reproducible PB-PEO superstructures is very challenging. Self-assembly performed under the discussed conditions yielded kinetically trapped structures which adopt a wide variety of different morphologies.

Analytics performed so far, only allowed for a qualitative description. The characterization tools used, i.e. light scattering and TEM might not be sufficient for a thorough investigation of these samples. Additionally, TEM is not an *in situ* technique, thus, the images might not reflect the situation in solution. Due to sample preparation, e.g. drying or interactions with the grid, and measurement conditions such as ultra high vacuum and a strong electron beam, the morphology of the assemblies might have been altered.

Preservation of the aggregation state in solution with e.g. quantitative cross-linking should enable artifact-free TEM imaging. Alternatively, systematic characterization by cryo-TEM might be useful to characterize the samples in their native state.

Furthermore, despite repeated extrusion cycles, the aggregates are still polydisperse regarding their size and shape. Nevertheless, the shape polydispersity was not discrete enough to reliably characterize different assemblies by for instance static light scattering.

In summary, only the aggregate preparation by THF displacement yielded structures with a reproducibility acceptable for the further spreading experiments.

Furthermore, with these conditions the highest concentration was achieved (about 0.2 mM). Since almost no precipitation occurred during THF evaporation, it can be assumed that this theoretical concentration is maintained throughout the superstructure preparation. Moreover, the superstructures were formed in a comparatively short preparation time of about 3-4 days. Consequently, this was the preparation protocol of choice for producing stable polymer assemblies with good concentration control for the spreading experiments discussed in detail in the next sections.

3.4.2 Aggregate spreading by non-covalent interactions

A pathway to solid-supported membranes by spreading comprised the deposition of PB-PEO-OH superstructures on oxygen plasma-treated glass substrates. After the plasma treatment, the glass surface is highly hydrophilic, leading to complete wetting upon addition of ultrapure water. The plasma-treated glass substrates were incubated with PB-PEO-OH dispersions containing sodium chloride (1.5 M). Compared to experiments where purely aqueous polymer dispersions were used, the polymer assemblies showed a higher tendency to spread. Since the polymer assemblies were prepared in pure water, the addition of salt resulted in a concentration gradient between the intra- and extraventricular space. The osmotic pressure leads to a decrease in the vesicle volume, while the membrane surface remains constant. This exerts a mechanical strain on the membrane surface, which destabilizes the polymer assemblies and facilitates their spreading (see Figure 34).

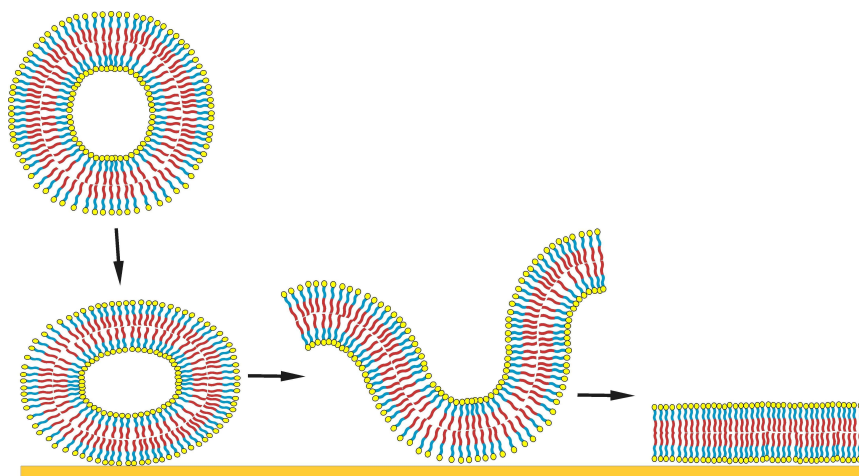


Figure 34. Vesicle spreading of PB-PEO superstructures on a solid support.

The result after incubation is shown in Figure 35. Remarkably, only very few non-ruptured polymer aggregates can be distinguished in the AFM height image. Once attached to the surface, the assemblies spread to form bilayer or multilayer patches. Nevertheless, the substrate was not fully covered by the polymer.

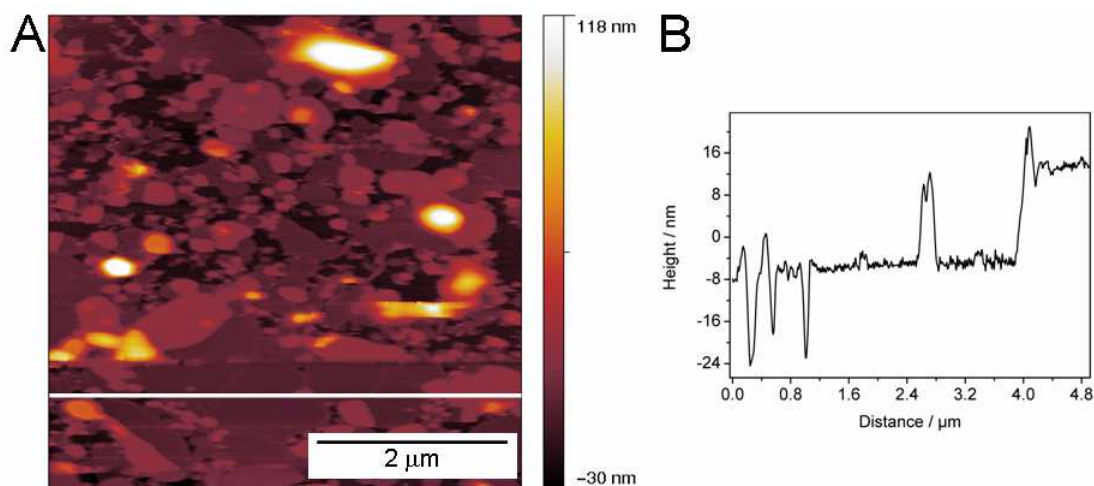


Figure 35. AFM height image of fused PB-PEO-OH assemblies on glass (A) and cross-section (B). The measurements were performed in NaCl solution (1.5 M).

The measured height steps of about 15-17 nm can be attributed to a single bilayer. It is slightly thicker compared to the bilayers prepared by sequential Langmuir film transfers on gold supports.^[123] As described in section 3.3.3, the thickness of such membranes was 11-12 nm. The thickness differences will be discussed in the following section.

In summary, spreading of PB-PEO-OH self-assemblies yields already a high surface coverage. However, non-covalent interactions between the hydrophilic glass surface and the hydroxyl-terminated polymer are not strong enough to induce complete fusion of the polymer aggregates. In order to increase the driving force of the fusion process, an approach utilizing covalent interactions between the polymer assemblies and the substrate was investigated.

3.4.3 Aggregate spreading by covalent interactions

In this section, PB-PEO-LA assemblies were spread on gold *via* covalent interactions. The spreading process was monitored by AFM and electrochemical impedance spectroscopy (EIS), as discussed below.

3.4.3.1 Characterization by AFM

First, a dispersion containing PB-PEO-LA assemblies in water was directly added to freshly cleaved gold substrates, without any further treatment. The AFM image in Figure 36 A displays that already a significant area of the surface is covered with the polymer, which indicates that most of the polymer assemblies directly spread on the gold surface. Single round discs, up to 200 nm in radius, can be identified, which might correspond to single fused polymer vesicles. This could be observed best, when the dispersions were diluted to 0.02-0.1 M. Then, the vesicles individually fused on gold. Unlike reported for lipid vesicles,^[124] direct contact between adjacent attached polymer assemblies is apparently not required to induce the spreading process.

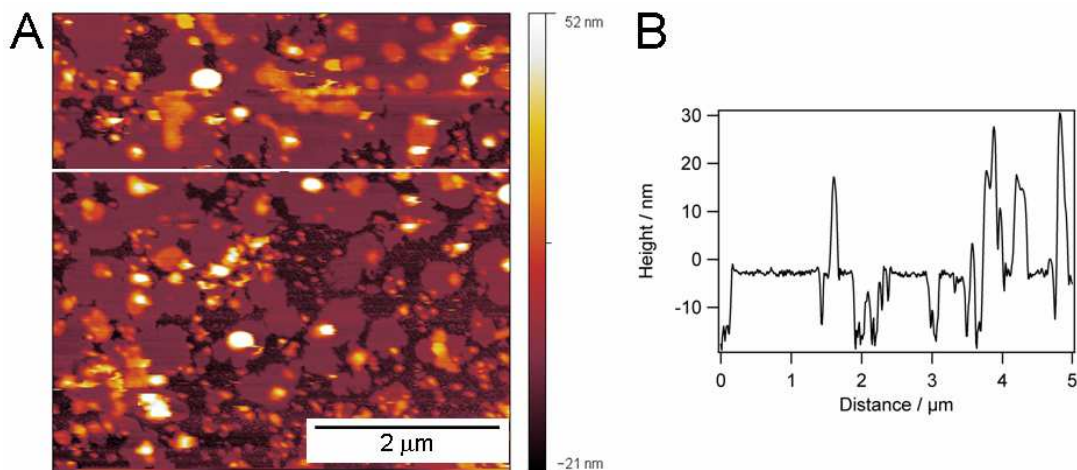


Figure 36. AFM height image of fused PB-PEO-LA assemblies on gold (A) and the corresponding height profile along the indicated line (B). The measurements were performed in water.

Apart from single round patches, also large multi- and bilayer patches can be distinguished in the AFM height image. The bilayer patches are as smooth as the supporting gold substrate with a mean surface roughness of 0.4 nm. Their height was measured to about 12 nm, as seen in Figure 36 B. Furthermore, these results are in agreement with those obtained from PB-PEO bilayer preparation *via* consecutive Langmuir film transfers.^[123]

As mentioned before, with a thickness of 15-17 nm, non-covalently immobilized PB-PEO-OH membranes on glass are slightly thicker than covalently bound PB-PEO-LA membranes on gold. PB-PEO-LA membranes, either prepared by consecutive film transfers, or by aggregate spreading in pure water or with added NaCl (results will be presented below), are about 11-12 nm thick. As explanation for the slightly increased thickness of the PB-PEO-OH membranes the following effects could be considered:

(i) Since the lipoic acid moiety is hydrophobic, it possibly folds back into the hydrophobic core of the membrane. Due to thermal fluctuations, an equilibrium between the folded and the unfolded conformation might establish. However, there is an argument that weakens this hypothesis: the lipoic acid-functionalized polymer contains still about 15-20% hydroxyl-terminated polymer. Even though it is assumed that some LA groups fold back, there should be still enough polymer chains available to span the membrane. Consequently, some folded PB-PEO-LA chains might rather lead to an increase in roughness, than to a decrease of the overall membrane thickness.

(ii) Polymer chain conformation might be influenced by the electrostatic properties of the support. The mainly negatively charged ions located on the glass surface might prefer to be surrounded by water, which has a higher dielectric constant compared to PEO. This might lead to stretching of the polymer chains.

(iii) The different end groups (OH and LA) might affect the self-assembly behavior, and thus the structure of the resulting membrane upon spreading on surfaces. Although the end group is small compared to the full chain length of the polymer, a strong influence of the end group has already been reported.^[122] Differences in polymer self-assembly depending on the end group were also described in section 3.4.1.2. Even though the polymer aggregates were prepared in the same way (in pure water upon evaporation of THF), self-assembly yielded different morphologies. In the case of PB-PEO-LA, the assemblies adopted a lamellar-like structure, either apparent as sub-structure of spherical aggregates, or as bent lamella in “octopi-like” assemblies. In the case of PB-PEO-OH, mainly small spherical aggregates with diameters of about 30-35 nm were formed.

(iv) The type of surface immobilization, covalently bound *versus* non-bound, might affect the orientation of the polymer chains. It was reported that covalently bound lipid bilayers on gold *via* lipoic acid anchors exhibit a slight tilt.^[83, 125] Probably, the covalent attachment of PB-PEO-LA onto gold led also to tilted films, thus to lower thicknesses.

Regarding the experimental and literature data,^[83, 122, 125] effects (iii) and (iv) might be the most pronounced ones in contributing to the slightly increased thickness of PB-PEO-OH membranes on glass. However, a more comprehensive explanation requires more systematic studies, on both, polymer self-assembly and aggregate spreading.

In order to further increase the surface coverage, NaCl (final salt concentrations of 0.3 M and 1.5 M, respectively) was added to the polymer dispersions prior to deposition on the gold surfaces. Once more, an osmotic effect is expected, as observed in the case of the PB-PEO-OH assemblies spread on glass surfaces (see section 3.4.2). Figure 37 evidently shows the effect of the added salt. Apart from some gaps, the surface coverage in Figure 37 A, corresponding to a final salt concentration of 0.3 M, increased significantly compared to Figure 36. A final salt concentration of 1.5 M, as shown in Figure 37 B, led to almost complete coverage. Also in the presence of salt, adsorbed polymer material, multilayer, and bilayer patches can be identified.

According to the profile measurements, the thickness of the first layer is about 12 nm, assuming that is a bilayer. The thickness was also confirmed by SPR measurements (see Figure 38).

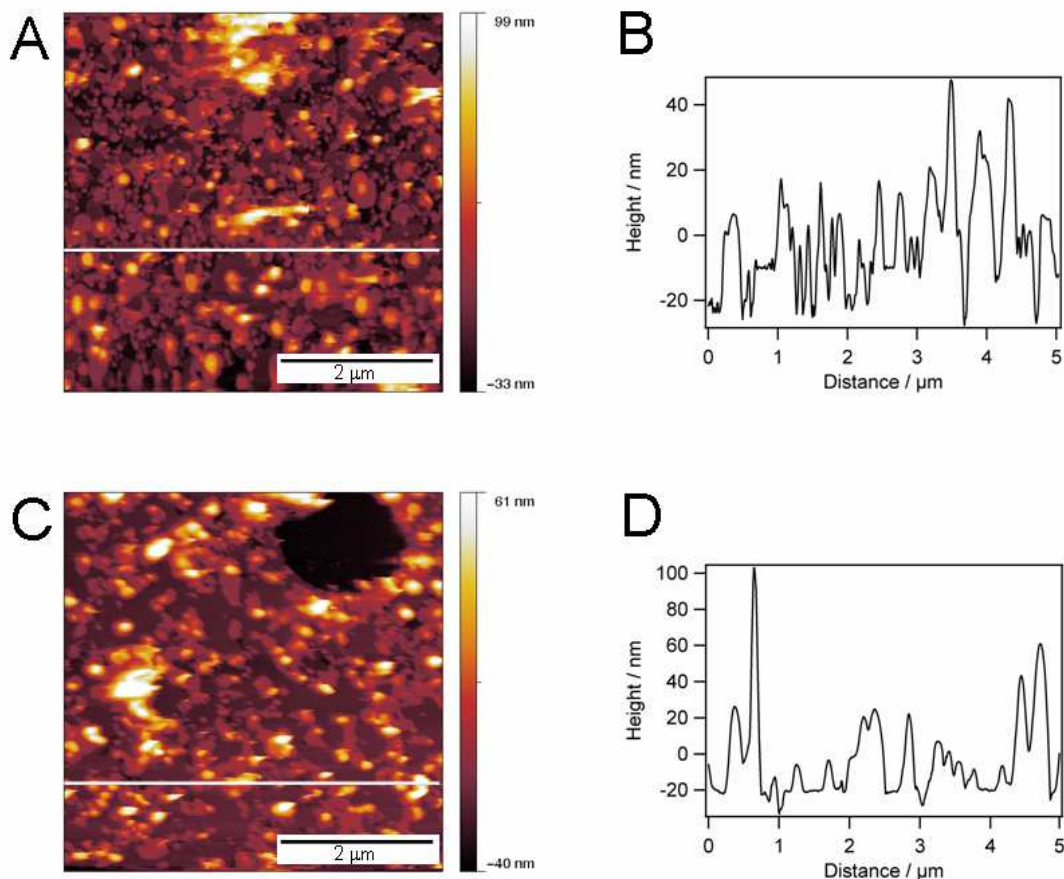


Figure 37. AFM height images of PB-PEO-LA assemblies spread on gold upon addition of different salt concentrations: (A) 0.3 M NaCl, (B) corresponding cross-section; (C) 1.5 M NaCl, (D) corresponding cross-section.

However, even at the high salt concentration, some gaps can be still identified in Figure 37 B. The big hole in the top right corner presumably stems from impurities in the gold film, so that the sulfur-functionalized polymer could not properly bind to the surface. The smaller grooves are indeed defect sites in the polymer bilayer. Apparently, due to their low mobility, the polymer chains in the top layer cannot close (“heal”) the small grooves. The glass transition temperature T_g of atactic 1,2-poly(butadiene) in bulk is about $-4\text{ }^\circ\text{C}$,^[119] thus rather high. The bulk value for T_g is not directly transferable to thin (mono- or bimolecular) polymer films, because it was shown, that

film thickness has a significant effect on the T_g .^[126] Nevertheless, a rather low polymer chain flexibility at room temperature can be assumed.

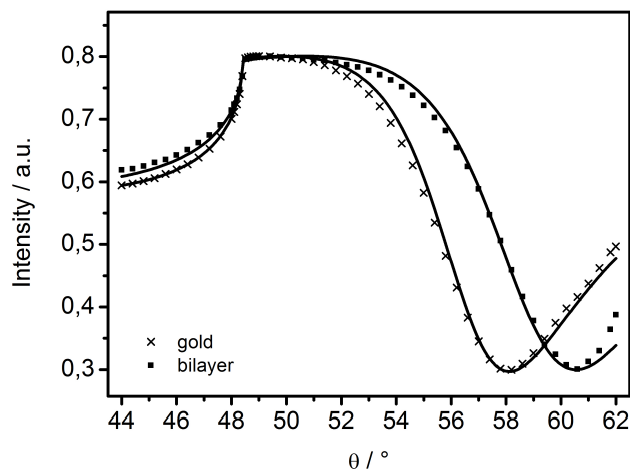


Figure 38. Angular SPR spectrum showing the shift of the reflectivity minimum of blank gold to a bilayer upon PB-PEO-LA aggregate spreading in 1.5 M NaCl. The solid lines represent the fit.

In order to optimize the surface coverage, the spreading was performed with 1.5 M final NaCl concentration in an incubation oven at 42-45°C. This should increase the fluidity of the membrane and facilitate the closure of the gaps. Figure 39 shows the formation of a very smooth and homogenous bilayer. Nevertheless, tiny gaps still remained even after this treatment. In any case, the treatment seems to have an effect on the adsorbed multilayer patches: bigger, more homogeneous patches compared to the previous samples were observed.

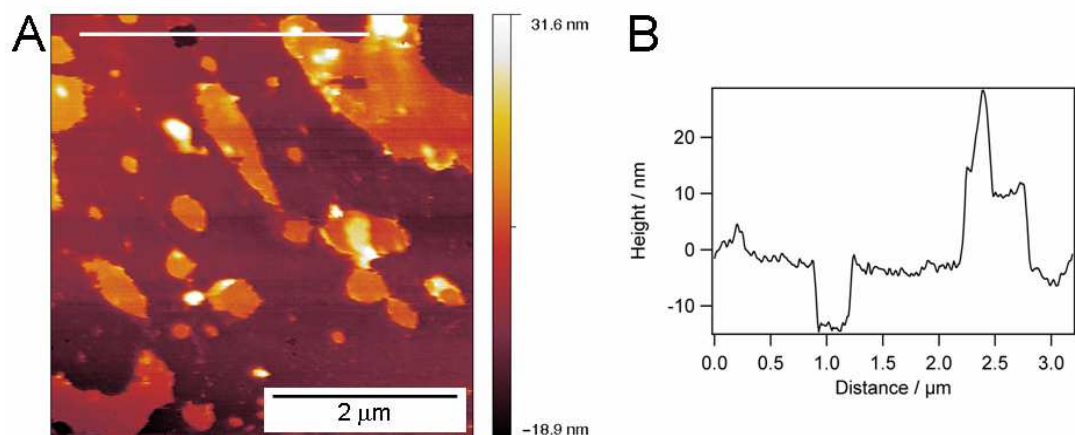


Figure 39. (A) AFM height image of a gold surface incubated with PB-PEO-LA assemblies (in 1.5 M NaCl solution and at 45 °C). (B) Height profile along the indicated line.

In addition, the sample was strongly rinsed with salt solution and blown dry under a stream of nitrogen for approximately 20 sec and consecutively rehydrated for the AFM measurement (Figure 40). Apart from some adsorbed polymer assemblies, this quick dehydration procedure removed most of the adsorbed polymer material (multilayers), while the bilayer itself remained unaffected by this procedure. In general, the bilayers formed by spreading are very stable. They have been stored for more than 14 days in water and no changes in the bilayer morphology could be detected by AFM.

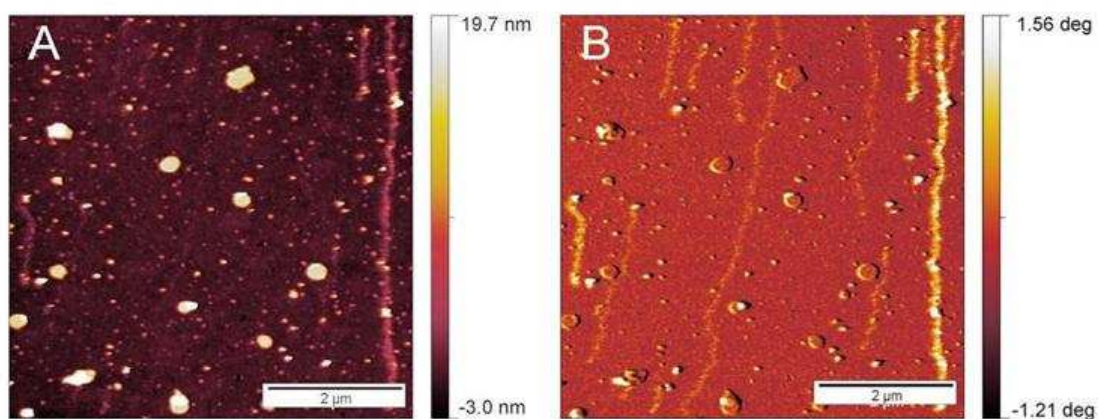


Figure 40. AFM height image (A) and AFM phase image (B) of fused PB-PEO-LA assemblies.

To ensure that the visualized films really consist of two individual membrane sheets, force-distance measurements, in analogy to the ones described in section 3.3.3.2, were performed. By repeatedly approaching and retracting the cantilever from the surface, adhesive and repulsive forces, as well as structural details can be obtained. Figure 41 A shows the force-distance curve of a bilayer. The characteristic peak in the force curve is visible at a distance of about 11 nm. The width of the following valley corresponds to approximately 6 nm, which is the thickness of a polymer monolayer.

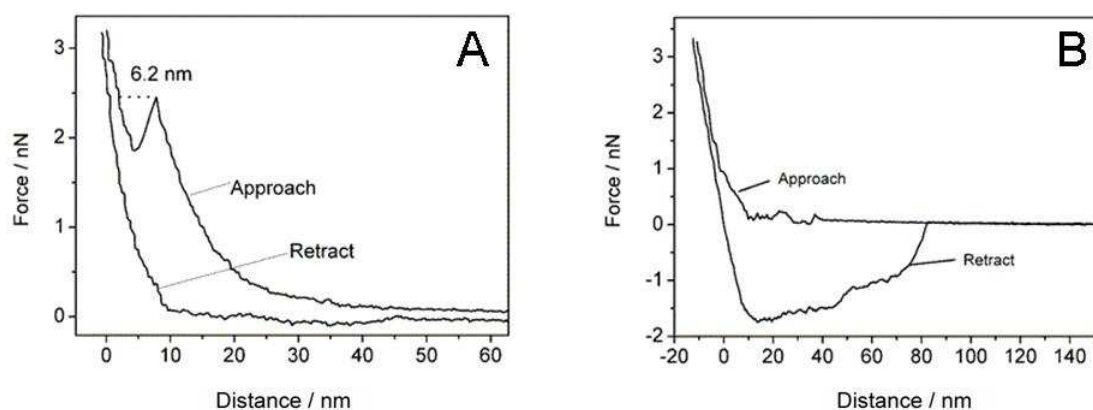


Figure 41. Force-distance measurements of an intact polymer bilayer (A) and a polymer monolayer after rinsing the sample with THF (B).

Further, the sample was rinsed with THF and dried, in order to perform force-distance measurements on a polymer monolayer. As shown in Figure 41 B, we do not observe any characteristic features in the approach curve, because the ability of the covalently bound polymer chains to reorganize upon perturbations by the cantilever is very limited.

Additionally, the surface has been rinsed with THF -a good solvent for the block copolymer- and investigated with AFM after rehydration. From the cross-sectional profile in Figure 42 B the layer thickness can be extracted. It is approximately 6 nm and corresponds very well to the thickness of a PB-PEO monolayer, consistent with our previous results (section 3.3.2). The larger defects visible in Figure 42 are presumably due to an incomplete and/or inhomogeneous fusion process. Additionally, the monolayer exhibits a very fine structure, probably due to conformational rearrangements of the polymer chains. This is not surprising since the image was

recorded in water so that the hydrophobic poly(butadiene) chains tend to minimize their free energy by rearranging on the surface. However, the freedom to reorient is limited by the covalent attachment to the substrate.

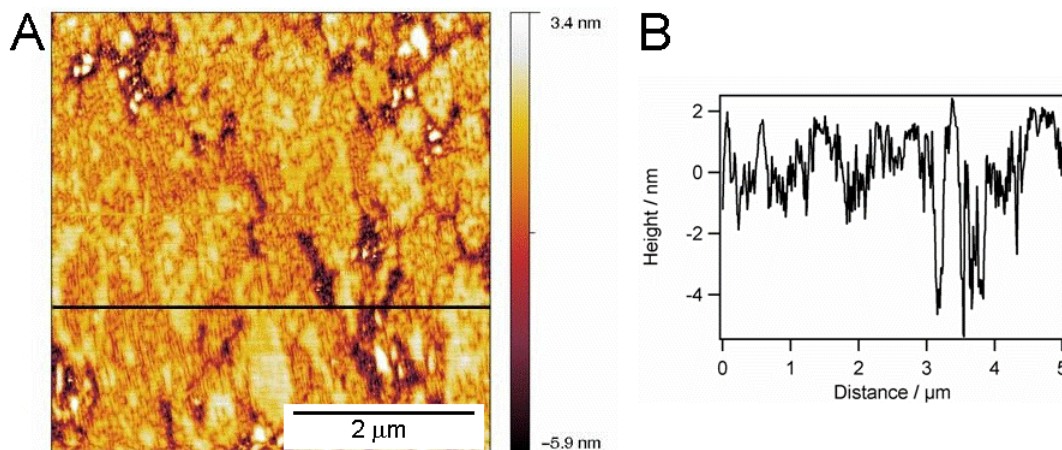


Figure 42. AFM image of a sample rinsed with THF and rehydrated with water (A) and the corresponding cross-section (B).

Moreover, solvent evaporation might have affected the morphological changes as well, since the samples were dried under a stream of nitrogen after washing. This assumption is supported by drying experiments, where the same fine structure appeared upon heating for minimum 12h. In summary, both measurements of the monolayer and the bilayer, are in agreement with the results reported earlier (see sections 3.3.2.3 and 3.3.3.2).

3.4.3.2 Characterization by EIS

Electrochemical impedance spectroscopy (EIS) is a sensitive and non-invasive technique to investigate and characterize the electrochemical properties of materials and their interfaces in contact with electrically conducting electrodes. Among others, the electrochemical (sealing) properties of artificial membranes, as well as the alterations upon reconstitution of e.g. channel proteins, can be probed by EIS.^[14, 15, 127]

The impedance Z is a measure for impeded flows of ions through solutions, interfaces, and coatings. In an EIS measurement, a sinusoidal alternating voltage of

about 5-50 mV of different frequencies is applied.^[128] The resulting current signal lags the voltage by a phase difference θ , as depicted in Figure 43.^[129]

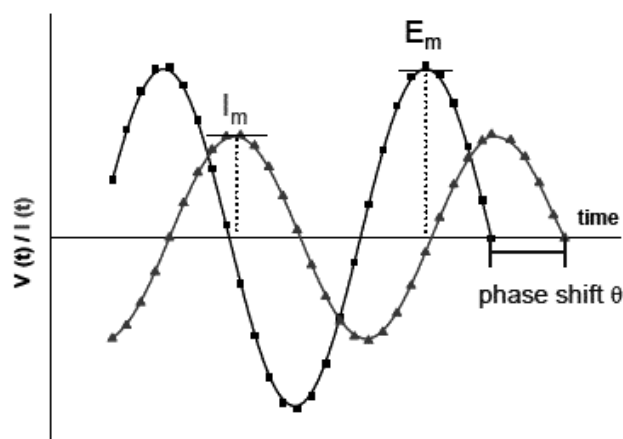


Figure 43. Sinusoidal potential and current response with a phase shift of $\theta=90^\circ$. I_m and E_m are the maximum amplitudes of the current and the potential, respectively.

A resistor will not show a phase shift, thus it equals the impedance. Whereas for an (ideal) capacitor, the phase difference between applied voltage and detected current is 90° . The total impedance of a system is a combination of the impedances of the individual components. Typically, EIS measurements are accompanied by theoretical considerations on an appropriate physical model of the studied system. An equivalent circuit, mainly consisting of capacitors and resistors, is derived from the model and necessary to fit the acquired data.^[129]

In section 3.3, the highly reproducible preparation of stable and homogenous polymer bilayers on gold by sequential Langmuir film transfers was evidenced. This is a prerequisite to measure the electrochemical properties, e.g. the resistance and the capacitance of a system. However, EIS measurements on such polymer membranes failed, most probably due to experimental limitations, i.e. these membranes cannot be prepared *in situ*. First, the membranes were prepared by LB/LS transfers, and afterwards, the samples were clamped into the EIS cell, where they are tightly pressed against an O-ring in order to properly seal the cell. Apparently, this procedure caused severe defects on the edges of the membranes, where they are in direct contact with the

O-ring. Since already slight disruptions of the membrane architecture can significantly influence the electrochemical properties of the system, we could not obtain reproducible and reliable results under these conditions. Therefore, membranes prepared *in situ* by polymer aggregate spreading were used for EIS measurements. Even though these membranes are less homogenous than the ones prepared by LB/LS, they at least allowed for the first feasibility study of polymer bilayers by EIS.

However, the conditions we identified optimal for spreading, i.e. addition of NaCl (1.5 M), yielded EIS data which were inconsistent with the AFM results. As detected by AFM, incubation of the gold surface with the salt-containing PB-PEO-LA dispersion led unambiguously to the formation of a polymer bilayer with almost complete surface coverage. Therefore, by recording the electrochemical impedance spectrum of such a bilayer, we expected the resistance to increase as well, since the ion flow should be impeded by the polymer. However, the resistance did not change at all after incubation with the polymer dispersion, meaning that a tight, sealing film like a bilayer was not formed, and the ions (sodium and chloride) could travel in an unperturbed way with respect to the applied voltage. Furthermore, an uncommon increase of the capacitance could be detected, which stabilized after about 20 min without changing any further. Usually, during bilayer formation, the capacitance should decrease until a stable value is obtained. This state corresponds to a well-packed bilayer, which is not able to host further charge carriers. In conclusion, first electrochemical measurements revealed a highly capacitive and non-resistive system that does not reflect at all the bilayer observed by AFM.

In an empirical approach, equal amounts of polymer dispersions containing 1.5 M NaCl were mixed with phosphate buffer. Figure 44 proves that these conditions led to almost the same results than the experiments presented in Figure 37.

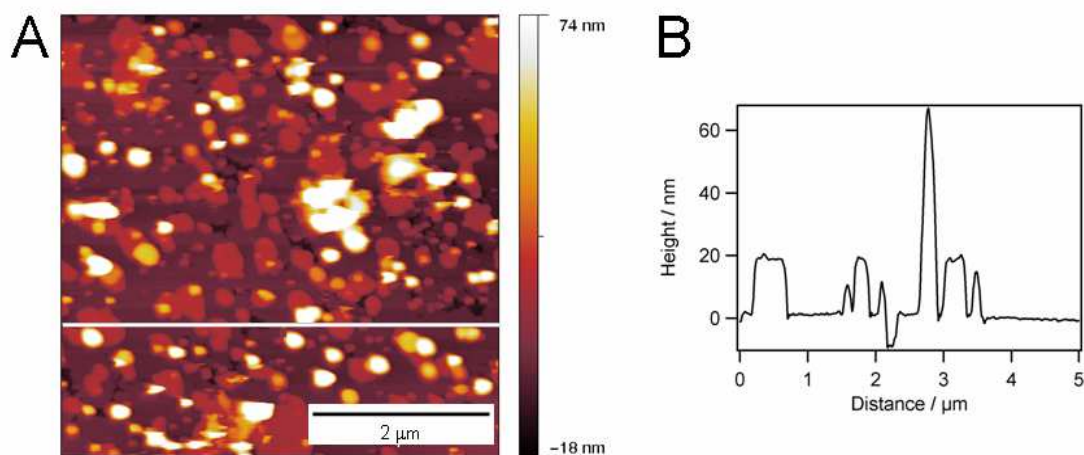


Figure 44. AFM height image of fused PB-PEO-LA assemblies on gold (A) and the corresponding height profile along the indicated line (B). Spreading was performed upon dilution of a 1.5 M NaCl-containing PB-PEO-LA dispersion with PBS (1:1).

The spreading process was recorded *in situ* in 20 to 60 min steps over a time period of 14 h by EIS. Quantitative values for the resistance and the capacitance were obtained by fitting the data to the equivalent circuit depicted in Figure 45 B. Every element in the equivalent circuit can be attributed to a part of the sample system. The supernatant electrolyte can be described by a single resistor R_{ele} . Ideally, the bilayer can be represented by a parallel resistor/capacitor (RC) element. In order to take surface heterogeneities into account, the capacitor can be replaced by a so-called constant phase element CPE, representing a non-ideal capacitor. A CPE is a capacitor, whose value is multiplied with a factor between 0 and 1. Finally, the processes at the interface between the gold electrode and a bilayer, which might act as ions reservoir, are represented by a capacitor C_{sc} . In Figure 45 A, the resistances and capacitances obtained by fitting are plotted in dependence of the time. It reveals that the spreading process is completed in approximately 2 h, and neither capacitance nor resistance change significantly any more. In addition, the spreading process was also monitored by SPR (see Figure 46) and confirmed the results obtained by EIS.

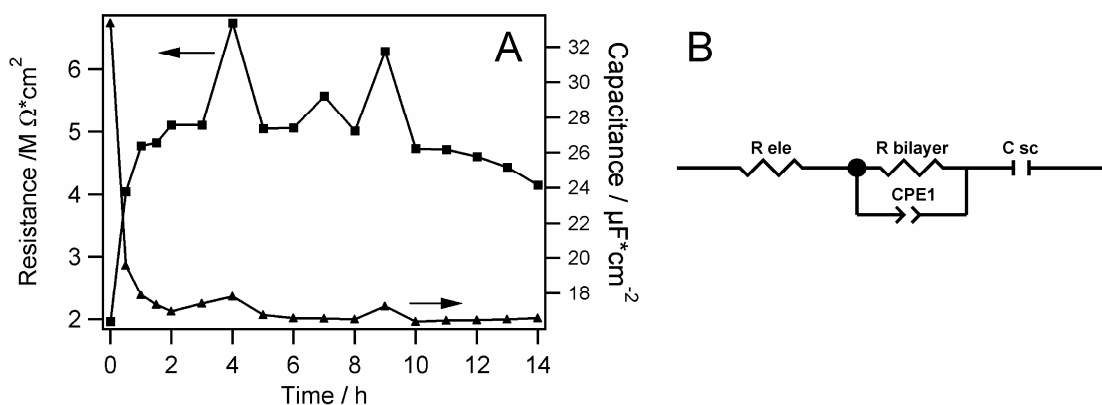


Figure 45. Plot of the resistance (■) and capacitance (▲) values (A), obtained from fitting EIS data, recorded during spreading, to an equivalent circuit (B).

The resistance R of the assembled bilayer architecture is $4\text{--}5 M\Omega cm^2$ and the capacitance C was calculated to $16 \mu F/cm^2$. The resistance of the polymer bilayer is comparable to what was obtained for lipid bilayers ($R = 1\text{--}20 M\Omega cm^2$).^[79] However, the capacitance of the polymer membrane is significantly higher compared to lipid membranes, which usually have capacitances of around $1 \mu F/cm^2$. A reason for the comparatively high capacitance value could be the high amount of double bonds in the poly(butadiene) blocks, leading to a higher polarizability of the polymer compared to lipids in general. Since the capacitance C is directly proportional to the electrical permittivity, which also takes into account the polarizability, the capacitance increases with the electrical permittivity. Additionally, the low packing of the polymer chains, as well as some defects in the bilayer contribute to the rather high capacitance values of the polymer membrane.

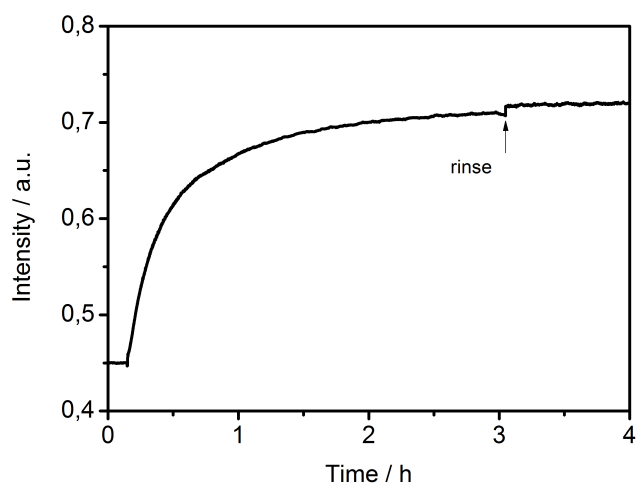


Figure 46. SPR kinetic measurement of PB-PEO-LA aggregate spreading recorded at a constant angle.

Nevertheless, EIS measurements can be performed on polymer membranes, and the electrochemical properties of the membrane can be described in a qualitative as well as in a quantitative way. This is important in order to monitor even small changes upon interactions with biologically relevant species such as peptides. In the following, the influence of peptides on the polymer bilayer is presented and discussed.

3.5 Influence of peptides on PB-PEO bilayers

In this section, it was our goal to investigate if the PB-PEO membrane is a suitable matrix for hosting peptides or proteins. One important limitation is that the size of most peptides or proteins may not fit with the increased thickness of the hydrophobic membrane core. However, despite the size-mismatch, theoretical and experimental work confirm the successful incorporation of membrane proteins into polymer membranes.^[130, 131]

Interactions of polymer membranes with peptides or proteins have not been discussed yet regarding fluidity in two dimensions. So far, all experimental studies available on protein or peptide insertion into polymer membranes were performed in vesicular systems,^[111] free-standing membranes,^[130] or monolayers at the air-water interface,^[132] where diffusion of the polymer chains might be less hindered. In the case of our planar PB-PEO membranes, diffusion is strongly hampered, because the bottom layer is almost completely covalently tethered to the gold support. As demonstrated earlier,^[123] the ability of the top layer to close intentionally created defects is limited, which is disadvantageous for post-insertion of proteins or peptides into the polymeric bilayers.

To evaluate if and how biologically relevant species interact with the supported polymer bilayer, different peptides were tested. The species investigated are alamethicin, polymyxin B, and α -haemolysin. Alamethicin is a peptidic antibiotic exhibiting an α -helical structure. In (cell) membranes, it forms voltage-gated nonspecific ion channels consisting of four to six molecules.^[133] It has been extensively studied in the context of pore formation,^[134] lipid-peptide and lipid-polymer interactions.^[45, 135]

Incubation of the polymer bilayer with alamethicin, even over night, did not show any effect as investigated by EIS. This result was unexpected, since it was reported that alamethicin spontaneously incorporates into (freely suspended) giant vesicles, made from a polymer very similar to ours.^[90] Probably the polymer chain mobility in the solid-supported bilayer was not sufficient to allow for successful peptide incorporation.

Furthermore, the interaction of the cyclic peptide polymyxin B with the polymer bilayer was tested. Polymyxin B causes alterations in the membrane structure similarly to detergents. In particular, it disrupts membranes consisting of lipopolysaccharides,

which are a major component of gram-negative bacterial membranes, leading to leakage of small ions and molecules and finally causing cell death.^[136] Polymyxin B is a promising candidate to interact with the polymer bilayer structures presented in this work since their hydrophilic PEO-block is chemically similar to the sugar chains of polysaccharides. The results of the incubation with polymyxin B are shown in Figure 47, representing the impedance spectra in a so-called Bode plot. In this plot, the absolute value of the impedance and the phase angle are plotted *versus* the frequency (impedance and frequency are plotted logarithmically). Impedance regions with a slope of -1, accompanied by a phase shift close to 90°, indicate that the impedance is dominated by capacitive effects in the corresponding frequency range. In contrast, flat impedance regions with slopes close to zero, accompanied by low phase angles (in the case of R_{ele} , θ is about zero), indicate the dominance of resistive effects. By extrapolation through the flat region, a preliminary value for Z can be obtained. Hence, the Bode representation gives a direct measure of the resistors under study, however, not for the capacitors.^[129] Therefore, to obtain quantitative values, EIS data has to be fitted by using appropriate equivalent circuits.

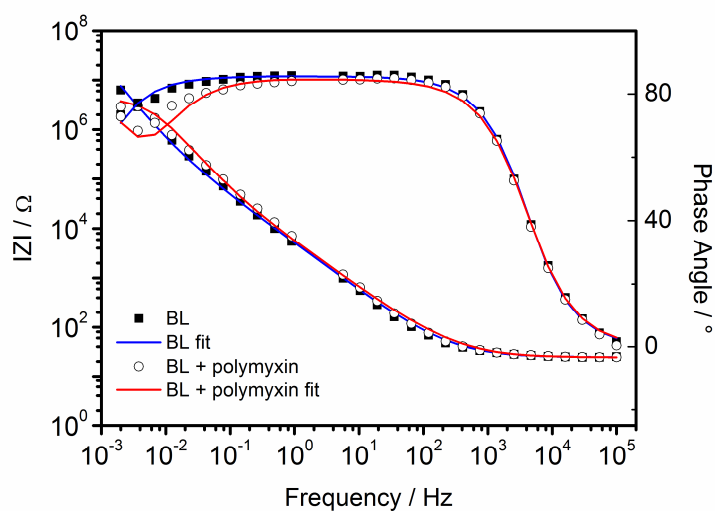


Figure 47. Electrochemical impedance spectra of a pure polymer bilayer (raw data: full squares; fit: blue solid lines) and a polymer bilayer incorporated with polymyxin B (raw data: open circles; fit: red solid lines), respectively. Data are represented in a Bode plot.

First, the bilayer formation by PB-PEO-LA aggregate spreading (without peptide) was probed. The measured data are depicted as full squares, whereas the fitted data as blue lines. Fitting to an equivalent circuit (see Figure 45 B) yields a membrane resistance of about $4.4 \text{ M}\Omega\text{cm}^2$, which proves the successful formation of a well-packed membrane. The plateau of the phase angle is approximately 83° , which is an indication for a high homogeneity of the membrane (surface). The bilayer was monitored over a time period of 14 h, and did not alter within this time. This is a prerequisite to detect even small changes of the membrane upon addition of a membrane-active species.

It was reported that the creation of transient defects by polymyxin requires a high local concentration.^[137] Therefore, a peptide concentration of 0.1 mg/mL was chosen. After incubation times of 15 and 60 min, respectively, the impedance spectra were recorded.

The measured data points after incubation with polymyxin B are depicted as open circles in Figure 47, and the fitted values are represented by the red lines. The fit reveals a decrease of the membrane resistance from $4.4 \text{ M}\Omega\text{cm}^2$ to $1.2 \text{ M}\Omega\text{cm}^2$. This decrease corresponds to a reduction of the electrochemical sealing properties of the membrane, and hints at the formation of additional pathways for charge carriers to travel across the membrane. The different incubation times did not affect the results, indicating that the peptide has an immediate effect on the bilayer. In contrast to the resistance, the capacitance of approximately $22 \text{ }\mu\text{F}/\text{cm}^2$ remained constant throughout the whole experiment, confirming the bilayer's integrity.

However, 7 h after incubation, the resistance returned to its initial value of about $4 \text{ M}\Omega\text{cm}^2$, evidencing the expected behavior of polymyxin B, i.e. it did not form a stable transmembrane pore. It interacts with the polymer membrane in a rather detergent-like way, i.e. it creates transient defects by partly disassembling the membrane structure. Such interactions have already been reported for lipid membranes.^[138] With time, the holes created by the peptide can heal, which is reflected by an increase of the membrane resistance. However, due to the rather low polymer chain mobility, the healing process takes much longer than for more fluid systems such as lipid bilayers.

Since polymyxin B is not a pore-forming peptide, the interactions of the channel-forming peptide α -haemolysin with the polymer membrane were probed as well. In its functional form, α -haemolysin is a heptameric pore.^[139] The mechanism of assembly is well understood and consists of three steps: first a monomeric unit attaches to the membrane, followed by assembly of an unfunctional heptameric structure, which is finally incorporated into the membrane as a functional transmembrane pore.^[140]

Again, first the bilayer produced by PB-PEO-LA aggregate spreading -without the peptide- was investigated by EIS over a time period of 14 h, in order to prove that neither resistance nor capacitance changed during the experiment and that the system is not susceptible to drifts caused by rearrangements or desorption of material. The spectrum of the pure bilayer is shown in Figure 48 A. The shorter plateau of the phase angle and the appearing slope at a frequency of 10 Hz hint at a lower surface homogeneity compared to the previous experiments. This might be due to different experimental procedures. For the previous measurements, the bilayers were prepared *in situ* in the EIS cell by spreading of the polymer aggregates. In the present case, the membranes were prepared by spreading, and afterwards the sample was clamped into the EIS cell. This might have caused defects at the membrane edges.

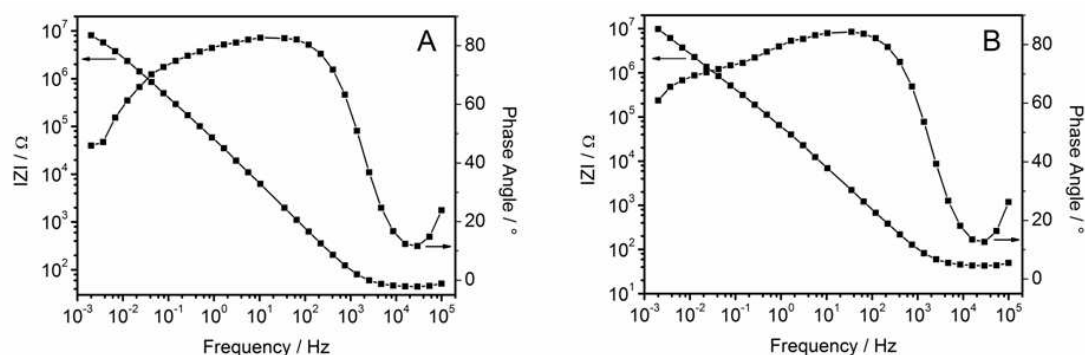


Figure 48. Measured EIS data of a polymer bilayer before (A) and after incubation with α -haemolysin (B).

Addition of α -haemolysin definitely affected the bilayers electrochemical properties, as seen in Figure 48 B. A significant decrease of the phase angle from about 83° to 70° at frequencies around 10^{-1} Hz can be noted. Actually, a decrease in the phase angle should be accompanied by a flattened slope in the impedance (ideally 0). Unfortunately, the zero slope region in the impedance is not unambiguously visible.

However, it is still questionable whether the peptide incorporated fully, i.e. as functional heptameric pore, or just partly in its monomeric form into the polymer bilayer. As shown before, the polymer chain mobility, thus the bilayer fluidity, is rather low, and maybe indeed too low to allow for complete reconstitution of α -haemolysin. Additionally, the protein-repellent character of the PEO block might also hamper the peptide insertion.

At the present stage, the interpretation of EIS data is purely qualitative. The first fitting attempts revealed that the typical fitting procedures used for lipids are not suitable to evaluate the data for a polymer bilayer. Probably, the polymer bilayers were too inhomogeneous. Thus, sample preparation and data processing have to be improved in order to obtain quantitative data from EIS measurements.

Even though quantitative data are not available yet and the recorded impedance spectra do not unambiguously show complete insertion of α -haemolysin into the polymer bilayer, it can be at least concluded that the peptide has some influence on the solid-supported polymer membrane.

4 Conclusions and outlook

In this thesis, novel solid-supported membranes from amphiphilic poly(butadiene)-*b*-poly(ethylene oxide)-based (PB-PEO) diblock copolymers are described. The polymers were synthesized by anionic polymerization and characterized in terms of molecular weight and individual block length. A chemical modification procedure yielded a sulfur-functionalized derivate, which could be covalently attached to ultrasmooth gold substrates. The covalent attachment of the proximal membrane layer to the solid support should endow the system with mechanical stability.

Two different preparation pathways were employed to prepare solid-supported polymer membranes. On the one hand, a combination of the well-controllable Langmuir-Blodgett-/Schaefer film transfers was employed to deposit individual polymeric monolayers on gold supports. In this way, for the first time, polymeric bilayers of defined morphology, molecular packing, and membrane thickness were produced. On the other hand, polymer bilayers on different substrates were produced by spreading of pre-organized superstructures. By this feasible one-step procedure physisorbed polymer bilayers on glass, as well as covalently bound membranes on gold could be prepared.

The polymer membranes were thoroughly characterized by surface-sensitive analytical techniques such as atomic force microscopy (AFM) and surface plasmon resonance spectroscopy (SPR) to gain insights into morphology, homogeneity, and thickness of the layers. SPR and AFM results indicated a thickness of 11-12 nm of the covalently immobilized PB-PEO bilayers on gold. Additionally, AFM measurements of the membranes prepared by Langmuir film transfers proved their flatness and homogeneity on several square millimeters. Furthermore, drying experiments proved air stability of these bilayers to a certain extent, however, the presence of water is still required to maintain the bilayer stability in the long term. The polymer used in this thesis rather falls into the molecular mass regime where entanglement between opposing layers only starts to occur, which is in agreement with reports from literature for this chain length. Therefore stability of this membrane system could be improved by using longer, thus more interpenetrating, polymers.

Nevertheless, the results presented in this thesis already suggest superior stability of the polymer membranes compared to conventional phospholipid bilayers.

SPR and AFM measurements on bilayers prepared upon polymer aggregate spreading on gold confirmed the thickness of 11-12 nm. AFM further revealed that the spreading approach not only yielded homogeneous bilayers, but also multilayers were formed. In any case, full surface coverage was not achieved by this method. However, surface coverage could be increased by the addition of NaCl to the polymer dispersions. This is ascribed to an osmotic effect exerting a mechanical strain on the membrane surface, which destabilizes the polymer assemblies and facilitates their spreading. Further treatments such as heating, rinsing, or quick dehydrations remarkably improved surface coverage and bilayer homogeneity. In order to demonstrate the membranes' biomimetic potential, bilayers prepared by spreading were incubated with peptides, polymyxin B and α -haemolysin. Occurring interactions between the peptides and the polymer membranes were detected by electrochemical impedance spectroscopy (EIS). The data suggest that the peptides definitely have an influence on the polymer bilayers, however, at this stage, a qualitative interpretation is not possible. The EIS fitting procedure was established for conventional lipid-based membranes, which differ significantly regarding physicochemical properties, conformation and molecular packing from the PB-PEO bilayers. Thus, improvements of the EIS data processing, as well as more systematic studies are required to extract qualitative data from these experiments. Nevertheless, we have some preliminary evidence for occurring interactions of membrane-active biological molecules interact with planar solid-supported polymeric bilayers. This might be relevant for further applications of solid-supported block copolymer membranes in the field of biosensing.

In this work, different methods of polymer synthesis, membrane preparation, and surface analytics were combined to create and characterize novel polymeric systems. This generic approach could be extended to different polymer chemistries or substrates, to help address questions in fundamental research, and to become a valuable platform for technological demands. As a consequence, this work might have an impact on research fields as diverse as drug screening or delivery, trace analysis, or sensor development.

5 Experimental part

All chemicals and solvents were purchased from Sigma Aldrich or Fluka (Switzerland) with the highest purity grade and, unless otherwise stated, used as received.

5.1 Synthesis of PB-PEO-OH

THF was refluxed and stirred over Na/K-alloy and Na/benzophenone complex until the typical purple color appeared. 1,3-butadiene (Bd) was cooled to -78°C ($\rho = 0.78 \text{ g/mL}$) and purified by cryo-distillation from CaH_2 and *n*BuLi. Ethylene oxide (EO) was cooled to -78°C ($\rho = 0.99 \text{ g/mL}$) and purified successively by distillation from CaH_2 , sodium mirror, and *n*BuLi.

PB-PEO was synthesized by sequential living anionic polymerization in an one-pot procedure carried out in a thoroughly flame-dried customized glass vacuum apparatus. Phosphazene base *t*BuP₄ (IUPAC name: 1-*tert*-butyl-4,4,4-tris(dimethylamino)-2,2-bis[tris(dimethylamino)-phosphoranylidenamino]-2 Λ^5 ,4 Λ^5 -catenadi(phosphazene) solution (20 mL; 20 mmol; 1.0 M in hexane) was introduced into the 1 L-Schlenk reactor under a stream of argon and the hexane was distilled off. The solid white base was dried for 1 h under vacuum. Sequentially, THF (500 mL) and 1,3-butadiene (68 mL; 924 mmol) were condensed into the reaction flask, and the solution was cooled to -78°C . The initiator *s*BuLi (13 mL; 18 mmol; 1.4 M in cyclohexane) was added via a sealed syringe. The yellow reaction mixture reacted at -78°C for 12 h. Before the sequential polymerization proceeded, a small aliquot (precursor) was taken and precipitated in cryo-degassed methanol for GPC and NMR characterization.

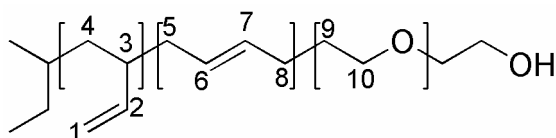
Afterwards, the reaction mixture was warmed to -40°C and a small amount of ethylene oxide (approx. 10% of the total volume, i.e. 25 mL; 554 mmol) was added by distillation. The slightly yellow, almost colorless mixture was allowed to react for 1 h and at the same time warmed to room temperature. Afterwards, the remaining ethylene oxide was added. The solution was warmed to 40°C and the polymerization proceeded for 72 h. In the course of the polymerization, the color of the mixture changed to dark blue or dark brown-red. After cooling the mixture to room temperature, the

polymerization was quenched with acetic acid (2 mL). Ion exchange resin (Dowex 50WX4-100) was added and the mixture was stirred for 2 h. After filtering, the solvent was evaporated until the mixture became viscous. The polymer was precipitated at least twice in cold acetone (-30°C) and dried under vacuum to constant weight. A slightly yellowish sticky solid was obtained.

The polymer was further purified by extractions. Therefore, about 2 g of PB-PEO were dissolved in 250 mL CHCl₃ and repeatedly extracted with 10% (v/v) HCl and water. The solution was dried over MgSO₄ and filtered. The solvent was evaporated under reduced pressure.

Characterization of PB-PEO-OH

The molecular weight of the block copolymer was determined by GPC (Agilent Technologies; column: PLgel 3 μm MIXED-E; Varian) and ¹H-NMR (Varian). A PB aliquot, drawn prior to the sequential copolymerization, was analyzed by GPC with THF as eluent (flow: 1 mg/mL; temperature: 30 °C). Narrow poly(butadiene) standards (PSS Polymer Standards Service, Germany) were used to calculate M_n , M_w , and the PDI of the PB block. The number of the ethylene oxide repeating units, thus the molecular weight, was calculated from the integral ratios in the ¹H-NMR spectrum of the block copolymer. The results are presented in section 3.2 (Table 1).



¹H-NMR (400 MHz, CDCl₃): δ [ppm] = 1.13-1.25 (m, 2H, H⁴), 1.86-2.12 (m, 5H, H^{3,5,8}), 3.60-3.67 (m, 4H, H^{9,10}), 4.85-4.97 (m, 2H, H¹), 5.31-5.58 (m, 3H, H^{2,6,7})

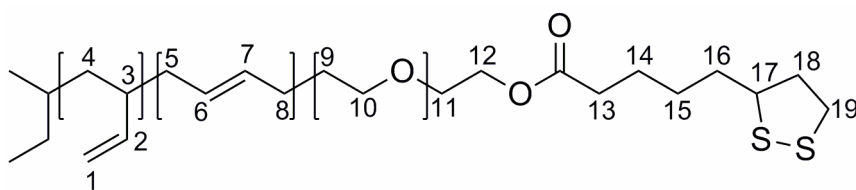
5.2 Synthesis of PB-PEO-LA

Lipoic acid (LA; 268 mg; 1.3 mmol), the coupling compound 1-ethyl-3-(3-dimethylaminopropyl)carbodiimide hydrochloride (EDC·HCl; 249 mg; 1.3 mmol), and 4-(dimethylamino)pyridine (DMAP; 12 mg; 0.1 mmol) were added to a flame-dried flask. The solids were dried under vacuum for 2 h. The mixture was dissolved in absolute DCM (10 mL), which was freshly distilled from CaH₂ prior to use. In a second flame-dried flask, the polymer (4.1 g; 1.0 mmol) was dried under vacuum for 2 h and dissolved in absolute DCM (10 mL). After NEt₃ (0.2 mL; 1.3 mmol) was added, the solution was injected into the first flask and the reaction mixture was stirred at room temperature for 72 h.

Afterwards the solution was washed with saturated NaHCO_{3(aq)}, 10% (v/v) HCl, and distilled water (three times each). The organic phase was dried over MgSO₄, filtered, and the solvent was evaporated under reduced pressure.

Characterization of PB-PEO-LA

The polymer was characterized by GPC and ¹H-NMR (see section 5.1). The results are presented in section 3.2 (Table 1).



¹H-NMR (400 MHz, CDCl₃): δ [ppm] = 1.13-1.45 (m, 4H, H^{4,15}), 1.61-1.73 (m, 4H, H^{14,16}), 1.86-2.12 (m, 6H, H^{3,5,8,18}), 2.35 (t, 2H, H¹³), 2.43-2.50 (m, 1H, H¹⁸), 3.08-3.21 (m, 2H, H¹⁹), 3.45-3.85 (m, 6H, H^{9,10,11}), 4.20-4.23 (m, 2H, H¹²), 4.85-4.97 (m, 2H, H¹), 5.31-5.58 (m, 3H, H^{2,6,7})

5.3 Mono- and bilayer preparation

5.3.1 Gold substrate preparation

Ultrasmooth template stripped gold (TSG) surfaces were prepared according to a procedure previously described by Naumann *et al.*^[141] where 50 nm thin gold films were deposited by electrothermal evaporation (0.8-1 Å/s; 5×10^{-6} mbar) on clean silicon wafers (CrysTec, Germany) and glued with epoxy glue (EPO-TEK 353ND4, USA) to clean microcrown glass slides (Menzel, Germany). The glued slides were cured for 1 h at 150 °C and stored until further use.

5.3.2 Monolayer transfer

PB-PEO-LA monolayers were transferred onto TSG substrates by the Langmuir-Blodgett (LB) technique, using a KSV 5000 (KSV Instruments, Finland) Langmuir TeflonTM trough (area 1860 cm²), placed on an antivibrational table in a plastic cabinet. Prior to film spreading, four freshly cleaved TSG substrates were immersed in the subphase using a dipper. After compressing a film to the pressure of 35 mN/m it was left for 15 min in order for the polymer chains to establish their most favorable orientation. Afterwards, a monolayer film was transferred at constant speed (0.3 mm/min) on dipper upstroke. Two PB-PEO-LA coated slides were used for surface investigations and the other two were subjected to a second monolayer transfer, completing the bilayer membrane. In this way, nearly identical conditions were created for one set of samples.

5.3.3 Bilayer preparation by LS transfer

A compressed PB-PEO-OH film (target pressure 35 mN/m) was produced at the air-water interface. PB-PEO-LA coated slides were placed in the dipper horizontally above the floating monolayer. At constant dipper speed (50 mm/min), the substrate was lowered through the interface. The water surface was thoroughly cleaned and the gold slides were placed, under water, into a crystallization dish.

5.3.4 Preparation of PB-PEO superstructures

The polymer (8 mg; PB-PEO-OH or PB-PEO-LA) was dissolved in THF or CHCl_3 (4 mL). Under vigorous stirring, ultrapure water (10 mL) were slowly (100 $\mu\text{L}/\text{min}$) added with a peristaltic pump to the polymer solution. During the addition of water, the solution became turbid, indicating the formation of superstructures. Under gentle stirring at room temperature, the organic solvent was evaporated within 4 days. CHCl_3 was also evaporated under reduced pressure. The resulting dispersions, with a theoretical concentration of approximately 0.2 mM, were consecutively extruded through 800 nm, 400 nm, and 200 nm pore-sized polycarbonate membranes (Whatman, United Kingdom) in a barrel extruder (Northern Lipids, Canada) at 5 bar.

5.3.5 Spreading of PB-PEO superstructures

For spreading on hydrophilic glass substrates, 500 μL of the polymer dispersion were mixed with 45 mg NaCl and applied directly to the surface.

For spreading on gold, LA-functionalized polymer self-assemblies were either added directly to freshly cleaved TSG surfaces, or were first mixed with 8 or 45 mg NaCl, vortexed until the salt was completely dissolved, and afterwards added to the TSG substrates. Some spreading experiments were additionally carried out in an oven at 45°C, as it is described in the text.

For AFM imaging, the surfaces were rinsed with ultrapure water, or NaCl solution, respectively, prior to the measurement.

5.3.6 Bilayer incubation with peptides

Bilayers formed by PB-PEO-LA aggregate spreading were rinsed with PBS and allowed to equilibrate for ~14 h inside the EIS cell. The equilibration process was monitored in 20-30 min and 1 h time intervals.

Alamethicin was added to the polymer bilayer inside the EIS sample cell. 50 μl peptide solution in ethanol (2 mg/mL) were added after bilayer equilibration.

In the case of polymyxin B, the sample volume inside the EIS sample cell was reduced to about 200 μL prior to peptide addition in order to prevent strong dilution of

the peptide aliquot by the electrolyte. Afterwards, 20 μl of the peptide in ultrapure water (1 mg/mL) were added and allowed to incubate for 15 min to 1 h. The EIS sample cell was filled with the required volume of electrolyte solution and spectra were recorded.

For the α -haemolysin measurement, the bilayer was prepared outside the impedance cell to check successful membrane formation by AFM. Subsequently, the sample was clamped into the EIS cell. 60 μL α -haemolysin solution in PBS (0.5 mg/mL) was added directly to the cell. The electrochemical impedance spectra were monitored over 14 h within time steps of 30 min to 1 h.

5.4 Mono- and bilayer characterization

5.4.1 Characterization at the air-water interface

Monolayers were investigated with a KSV 2000 Langmuir TeflonTM trough (KSV Instruments, Finland), area 420 cm², equipped with two symmetric, hydrophilic DelrinTM barriers and a Wilhelmy plate (ashless filter paper strips, perimeter 23 mm) to monitor the surface pressure with an accuracy of 0.1 mN/m. The trough was placed in a plastic cabinet to prevent dust contaminations. All experiments were carried out in an air-conditioned lab (20 °C). Monolayers were spread drop-wise on ultrapure water (18.2 M Ωm ; Millipore, Germany) surface from chloroform solutions (typically 1-2 mg/mL). The solvent was allowed to evaporate for 15 min, and the monolayers were compressed at the rate of 1 mm/min.

5.4.2 Contact angle measurements

Contact angle measurements of the covalently attached monolayer were performed applying the static sessile drop method with a fully computer-controlled instrument (DSA 10, Krüss, Germany). The measurements were carried out under constant ambient conditions and constant drop size (3 μL). Ultrapure water was used as medium.

5.4.3 ATR infrared spectroscopy

ATR-IR measurements were acquired using a FTIR-8400S spectrometer (Shimadzu). Spectra were recorded with 128 scans and a resolution of 2 cm^{-1} .

5.4.4 Surface plasmon resonance spectroscopy

SPR measurements were performed using a home-built setup in the Kretschmann configuration with a He/Ne laser ($\lambda = 633\text{ nm}$).^[142] In scan mode, reflectivity is monitored as a function of the incident angle. In kinetic mode, reflectivity changes occurring at a fixed angle are recorded as a function of time. In order to achieve the high in-plane wave vectors of the exciting light at moderate coupling angles, the microcrown slide was attached to a LaSFN9 Prism ($n = 1.845$). Spectra were analyzed using a four layer model including the prism, gold, mono- or bilayer, and the surrounding medium (water or air). A refractive index $n = 1.5$ was assumed for both, mono- and bilayer.^[143]

5.4.5 Atomic force microscopy

AFM was carried out on a Nanowizard (JPK Instruments, Germany), installed on an inverted microscope (Axiovert; Zeiss, Germany). Measurements were performed in intermittent contact mode in liquid environment. For imaging and force distance measurements oxide sharpened silicon nitride tips (NP-S; Veeco Instruments, Germany) with a nominal spring constant of 0.32 N/m were used, whereas for scratching experiments silicon cantilevers (OMCL-AC240TS; Olympus, Germany) with a nominal spring constant of 2 N/m were utilized. Typical scan rates ranged from $0.8\text{--}1.2\text{ Hz}$. Cantilevers were not calibrated for force distance measurements; the nominal spring constant was chosen.

5.4.6 Electrochemical impedance spectroscopy

Measurements were conducted using an Autolab spectrometer PGSTAT 12 (Eco Chemie, Netherlands). Spectra were recorded for frequencies between 2 mHz and 100 kHz at 0 V bias potential with an AC modulation amplitude of 10 mV. Raw data were analyzed using the ZVIEW software package (Version 2.90, Scribner Associates). Three-electrode measurements were performed with the gold substrate as the working electrode, a coiled platinum wire as the counter electrode, and a DRIFEF-2 reference electrode (World Precision Instruments, Germany). The home-built TeflonTM cells had a buffer volume of 1 mL and an electrochemically active area on the substrates of about 0.28 cm².

By measuring the impedance of the system at different frequencies, the resistances and capacitances of the tethered bilayer/electrode assembly can be determined using a model equivalent circuit consisting of resistors (R) and capacitors (C).^[144] In this work, we used a R(RC)C-circuit consisting of a RC element describing the bilayer in series with a capacitor C_{sc} and an electrolyte resistance R_{ele} . To model the actual surface architecture, a constant phase element (CPE) was used instead of a capacitor. The CPE represents a distribution of capacitors taking the surface heterogeneity into account. The C_{sc} element represent the charge separation due to the spacer region combined with the effects of the electrochemical double layer at the gold interface.^[127, 141] The data can be displayed in Bode plots, where pure capacitances show up as slopes of -1 with high phase shifts of -90°, whereas ideal resistances are represented as horizontal regions of low phase angles.^[144]

5.4.7 Dynamic light scattering

DLS studies were carried out using a commercial goniometer (ALV, Germany) equipped with a He-Ne laser ($\lambda = 633$ nm) at $T = 293$ K \pm 0.05 K. The photon intensity auto correlation function $g^2(t)$ was determined with an ALV-5000E correlator at scattering angles between 40° and 140°. DLS data were analyzed via the CONTIN algorithm.

5.4.8 Transmission electron microscopy

TEM images were taken on a Philips EM 400 (Philips Electronics, Netherlands) operated at 80 kV, equipped with a Megaview III charge-coupled device camera (CCD) and controlled with Morgagni 268D control and image acquisition software. 5 μ L sample was absorbed on a glow-discharged, parlodion- and carbon-coated, 200 mesh copper grid and incubated for 1 min, before the droplet was blotted on a filter paper. Afterwards, the samples were stained with 2% uranyl acetate.

6 Additional polymers synthesized

In this section, the synthesis and characterization of two end-functionalized PB-PEO polymers are described.

6.1 Biotin-functionalized PB-PEO

This polymer can be used for specific immobilization on streptavidin-modified surfaces,^[27, 86] or for probing specific binding to streptavidin-tagged compounds such as peptides or proteins. The biotin-streptavidin approach can be applied to glass surfaces, which allows for (single-molecule) investigations by fluorescence spectroscopy. This is an advantage compared to the immobilization *via* gold-sulfur interactions: since gold quenches fluorescence, fluorescence spectroscopy can usually not be performed on gold surfaces.

Biotin (489 mg; 2.0 mmol), the coupling compound EDC·HCl (383 mg; 2.0 mmol), and DMAP (24 mg; 0.2 mmol) were added to a flame-dried flask. The solids were dried under vacuum for 2 h. The mixture was dissolved in absolute DCM (10 mL), which was freshly distilled from CaH₂ prior to use. In a second flame-dried flask, the polymer (820 mg; 0.2 mmol) was dried under vacuum for 2 h and dissolved in absolute DCM (10 mL). After NEt₃ (0.3 mL; 2.0 mmol) was added, the solution was injected into the first flask and the reaction mixture was stirred at room temperature for 72 h.

Afterwards the solution was washed with saturated NaHCO_{3aq}, 10% (v/v) HCl, and distilled water (three times each). The organic phase was dried over MgSO₄, filtered, and the solvent was evaporated under reduced pressure. The ¹H-NMR spectrum is displayed in Figure 49.

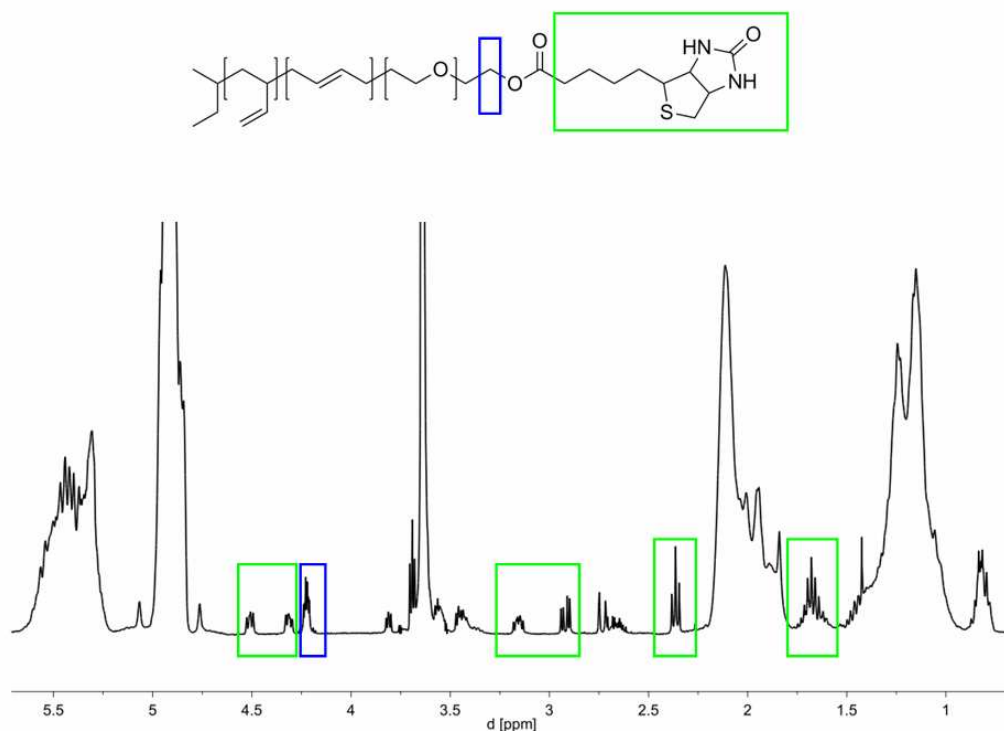


Figure 49. Structure and representative $^1\text{H-NMR}$ spectrum of PB-PEO-biotin. The biotin signals are highlighted in green. The signal at $\delta = 4.23$ ppm, highlighted in blue, corresponds to the methylene group in the backbone, which is adjacent to the newly formed ester group.

As determined by $^1\text{H-NMR}$, the degree of functionalization is ca. 80%. DOSY measurements proved covalent coupling of biotin to the polymer ($\delta_{\text{diff}} = 1.88 \cdot 10^{-10} \text{ m}^2/\text{s}$ for $\delta = 4.94$ and $\delta_{\text{diff}} = 1.95 \cdot 10^{-10} \text{ m}^2/\text{s}$ for $\delta = 4.32$ and 4.52).

6.2 Fluorophore-functionalized PB-PEO

PB-PEO-OH was functionalized with a fluorescent dye. Covalently dye-labeled polymers might be useful for diffusion measurements by fluorescence correlation spectroscopy for instance.^[111] Fluorescein- and rhodamine-based fluorophores were used to functionalize the polymer. First, a native carboxyfluorescein was used for labeling. However, the reaction was not successful. Probably, the dye was not reactive enough due to its pH sensitivity, or due to the equilibrium with its lactone form. The next attempts to label the polymer were carried out using *N*-hydroxysuccinimide ester-activated carboxyfluorescein and an activated derivate of a sulforhodamine dye. Both syntheses were not successful either. Finally, PB-PEO-OH was converted with an azide derivate of a rhodamine-based dye (tetramethylrhodamine-5-carbonyl azide; TMRA; Invitrogen, Switzerland).

PB-PEO-OH (24.6 mg; 6.0 μmol) and the TMRA (8.2 mg; 18.0 μmol) were dried separately under vacuum for 2 h. The components were dissolved in 3 mL MEK each. After the polymer solution was added to the fluorophore solution, the reaction mixture was refluxed at 80 °C for 72 h (the azide was converted *in situ* in a Curtius reaction into an intermediate isocyanate, which forms stable carbamates with the hydroxyl polymer end groups).

The solvent was evaporated under vacuum and the pink crude product was dissolved in DCM and extracted with several liters of water until the aqueous phase was colorless.

As determined by ¹H-NMR (see Figure 50), the degree of functionalization is ca. 50%. DOSY measurements proved covalent coupling of biotin to the polymer ($\delta_{\text{diff}} = 2.35 \cdot 10^{-10} \text{ m}^2/\text{s}$ for $\delta = 4.94$ and $\delta_{\text{diff}} = 2.49 \cdot 10^{-10} \text{ m}^2/\text{s}$ for $\delta = 6.41$ and 6.62).

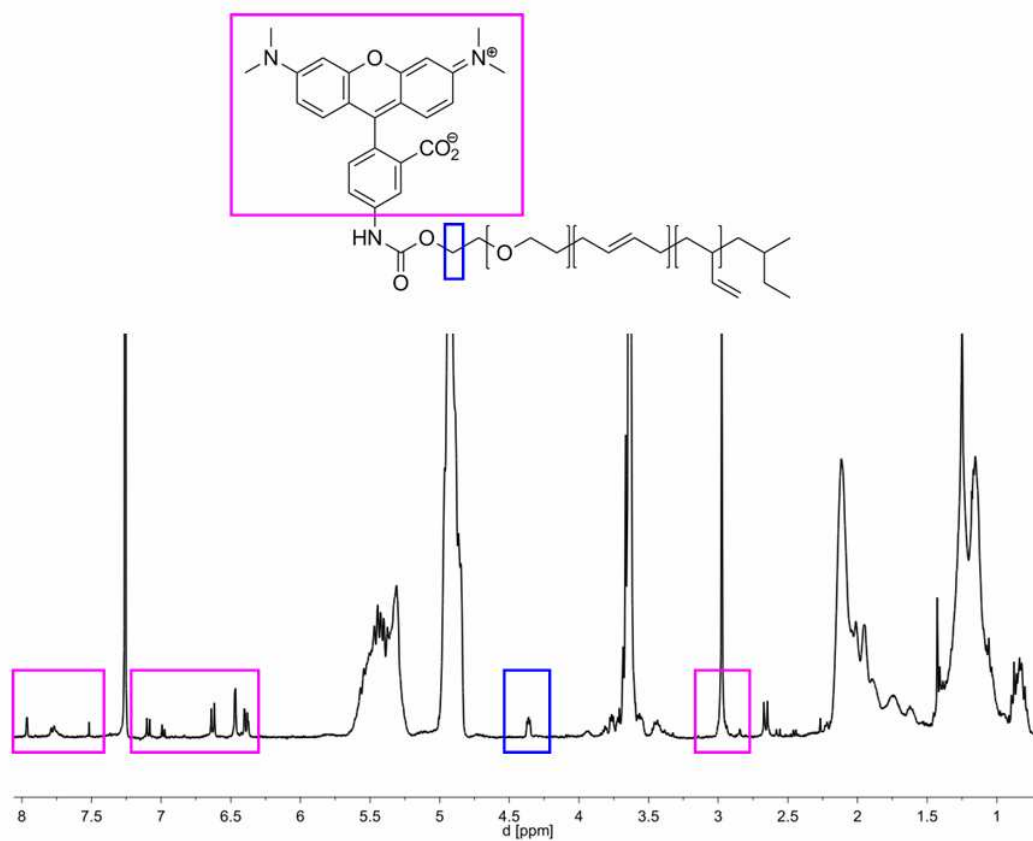


Figure 50. Structure and representative ¹H-NMR spectrum of PB-PEO-TMRA. The fluorophore signals are highlighted in purple. The signal at $\delta = 4.36$ ppm, highlighted in blue, corresponds to the methylene group in the backbone, which is adjacent to the newly formed carbamate group.

7 References

- [1] C. Steinem, A. Janshoff, *Chem. Unserer Zeit* **2008**, *42*, 116.
- [2] B. Alberts, A. Johnson, J. Lewis, M. Raff, K. Roberts, P. Walter, *Molecular biology of the cell*, Garland Science, New York, **2002**.
- [3] S. J. Singer, G. L. Nicolson, *Science* **1972**, *175*, 720.
- [4] <http://cellbiology.med.unsw.edu.au/units/science/lecture0803.htm>, accessed on March, 30 **2010**.
- [5] J. N. Israelachvili, D. J. Mitchell, B. W. Ninham, *Biochim. Biophys. Acta, Biomembr.* **1977**, *470*, 185.
- [6] R. Nagarajan, E. Ruckenstein, *Langmuir* **1991**, *7*, 2934.
- [7] C. Tanford, *Science* **1978**, *200*, 1012.
- [8] K. Simons, E. Ikonen, *Nature* **1997**, *387*, 569.
- [9] C. Peetla, A. Stine, V. Labhasetwar, *Mol. Pharmaceutics* **2009**, *6*, 1264.
- [10] C. H. Nielsen, *Anal. Bioanal. Chem.* **2009**, *395*, 697.
- [11] M. A. Shannon, P. W. Bohn, M. Elimelech, J. G. Georgiadis, B. J. Marinas, A. M. Mayes, *Nature* **2008**, *452*, 301.
- [12] W. Knoll, F. Yu, T. Neumann, S. Schiller, R. Naumann, *Phys. Chem. Chem. Phys.* **2003**, *5*, 5169.
- [13] J. Spinke, J. Yang, H. Wolf, M. Liley, H. Ringsdorf, W. Knoll, *Biophys. J.* **1992**, *63*, 1667.
- [14] C. Steinem, A. Janshoff, W.-P. Ulrich, M. Sieber, H.-J. Galla, *Biochim. Biophys. Acta, Biomembr.* **1996**, *1279*, 169.
- [15] I. K. Vockenroth, P. P. Atanasova, J. R. Long, A. T. A. Jenkins, W. Knoll, I. Koeper, *Biochim. Biophys. Acta, Biomembr.* **2007**, *1768*, 1114.
- [16] S. H. White, *Biophys. J.* **1970**, *10*, 1127.
- [17] S. Foerster, *Top. Curr. Chem.* **2003**, *226*, 1.
- [18] S. Foerster, M. Antonietti, *Adv. Mater.* **1998**, *10*, 195.
- [19] S. Forster, T. Plantenberg, *Angew. Chem. Int. Ed.* **2002**, *41*, 688.
- [20] K. Kita-Tokarczyk, M. Junginger, S. Belegriou, A. Taubert, in *Adv. Polym. Sci.*, Springer-Verlag, Berlin Heidelberg, **2010**, p. DOI: 10.1007/12_2010_58.
- [21] K. Kita-Tokarczyk, J. Grumelard, T. Haefele, W. Meier, *Polymer* **2005**, *46*, 3540.
- [22] K. Kita-Tokarczyk, W. Meier, *Chimia* **2008**, *62*, 820.
- [23] A. Mecke, C. Dittrich, W. Meier, *Soft Matter* **2006**, *2*, 751.
- [24] V. Malinova, S. Belegriou, D. d. B. Ouboter, W. P. Meier, *Adv. Polym. Sci.* **2010**, *224*, 113.
- [25] A. Graff, C. Fraysse-Ailhas, C. G. Palivan, M. Grzelakowski, T. Friedrich, C. Vebert, G. Gescheidt, W. Meier, *Macromol. Chem. Phys.* **2010**, *211*, 229.
- [26] A. Graff, M. Sauer, P. Van Gelder, W. Meier, *Proc. Natl. Acad. Sci. USA* **2002**, *99*, 5064.
- [27] M. Grzelakowski, O. Onaca, P. Rigler, M. Kumar, W. Meier, *Small* **2009**, *5*, 2545.
- [28] M. Kumar, M. Grzelakowski, J. Zilles, M. Clark, W. Meier, *Proc. Natl. Acad. Sci. USA* **2007**, *104*, 20719.
- [29] C. Nardin, W. Meier, *Rev. Mol. Biotechnol.* **2002**, *90*, 17.
- [30] D. E. Discher, A. Eisenberg, *Science* **2002**, *297*, 967.

-
- [31] K. Yu, A. Eisenberg, *Macromolecules* **1998**, *31*, 3509.
- [32] H. Bermudez, A. K. Brannan, D. A. Hammer, F. S. Bates, D. E. Discher, *Macromolecules* **2002**, *35*, 8203.
- [33] A. Taubert, A. Napoli, W. Meier, *Curr. Opin. Chem. Biol.* **2004**, *8*, 598.
- [34] S. Svenson, *J. Dispersion Sci. Technol.* **2004**, *25*, 101.
- [35] S. Segota, D. Tezak, *Adv. Colloid Interface Sci.* **2006**, *121*, 51.
- [36] C. Nardin, M. Winterhalter, W. Meier, *Langmuir* **2000**, *16*, 7708.
- [37] M. Winterhalter, C. Hilty, S. M. Bezrukov, C. Nardin, W. Meier, D. Fournier, *Talanta* **2001**, *55*, 965.
- [38] P. Mueller, D. O. Rudin, H. T. Tien, W. C. Wescott, *Nature* **1962**, *194*, 979.
- [39] M. Montal, P. Mueller, *Proc. Nat. Acad. Sci.* **1972**, *69*, 3561.
- [40] P. Mueller, D. O. Rudin, *Nature* **1967**, *213*, 603.
- [41] L. N. Ermishkin, K. M. Kasumov, V. M. Potzeluyev, *Nature* **1976**, *262*, 698.
- [42] B. Franklin, *Philos. Trans. Royal Chem. Soc.* **1774**, *64*, 445.
- [43] I. Langmuir, *J. Am. Chem. Soc.* **1917**, *39*, 1848.
- [44] G. Brezesinski, H. Mohwald, *Adv. Colloid Interface Sci.* **2003**, *100-102*, 563.
- [45] T. Haefele, K. Kita-Tokarczyk, W. Meier, *Langmuir* **2006**, *22*, 1164.
- [46] K. Kita-Tokarczyk, F. Itel, M. Grzelakowski, S. Egli, P. Roszbach, W. Meier, *Langmuir* **2009**, *25*, 9847.
- [47] M. Angelova, D. Dimitrov, *Faraday Discuss. Chem. Soc.* **1986**, *81*, 303.
- [48] J. M. H. Kremer, M. W. Van der Esker, C. Pathmamanoharan, P. H. Wiersema, *Biochemistry* **1977**, *16*, 3932.
- [49] F. Olson, C. A. Hunt, F. C. Szoka, W. J. Vail, D. Papahadjopoulos, *Biochim. Biophys. Acta, Biomembr.* **1979**, *557*, 9.
- [50] M. Ollivon, A. Walter, R. Blumenthal, *Anal. Biochem.* **1986**, *152*, 262.
- [51] N. Oku, R. C. MacDonald, *Biochemistry* **1983**, *22*, 855.
- [52] G. Sessa, G. Weissmann, *J. Lipid Res.* **1968**, *9*, 310.
- [53] J. L. Rigaud, B. Pitard, D. Levy, *Biochim. Biophys. Acta* **1995**, *1231*, 223.
- [54] M. Nallani, S. Benito, O. Onaca, A. Graff, M. Lindemann, M. Winterhalter, W. Meier, U. Schwaneberg, *J. Biotechnol.* **2006**, *123*, 50.
- [55] C. Nardin, S. Thoeni, J. Widmer, M. Winterhalter, W. Meier, *Chem. Commun.* **2000**, 1433.
- [56] L. Zhang, A. Eisenberg, *Science* **1995**, *268*, 1728.
- [57] H.-J. Choi, C. D. Montemagno, *Nano Lett.* **2005**, *5*, 2538.
- [58] M. Antonietti, S. Foerster, *Adv. Mater.* **2003**, *15*, 1323.
- [59] Z. G. Wang, *Macromolecules* **1992**, *25*, 3702.
- [60] Y.-Y. Won, A. K. Brannan, H. T. Davis, F. S. Bates, *J. Phys. Chem. B* **2002**, *106*, 3354.
- [61] S. Burke, H. Shen, A. Eisenberg, *Macromol. Symp.* **2001**, *175*, 273.
- [62] A. Blanazs, S. P. Armes, A. J. Ryan, *Macromol. Rapid Commun.* **2009**, *30*, 267.
- [63] S. Jain, F. S. Bates, *Macromolecules* **2004**, *37*, 1511.
- [64] A. A. Reinecke, H.-G. Doebereiner, *Langmuir* **2003**, *19*, 605.
- [65] L. Luo, A. Eisenberg, *Langmuir* **2001**, *17*, 6804.
- [66] L. Luo, A. Eisenberg, *Langmuir* **2002**, *18*, 1952.
- [67] L. Chen, H. Shen, A. Eisenberg, *J. Phys. Chem. B* **1999**, *103*, 9488.
- [68] M. L. Wagner, L. K. Tamm, *Biophys. J.* **2000**, *79*, 1400.
- [69] K. B. Blodgett, *J. Am. Chem. Soc.* **1935**, *57*, 1007.
- [70] I. Langmuir, V. J. Schaefer, *J. Am. Chem. Soc.* **1938**, *60*, 2803.
- [71] H. Lang, C. Duschl, H. Vogel, *Langmuir* **1994**, *10*, 197.

- [72] V. Von Tscharner, H. M. McConnell, *Biophys. J.* **1981**, *36*, 409.
- [73] A. A. Brian, H. M. McConnell, *Proc. Natl. Acad. Sci. USA* **1984**, *81*, 6159.
- [74] L. K. Tamm, H. M. McConnell, *Biophys. J.* **1985**, *47*, 105.
- [75] E. Sackmann, *Science* **1996**, *271*, 43.
- [76] M. Tanaka, E. Sackmann, *Phys. Stat. Sol. (a)* **2006**, *203*, 3452.
- [77] E. K. Sinner, W. Knoll, *Curr. Opin. Chem. Biol.* **2001**, *5*, 705.
- [78] M. Tanaka, E. Sackmann, *Nature* **2005**, *437*, 656.
- [79] C. Rossi, J. Chopineau, *Eur. Biophys. J.* **2007**, *36*, 955.
- [80] W. Knoll, C. W. Frank, C. Heibel, R. Naumann, A. Offenhausser, J. Ruhe, E. K. Schmidt, W. W. Shen, A. Sinner, *Rev. Mol. Biotechnol.* **2000**, *74*, 137.
- [81] N. Bunjes, E. K. Schmidt, A. Jonczyk, F. Rippmann, D. Beyer, H. Ringsdorf, P. Graeber, W. Knoll, R. Naumann, *Langmuir* **1997**, *13*, 6188.
- [82] A. Foertig, R. Jordan, K. Graf, G. Schiavon, O. Purrucker, M. Tanaka, *Macromol. Symp.* **2004**, *210*, 329.
- [83] S. M. Schiller, R. Naumann, K. Lovejoy, H. Kunz, W. Knoll, *Angew. Chem. Int. Ed.* **2003**, *42*, 208.
- [84] E. Rakhmatullina, A. Manton, T. Burgi, V. Malinova, W. Meier, *J. Polym. Sci., Part A: Polym. Chem.* **2008**, *47*, 1.
- [85] E. Rakhmatullina, W. Meier, *Langmuir* **2008**, *24*, 6254.
- [86] T. Rosenkranz, A. Katranidis, D. Atta, I. Gregor, J. Enderlein, M. Grzelakowski, P. Rigler, W. Meier, J. Fitter, *ChemBioChem* **2009**, *10*, 702.
- [87] E. Rakhmatullina, T. Braun, M. Chami, V. Malinova, W. Meier, *Langmuir* **2007**, *23*, 12371.
- [88] J. C.-M. Lee, H. Bermudez, B. M. Discher, M. A. Sheehan, Y.-Y. Won, F. S. Bates, D. E. Discher, *Biotechnol. Bioeng.* **2001**, *73*, 135.
- [89] R. Matmour, T. J. Joncheray, Y. Gnanou, R. S. Duran, *Langmuir* **2007**, *23*, 649.
- [90] K. Vijayan, D. E. Discher, J. Lal, P. Janmey, M. Goulian, *J. Phys. Chem. B* **2005**, *109*, 14356.
- [91] K. Hong, D. Uhrig, J. W. Mays, *Curr. Opin. Solid State Mater. Sci.* **2000**, *4*, 531.
- [92] J. Jagur-Grodzinski, *J. Polym. Sci., Part A: Polym. Chem.* **2002**, *40*, 2116.
- [93] B. Esswein, M. Moeller, *Angew. Chem. Int. Ed.* **1996**, *35*, 623.
- [94] S. Foerster, E. Kraemer, *Macromolecules* **1999**, *32*, 2783.
- [95] J. S. Gounarides, A. Chen, M. J. Shapiro, *J. Chromatogr., B: Biomed. Sci. Appl.* **1999**, *725*, 79.
- [96] R. Huo, R. Wehrens, J. Van Duynhoven, L. M. C. Buydens, *Anal. Chim. Acta* **2003**, *490*, 231.
- [97] D. J. Crisp, *J. Colloid Sci.* **1946**, *1*, 161.
- [98] G. Jura, W. D. Harkins, *J. Chem. Phys.* **1944**, *12*, 113.
- [99] A. M. Goncalves da Silva, E. J. M. Filipe, J. M. R. d'Oliveira, J. M. G. Martinho, *Langmuir* **1996**, *12*, 6547.
- [100] W. D. Harkins, *Physical Chemistry of Surface Films*, Reinhold Publishing Corp., New York **1952**.
- [101] S. M. Baker, K. A. Leach, C. E. Devereaux, D. E. Gragson, *Macromolecules* **2000**, *33*, 5432.
- [102] J. A. Zasadzinski, R. Viswanathan, L. Madsen, J. Garnaes, D. K. Schwartz, *Science* **1994**, *263*, 1726.
- [103] C. L. Brosseau, J. Leitch, X. Bin, M. Chen, S. G. Roscoe, J. Lipkowski, *Langmuir* **2008**, *24*, 13058.

-
- [104] D. K. Schwartz, *Surf. Sci. Rep.* **1997**, *27*, 241.
- [105] I. Pera, R. Stark, M. Kappl, H.-J. Butt, F. Benfenati, *Biophys. J.* **2004**, *87*, 2446.
- [106] G. Battaglia, A. J. Ryan, *J. Am. Chem. Soc.* **2005**, *127*, 8757.
- [107] R. F. Roskamp, I. K. Vockenroth, N. Eisenmenger, J. Braunagel, I. Koeper, *ChemPhysChem* **2008**, *9*, 1920.
- [108] F. Albertorio, V. A. Chapa, X. Chen, A. J. Diaz, P. S. Cremer, *J. Am. Chem. Soc.* **2007**, *129*, 10567.
- [109] F. Albertorio, A. J. Diaz, T. Yang, V. A. Chapa, S. Kataoka, E. T. Castellana, P. S. Cremer, *Langmuir* **2005**, *21*, 7476.
- [110] Y. Deng, Y. Wang, B. Holtz, J. Li, N. Traaseth, G. Veglia, B. J. Stottrup, R. Elde, D. Pei, A. Guo, X. Y. Zhu, *J. Am. Chem. Soc.* **2008**, *130*, 6267.
- [111] J. C. M. Lee, M. Santore, F. S. Bates, D. E. Discher, *Macromolecules* **2002**, *35*, 323.
- [112] S. Jain, F. S. Bates, *Science* **2003**, *300*, 460.
- [113] B. M. Discher, Y.-Y. Won, D. S. Ege, J. C. M. Lee, F. S. Bates, D. E. Discher, D. A. Hammer, *Science* **1999**, *284*, 1143.
- [114] H. Ringsdorf, B. Schlarb, J. Venzmer, *Angew. Chem.* **1988**, *100*, 117.
- [115] F. M. Menger, M. I. Angelova, *Acc. Chem. Res.* **1998**, *31*, 789.
- [116] A. A. Choucair, A. H. Kycia, A. Eisenberg, *Langmuir* **2003**, *19*, 1001.
- [117] W. Su, Y. Luo, Q. Yan, S. Wu, K. Han, Q. Zhang, Y. Gu, Y. Li, *Macromol. Rapid Commun.* **2007**, *28*, 1251.
- [118] Y. Zhou, D. Yan, *J. Am. Chem. Soc.* **2005**, *127*, 10468.
- [119] <http://www3.oup-usa.org/pdh/>, accessed on Mai, 25 **2010**.
- [120] A. K. Brannan, F. S. Bates, *Macromolecules* **2004**, *37*, 8816.
- [121] F. Meng, C. Hiemstra, G. H. M. Engbers, J. Feijen, *Macromolecules* **2003**, *36*, 3004.
- [122] M. Maskos, *Polymer* **2006**, *47*, 1172.
- [123] S. Belegriinou, J. Dorn, M. Kreiter, K. Kita-Tokarczyk, E.-K. Sinner, W. Meier, *Soft Matter* **2010**, *6*, 179.
- [124] I. Reviakine, A. Brisson, *Langmuir* **2000**, *16*, 1806.
- [125] J. Leitch, J. Kunze, J. D. Goddard, A. L. Schwan, R. J. Faragher, R. Naumann, W. Knoll, J. R. Dutcher, J. Lipkowski, *Langmuir* **2009**, *25*, 10354.
- [126] O. Prucker, S. Christian, H. Bock, J. Ruehe, C. W. Frank, W. Knoll, *Macromol. Chem. Phys.* **1998**, *199*, 1435.
- [127] V. Atanasov, P. P. Atanasova, I. K. Vockenroth, N. Knorr, I. Koeper, *Bioconjugate Chem.* **2006**, *17*, 631.
- [128] M. Moisel, M. A. F. Lorenzo de Mele, W.-D. Mueller, *Adv. Biomater.* **2008**, B33.
- [129] I. K. Vockenroth, University of Bath **2007**.
- [130] W. Meier, C. Nardin, M. Winterhalter, *Angew. Chem. Int. Ed.* **2000**, *39*, 4599.
- [131] V. Pata, N. Dan, *Biophys. J.* **2003**, *85*, 2111.
- [132] D. Ho, S. Chang, C. D. Montemagno, *Nanomedicine* **2006**, *2*, 103.
- [133] H. Duclohier, H. Wroblewski, *J. Membr. Biol.* **2001**, *184*, 1.
- [134] F.-Y. Chen, M.-T. Lee, H. W. Huang, *Biophys. J.* **2003**, *84*, 3751.
- [135] A. Spaar, C. Muenster, T. Salditt, *Biophys. J.* **2004**, *87*, 396.
- [136] R. A. Dixon, I. Chopra, *J. Antimicrob. Chemother.* **1986**, *18*, 557.
- [137] A. Wiese, M. Munstermann, T. Gutschmann, B. Lindner, K. Kawahara, U. Zahringer, U. Seydel, *J. Membr. Biol.* **1998**, *162*, 127.
- [138] G. Schroeder, K. Brandenburg, U. Seydel, *Biochemistry* **1992**, *31*, 631.

-
- [139] T. Tomita, M. Watanabe, T. Yasuda, *J. Biol. Chem.* **1992**, 267, 13391.
- [140] L. Song, M. R. Hobaugh, C. Shustak, S. Cheley, H. Bayley, J. E. Gouaux, *Science* **1996**, 274, 1859.
- [141] R. Naumann, S. M. Schiller, F. Giess, B. Grohe, K. B. Hartman, I. Kaercher, I. Koeper, J. Luebben, K. Vasilev, W. Knoll, *Langmuir* **2003**, 19, 5435.
- [142] J. R. Sambles, G. W. Bradbery, F. Yang, *Contemp. Phys.* **1991**, 32, 173.
- [143] J. Brandrup, E. H. Immergut, *Polymer Handbook*, John Wiley & Sons, New York, **1975**.
- [144] J. R. Macdonald, *Impedance Spectroscopy*, John Wiley & Sons, New York, **1987**.

Curriculum vitae

Personal Data

Name	Serena Belegriou
Date and place of birth	21.08.1982 in Augsburg (Germany)
Nationality	German

Education

02/2007 - present PhD studies supervised by Prof. Dr. Wolfgang Meier
(University of Basel, Switzerland)

09/2006 Diploma in chemistry (University of Ulm, Germany)

Diploma thesis supervised by PD Dr. Hubert Rauscher (Joint Research Centre of the European Commission in Ispra, Italy) and Prof. Dr. Katharina Landfester (University of Ulm, Germany)

06/2001 A-levels (“Abitur”)
(Paul-Klee-Gymnasium Gersthofen, Germany)

The following lecturers participated in the educational training during the PhD studies:
Thomas Briellmann, Franz E. Dussy, Daniel Gygax, Peter C. Hauser, Philipp Hübner,
Katarzyna Kita-Tokarzyk, Hanno Langen, Wolfgang Meier, Uwe Piele, Hans-Rudolf Schmutz, André Scholer, Maria Anna Schwarz, Corinne Vebert

Publications and conference posters

Publications

S. Belegriou, V. Malinova, R. Masciadri, W. Meier

Synth. Commun. **2010**, accepted

K. Kita-Tokarczyk, M. Junginger, S. Belegriou, A. Taubert

Adv. Polym. Sci. **2010**, DOI: 10.1007/12_2010_58

V. Malinova, S. Belegriou, D. de Bruyn Ouboter, W. Meier

Adv. Polym. Sci. **2010**, 224, 113

S. Belegriou, J. Dorn, M. Kreiter, K. Kita-Tokarczyk, E.-K. Sinner, W. Meier

Soft Matter **2010**, 6, 179

S. Belegriou, I. Manelli, P. Lisboa, F. Bretagnol, A. Valsesia, G. Leccone, P. Colpo, H. Rauscher, F. Rossi; *Langmuir* **2008**, 24, 7251

S. Belegriou, I. Manelli, L. Sirghi, F. Bretagnol, A. Valsesia, H. Rauscher, F. Rossi

J. Phys. Chem. B **2007**, 111, 8713

In preparation:

S. Belegriou, P. Rossbach, K. Kita-Tokarczyk, M. Grzelakowski, J. Thoma,

W. Meier

S. Belegriou, S. Menon, D. Dobrunz, W. Meier

Invited review, *Soft Matter*

J. Dorn, S. Belegriou, M. Kreiter, E.-K. Sinner, W. Meier

J. Dorn, M. Geissbühler, I. Märki, S. Belegriou, M. Kreiter, E.-K. Sinner, T. Lasser

Conference Posters

Spring Meeting of the Swiss Chemical Society, Zürich (Switzerland), 12.06.2009

S. Belegriou, J. Dorn, M. Kreiter, E.-K. Sinner, W. Meier

Frontiers in Polymer Science, Mainz (Germany), 07.-09.06.2009

S. Belegriou, J. Dorn, M. Kreiter, E.-K. Sinner, W. Meier

11. European Conference on Organized Films, Potsdam, Germany, 8.-11.07.2008,

S. Belegriou, J. Dorn, M. Kreiter, , E.-K. Sinner, W. Meier

Fall Meeting of the Swiss Chemical Society, Lausanne (Switzerland) 12.09.2007

S. Belegriou, R. Nehring, K. Kita-Tokarczyk, V. Malinova, W. Meier

International Max Planck Research Schools for Polymer Science/National Science Foundation, Playa del Aro, Spanien, 28.06.- 01.07.2007

S. Belegriou, R. Nehring, M. Grzelakowski, P. Rigler, V. Malinova, W. Meier